Spatio-Temporal Analysis of Urban Heat Vulnerability: The Case study of Dire Dawa City, Ethiopia

By:-Habtamu Lensha Osman

A Thesis Submitted to

The department of Geomatics Engineering,

School of Civil Engineering and Architecture Presented in Partial Fulfillment of the Requirements for the Degree of

Master's in Geo-informatics Engineering

Office of Graduate Studies

Adama Science and Technology University

June, 2022

Adama, Ethiopia

Spatio-Temporal Analysis of Urban Heat Vulnerability: The Case study of Dire Dawa City, Ethiopia

By:-Habtamu Lensha Osman

Major Advisor: Getachew Brhanemeskel (PhD)

Co-Advisor: Boja Mekonon (PhD)

A Thesis Submitted to
The department of Geomatics Engineering,
School of Civil Engineering and Architecture Presented in Partial Fulfillment
of the Requirements for the Degree of
Master's in Geo-informatics Engineering

Office of Graduate Studies

Adama Science and Technology University

June, 2022

Adama, Ethiopia

DECLARATION

I hereby declare that this Master Thesis entitled “Spatio-Temporal Analysis of Urban Heat Vulnerability: The Case study of Dire Dawa City, Ethiopia” The thesis is my original work and has not been presented and submitted to any other university anywhere for the award of any academic degree, diploma or certificate. All sources or materials that I used in this thesis have been duly acknowledged through citation.

Habtamu Lensha Osman	________________	________________
Name	Signature	Date

RECOMMENDATION

This is to certify that the thesis entitled “Spatio-Temporal Analysis of Urban Heat Vulnerability: The Case study of Dire Dawa City, Ethiopia”. Submitted in partial fulfillment of the requirements for the degree of Master’s in Geo-informatics Engineering, the Graduate program of the department of Geomatics Engineering, and has been carried out by Habtamu Lensha Osman, ID. PGR/19367/12 was under our supervision. Therefore, we recommend that the student has fulfilled the requirements and hence he can submit the thesis to the department.

Getachew Brhanemeskel (PhD)	______________	______________
Name of major Advisor	Signature	Date
Boja Mekonon (PhD)	_______________	_______________
Name of Co-Advisor	Signature	Date

BOARD OF EXAMINERS APPROVAL

We, the advisors of the thesis entitled "Spatio-Temporal Analysis of Urban Heat Vulnerability: The Case study of Dire Dawa City, Ethiopia" and developed by (Habtamu Lensha Osman), hereby certify that the recommendation and suggestions made by the board of examiners are appropriately incorporated into the final version of the thesis.

Getachew Brhanemeskel (PhD) ____	______________________	________________
Major Advisor	Signature	Date
Boja Mekonon (PhD) ____	______________________	________________
Co-Advisor	Signature	Date

We, the undersigned, members of the Board of Examiners of the thesis by Habtamu Lensha Osman have read and evaluated the thesis entitled "Spatio-Temporal Analysis of Urban Heat Vulnerability: The Case study of Dire Dawa City, Ethiopia" and examined the candidate during open defense. This is, therefore, to certify that the thesis is accepted for partial fulfillment of the requirement of the degree of Master of Science in Geo-informatics Engineering.

______________________	______________________	______________________
Chairperson	Signature	Date
______________________	______________________	______________________
Internal Examiner	Signature	Date
______________________	______________________	______________________
External Examiner	Signature	Date

Final approval and acceptance of the thesis is contingent upon submission of its final copy to the Office of Postgraduate Studies (OPGS) through the Department Graduate Council (DGC) and School Graduate Committee (SGC).

______________________	______________________	______________________
Department Head	Signature	Date
______________________	______________________	______________________
School Dean	Signature	Date
______________________	______________________	______________________
Office of Postgraduate Studies, Dean	Signature	Date

ACKNOWLEGMENTS

First and foremost, I want to praise, and thanks to Almighty God, the Lord of everything, who is credited with all of the completion of this Thesis work.

This work wouldn’t be completed without the assistance of several persons and organizations, all of whom I grateful acknowledgement. I would like to express my sincerest thanks and appreciation to my advisors who indeed contributed to the complement of this study. I would like to deeply acknowledge My Main Advisor Dr. Getachew Brhanemeskel (PhD), Co-Advisor Dr. Boja Mekonon (PhD) and Daniel Alemayehu (PhD, Asst. Prof.) for their supervision, support, guidance, helping me overcoming the obstacles, and answering all my questions during the time of my thesis work.

Special thanks to Adama Science and Technology University (ASTU) and Dire Dawa University for financial support to pursue my studies and related research activities to achieve my research objectives.

From the bottom of my heart, I would like to thanks my Mother Inspector Yashi Lami Badhane, for her supporting and encouraging me day night in my life past and future; I love you forever! Last but not least, with all love and respect I would like to thank my friends (Adisu Teshome, Amanuel Atnafu, Abdi Tadese and Baselam Shimalis) for their thoughtful encouragement all the time during my thesis work.

TABLE OF CONTENTS

Contents **Page**

LIST OF TABLES

Table Title **Page**

LIST OF FIGURES

LIST OF ACRONYMS

BT	Brightness Temperature
CSA	Central Statistical Agency
ERDAS	Earth Resources Data Analysis System
GIS	Geographic Information System
GPS	Global Positioning System
HVI	Heat Vulnerability Index
IDW	Inverse Distance Weighted
IPCC	Intergovernmental Panel on Climate Change
LST	Land Surface Temperature
LULC	Land Use Land Cover
NDVI	Normalized Difference Vegetation Index
OLI	Operational Land Imager`
TIRS	Thermal Infrared Sensor
TM	Thematic Mapper
TOA	Top of Atmosphere
UHI	Urban Heat Island
UHV	Urban Heat Vulnerability
USGS	United States Geological Survey
UTM	Universal Transverse Mercator
WGS	World Geodetic System

ABSTRACT

Dire Dawa City has faced the adverse effect of climate change with the problem of overwhelming increase in temperature as compared from year to year. The effects significantly influence internal urban microclimate at a local scale. And, the rapid urbanization has produced a remarkable effect on the surface thermal response. Thus, the aim of this study was to analyze spatio-temporal distribution of urban heat vulnerability in Dire Dawa City by employing geospatial technologies tools. To achieve the objective of the study, heat vulnerability index through aggregation (additive approach) were used to identify vulnerable areas to heat. Based on Intergovernmental Panel on Climate Change (IPCC's) approach of vulnerability assessment which comprises exposure, sensitivity and adaptive capacity. Four sub components of vulnerability indicators were identified and their values were normalized to a number which ranges between 0-1, as the values approaches to 1, vulnerability increases. In this study, land surface temperature and land use land cover types extracted from Landsat 5 TM (1995) and Landsat 8 OLI/TIRS (2020). Erdas imagine 2014 and ArcGIS 10.8 were used for data pre-processing, preparation and map composition. Results from land use land cover dynamics in relation to land surface temperature changes between 1995 and 2020 revealed that, a noticeable increase in built-up area by 5.38 km^2 exhibited a high change of surface temperature by 5.12^0C. While, sparse vegetation has been gradually decline by 2.07 km^2 exposed surface temperature to increase by 5.03^0C. Also, urban land development raised surface temperature by 6.87 ^{0}C (highest) for kebele 02 and 5.30 ^{0}C (lowest) for kebele 07. And, the normalized values of spatial distribution of population per kebele score of sensitivity result were highest (1.0) for kebele 02 and lowest for kebele 06 (0.0). On the other hand, normalized average adaptive capacity result shows highest (1.00) for kebele 06 and lowest (0.06) for kebele 03. Relative heat vulnerability index score ranges from 0.12(lowest) in kebele 03, goes to 0.63 (highest) found in kebele 07; by superimposing the heat vulnerability indicators, kebele 07, 02, 09, 06 and 08 kebeles were identified as highly vulnerable to heat incidence; highest heat vulnerability are derived from factors associated with the raised land surface temperature, high population density, limited green area coverage's and poor accessibility of water. Generally, urban heat vulnerability maps that developed for Dire Dawa City are able to identify not only where are the hottest areas are located but also where the most vulnerable people of the City are located in the City. In addition, there are also able to visualize the current state of adaptive capacity to extreme heat based on the availability of greenery, water accessibility for public health.

Keywords: Urban Heat Vulnerability, Exposure, Sensitivity and Adaptive Capacity

CHAPTER I: INTRODUCTION

1.1 Background of the study

According to the Intergovernmental Panel on Climate Change (IPCC, 2014b) vulnerability is defined as a function of exposure, sensitivity, and adaptive capacity. These three components are the key elements in determining a vulnerability to climate change and provide useful information for analyzing the adverse effect of climate change and reducing climatic intimidations. Different scientific communities apply different definitions for connecting an adverse effect with urban heat vulnerability. Exposure is the extent to which urban populations are in contact with, or subject to hazards and size of the area or system, sector or group affected under climate change; The most common indicator for analyzing exposure is land surface temperature change (Reid, 2009; Huang., 2011; Feyissa, 2019). Sensitivity is defined as the extent to which a community will be affected by a change in climatic conditions (Kell, 2000). While, adaptive capacity is also considered as a function of infrastructure and access to resources (Inostroza, 2016).

Urban heat vulnerability is one of the by-products of the human alteration to natural landscapes and landscapes of man-made materials like asphalt and concrete that retain heat (Stone, 2012). Many studies on urban thermal environment indicate that settlement and impervious surfaces are highly expanded at the expense of green areas, and open spaces (Mutiibwa, 2014). Similarly, Odindi, (2015) stated that the conversion of urban greenery to impervious landscapes has been recognized as a key factor influencing the distinctive urban heat and associated consequences. Population density levels and lack of green areas are also the main drivers for urban heat vulnerability (Rizwan, 2008). Moreover, heat stress becomes aggravated due to reduced levels of evapotranspiration and occurs in high-density of industrial zones, thus affecting public health (Baklanov, 2016).

With specific reference to heat health risk, multiple studies have shown that increased population density results in increased heat vulnerability (Harlan, 2006; Tan J:, 2008). The studies showed that the high rate of heat vulnerability has effect on the health of people thereby leading to heat related diseases such as fatigue, sunstroke, muscle cramps, heat stroke and heat exhaustion (Alaigba, 2017). FDRE ministry of health report reveals that, re-emergence of Dengue fever in eastern parts of Ethiopia has been increased; this Dengue fever is among climate sensitive diseases that are believed to intensify with the rise of temperature (FDRE Ministry of Health, 2015).

Currently, various cities around the world are focusing on the creation of green space and increasing supplies of freshwater in order to lower effect of heat vulnerability. Urban green space, such as open parks, forests, and grasslands, have been increasingly recognized as key components of urban planning (Santamouris, 2001). Scholars agree on the role of urban green space to mitigate highest temperature changes in urban areas (Norton, *et al.,* 2015; Zhang *et al.,* 2017). According to the previous studies, green space can provide a mitigation effect of the heat vulnerability (Reid, 2009; Yue *et al,* 2019). They can also provide critical ecosystem services that could improve residents' health and wellbeing. green space forms cool islands and improve outdoor thermal comfort throughout warm seasons, as well as significantly reduce environmental stress produced by heat island (Chang and Akpina, 2014). For example, a study by Spronken-Smith, *et al.,* (2001) and Klok, *et al.,* (2012) concluded that identifying hot spots spatial location and strategically placing green space is the first step towards adaptation to future climate change.

The global trend of urbanization and the growing population of cities require increasing volumes of water to be extracted and transported (Hunt *et al*., 2010). Since urban population is expected to grows increasing the amount of existing water supply to meet the rising demand (Hanak and Lund, 2011). Studies suggested that, an additional sources of water supply (like from the ground water) is required in order to maintain inhabited consumption levels (Alexander *et al*., 2010). Securing sufficient supplies of freshwater for growing cities is recognized as primary concern, and may be seriously hindered by the spatial and temporal variability of water demand and supply (Buytaert, *et al.*, 2012).

Research on urban heat vulnerability has been expanded rapidly since the early 1990s in various academic disciplines due to recent advances in the integration of geospatial information that allows for a spatially explicit characterization of extreme heat vulnerability in urban environments (Wilhelmi *et al*., 2004). However, Bao *et al*., (2015) concluded that, studies on assessing heat vulnerability are mainly performed in Europe and the United States. In Ethiopia, the impact of climate change was studied largely at the country level in different sectors mainly emphasizing the impacts of agricultural productivity and water sectors (Feyissa, 2019). Likewise, studies concerning on the application of heat vulnerability is also needed. Since, urban heat vulnerability analysis is conducted to address certain objectives, such as to identify vulnerable location for mitigating heat risks to the public and for monitoring the effects of temperature changes, which lead to heat vulnerability.

The above mentioned objectives and gaps are addressed in this research by using an integrated framework that combines remote sensing and GIS. In some of previous studies different methods are typically utilized to determine urban heat vulnerability. None of the methods are necessarily superior to the others, but the choice of method were depend on objectives, data availability and the time frame for the analysis (Sherbinin, 2014; Reid, *et al.,* 2009; Rinner *et al.,* 2010). After confirming the determinants of heat vulnerability, many researchers have normalized the values of the determinants to relative positions between 0 and 1, as the values increased to 1 vulnerability to climate change increases. The normalized values of all determinants were aggregated to form a composite Heat Vulnerability Index (Aubrecht and Ozceylan, 2013 ; Wolf et al., 2014). Indicator standardization (a 0–1 range) and aggregation (additive approach) are a common approach in indicator composition and this approach helps avoid additional subjectivity in the index development (Tapsell, et al., 2002; Turvey, 2007).

Generally speaking, this study aims to fill a portion of that gap by outlining and prioritizing the heat vulnerabilities faced by the residents of Dire Dawa City. And also for building academic knowledge and provide base for further career improvement. Keeping in view, the detailed land use land cover map of the City will further helps municipal land use information demand in the planning and arrangement of urban green space requirements. The result also helps to implement sound plans at local level for improvement of strategic placements of urban green space and to ensure equitable access to water in Dire Dawa City.

1.2 Statement of the Problem

Dire Dawa City has perceived a notable spatial expansion, population growth and many developmental activities such as industries, building construction and many other activities. Based on contemporary finding on the study areas which is done by Haylemariyam, (2018) shows that the changes in land use land cover is because of urban growth, settlement expansion, and construction of newly built-up units in Dire Dawa City; has led to increment in land surface temperature. As well, the result in land use land covers change that causes extensive reduction on abundance of vegetation bounce urban land surface temperatures to rise. Also lack of appropriate land use policies and regulations, lack of considering the role of green space during planning and designing period and also, uneven accessibility of safe water is continuing as a challenge which can aggravate heat vulnerability problem. While, the degree of urban heat vulnerability was not investigated for designing the appropriate mitigation policies towards urban heat vulnerable areas.

The climatic condition of Dire Dawa City is characterized by warm and dry climate with a relatively low level of precipitation. Increasing temperature due to urbanization has been observed in Dire Dawa City Administration. For instance, based on national meteorology agency availed data the mean annual temperature of 1995 was 25.85°C, on the other hand in 2020 the mean annual temperature was 26.61°C; this implies that the mean annual temperature difference between 1995 and 2020 was 0.74°C. For the last two decades, the average annual temperature of the City was increasing by 0.6°C per decade, especially in the cool months(D.D.E.P.A, 2020). Moreover, the assessments made by National Meteorological Agency (2007), reported that in case of IPCC mid-range (A1B) emission scenario, the mean annual temperature in Dire Dawa will increase up to 1°C by 2030, 1.8°C by 2050 and 3°C by 2080 compared to the 1961-1990 normal. The climate warming trend and City growth contribute to excessive heat in urban areas (Ahmed, 2015).

In conditions of climate change, urban areas suffer the most heat load, which negatively affects human health. For instance, based on national Meteorological Agency (2020), report on " Climate Information for the Health Sector" the degree of human comfort with respect heat stress, Dire Dawa recorded 23 days uncomfortable conditions out of 29 days during the month of May 2020. All human well-being is needed to be comfortable but the adverse effect of climate change increased heat stress in Dire Dawa City. However, there is acute shortage of urban heat vulnerability monitoring in groundwork. These serious problems are initiated to do this study.

Heat vulnerability problem in Dire Dawa City, by now it is researchable problem. Especially, identifying the spatial location of urban heat vulnerability is one of the most important problems in Dire Dawa City. Because, historical trends of temperature within the past decades was not identified and quantified at kebele levels of administrative boundaries; again, due to physical, demographic characteristics the sensitivity of populations to heat stressors and adaptive capacities difference over the kebele boundary, all kebeles have not similar heat vulnerability. Surprisingly, methods of identifying the hotspot location that support the strategic placement of green space and equitable access to water in city in the context of identified urban heat vulnerable locations is not developed. Therefore, these studies were focused on the identification of vulnerable areas (kebeles) to heat and propose the areas (kebeles) which require priority for the development of specific climate change adaptation strategies to mitigate urban heat vulnerability within the study area.

1.3 Objective of the study

1.3.1 General objective

The general objective of the study is to analyze spatio-temporal distribution of urban heat vulnerability hotspot areas in the Dire Dawa City from the year 1995 – 2020 by using geospatial technologies tools.

1.3.2 Specific objectives

The specific objective of the study is to:

- Examine the spatio-temporal variation of land surface temperature in relation to land use land cover dynamics from 1995 to 2020.
- Quantify the spatial distribution of heat vulnerability based on vulnerability indices (exposure, sensitivity and adaptive capacity).
- Identify the spatial distribution of urban heat vulnerability hotspot areas in Dire Dawa City.

1.4 Research questions

- How the land surface temperature distribution was influenced by land use land cover dynamics?
- How heat vulnerability indicators are quantified and mapped by Heat Vulnerability Index?
- Which areas of the City is most vulnerable to heat?

1.5 Significance of the Study

The study's relevance could be that it provides information on the area's LU/LC and LST change trends. Additionally, it could be utilized as a source of information for government policymakers, urban land managers, natural resource managers, environmental experts, and other interested parties in making decisions on how LU/LC and LST evolve through time.

The overall aim of this research is to create an understanding of heat vulnerability at a local scale, its impacts and the ways in which impacts are reduced by adaptation and mitigation activities. The output or findings can serve as the basis to give more detailed information (spatially) about heat vulnerability. Heat vulnerability analyses also help to strengthen mitigation activities and prioritize kebeles of Dire Dawa City based on their degree of heat vulnerability. More specifically, the maps and graphs obtained from these studies can be used as planning support and as a solution to the reduction of heat vulnerability. Furthermore, it can be used as a starting point or a reference for future researchers based on the study's finding.

1.6 Delimitations and Limitations of the study

The scope of present research was limited to the geographical coverage of Dire Dawa City, Ethiopia. The thematic scope of this studies were focused on identification of the most vulnerable kebeles to heat over the city and propose the areas which require priority for adaptation strategies to mitigate urban heat vulnerability within the study area. To achieve these objectives, the study were selected the sub neighborhood (kebeles) as the analytical unit, which is the smallest territorial unit in administrative division at which most of the local urban planning and management decisions are designed and implemented. This study attempted to see all significant pointers that have contributed to urban heat vulnerability by integrating all possible efforts in acquiring required inputs in the form of secondary data collection, analysis and interpretation of the results, conclude and recommend for further researchers.

1.7. Thesis Organization

This thesis is presented into five chapters. The first chapter introduces the proposed topic, Spatio-Temporal Distribution of Urban Heat Vulnerability: The Case of Dire Dawa City, Ethiopia. It also includes the problem statements, objectives, and research questions, significances of the study, delimitations and limitations of the study. The second chapter is literature review. This includes both theoretical and empirical frameworks. A comprehensive review of urban heat vulnerability concepts and the environmental and social impacts of urban heat vulnerability, urban heat vulnerability mitigation alternatives and methods were covered under theoretical framework and empirical framework which includes previous studies related to this study. Afterwards, chapter 3 has a closer look to the materials and methods. This chapter gives an overview of description of the study area, materials used, data analysis methods and conceptual framework of the study. Results obtained from the data analysis to achieve the objectives of the study follow in chapter 4, together with interpretation of results and discussion. Based on the result of the study conclusion and recommendations for future studies were covered under Chapter 5.

CHAPTER II: LITERATURE REVIEW

This chapter explores both theoretical and empirical frameworks. A comprehensive review of urban heat vulnerability concepts and the environmental and social impacts of urban heat vulnerability, urban heat vulnerability mitigation alternatives and review of different recent studies which was studied by different scholars in different countries were covered under theoretical framework. And an empirical framework covers different literatures concerned with methodology used for urban heat vulnerability analysis in different countries.

2.1. Theoretical Framework.

2.1.1 Overview of Climate Change

According to IPCC, (2014), climate change refers to a change in the state of the climate that can be identified by changes in the mean and/or the variability of its properties and that persists for an extended period, typically decades or longer. Similarly, the World Meteorological Organization explains the differences between climate change and variability as "climate variability looks at change that occurs within smaller time frames as a month, a season or a year, and climate change considers changes that occur over a longer period of time, typically over decades or longer" (WMO, 2020). United Nations Framework Convention on Climate Change by its part defines climate change as a change of climate which is attributed directly or indirectly to human activity that alters the composition of the global atmosphere and which is in addition to natural climate variability observed over comparable time periods (UNFCCC, 1992). In most cases, vulnerability, resilience, and adaptive capacity are the central concepts for the analyses and understanding of the impacts of climate change, or amplify the consequences of environmental changes (Feyissa, 2019).

2.1.2 Trends of Climate Change in Ethiopia

So far, some studies predict long-term future climate change situations that could prevail up to the end of this century in Ethiopia (Mcsweeney *et al.*, 2010). National Meteorological Agency report, reveals that there has been a warming trend in the annual minimum temperature over the past 55 years (1951-2006), in the indicated period, the temperature has been increasing by about 0.37 °C every ten year (NMA, 2007). Warming is expected to continue in Ethiopia, for all seasons, in all regions, and even if emissions decrease (Feyissa, 2019). The multi-model average shows warming in all four seasons in all regions, with annual warming in Ethiopia by the 2020s of 1.2 °C with a range of 0.7–2.3 °C (2050s 2.2°C, range 1.4–2.9°C) (Conway, *et al.*, 2011).

Both average maximum and minimum temperatures are characterized by high inter-annual variability for all regions with different trends for the regions (NMA, 2007). The assessments that are undertaken in major Ethiopian towns indicate that the temperature has increased and continue to increase in the future. For instance, the temperature trends indicates increment in major towns like, Mekelle, Bahirdar, Gondar, Adama, Dire Dawa, Gode Jigjiga, Batu, Arbamich and others (Beyene, 2016; Mulugeta, *et al.*, 2017). In general in Ethiopia, historical data indicate that temperatures are increasing and the number of extreme events is likely increasing(Chemonics International, 2015).

2.1.3 Vulnerability to Climate Change

The knowledge of vulnerability to climate change can assist decision makers in recommending the existing adaptation measures and prioritizing resource allocation for adaptation measures to future impacts of climate change (Gizachew *et al.*, 2014). Yamin, *et al*. (2005) also refer to vulnerability as, "the manner and degree in which a community is susceptible to conditions that directly and indirectly affect the well-being or sustainability of a community". Furthermore, Füssel and Klein (2006) define vulnerability as an integrated measure of the expected magnitude of adverse effects to a system caused by a given level of particular external stressors. Vulnerability measures the country's exposure, sensitivity, and ability to cope with the negative effects of climate change by considering vulnerability in six life-supporting sectors: food, water, ecosystem service, health, human habitat and infrastructure(IPCC, 2014a).

Vulnerability to a climatic stressor is essentially a composite of exposure, a degree of sensitivity to the stressor, and the facility of the system to handle the stressor and vulnerability analysis are conducted for various reasons ranging from identifying worldwide mitigation targets to selecting local adaptation strategies (Fussel and Klein 2006 ; Smit and Wandel 2006). Vulnerability is mostly considered to be a local phenomenon that is investigated by local-scale studies in which the specific societal and physical situation can be taken into account much better than in a global scale study (Doll, 2009).

Consistent throughout the literature the notion that the vulnerability of any system (at any scale) is reflective of (or a function of) the exposure and sensitivity of that system to hazardous conditions and the ability or capacity or resilience of the system to cope, adapt or recover from the effects of those conditions (Smit Barry and Johanna Wandel., 2006). The three components can be expanded on as follows:

I. Exposure:

Exposure concerns the nature and intensity of environmental stress experienced by a system, encompassing both long-term changes in climatic conditions and the variability represented by extreme events (O'Brien, *et al.*, 2004; Adger, 2006). Heat exposure can be measured directly using surface temperature or indirectly quantified by remotely sensed satellite imagery that provides multiple affordable and accurate metrics of heat exposure (Uejio *et al.*, 2011). The most common indicator for analyzing exposure is land surface temperature (LST) (Reid, 2009; Huang, *et al.*, 2011; Feyissa, 2019).

II. Sensitivity:

According to McCarty, *et al.*, (2001), sensitivity is the degree to which a population can be affected by climate change, whether directly or indirectly, and is related to the intrinsic characteristics of the impacted system. The study worked with the indirect effects of climate resulting from the possible damage that can occur, more specifically on specific population groups (Menezes *et al.*, 2018), was used to associate existing socio environmental characteristics of municipalities with climate change scenarios in order to identify those that might be most affected by climate change.

III. Adaptive capacity:

Adaptive capacity is similar to or closely related to a host of other commonly used concepts, including adaptability, coping ability, management capacity, stability, robustness, flexibility, and resilience (Adger, and Kelly, 1999; Brooks, 2003; Füssel, and Klein 2006). Local adaptive capacity is reflective of broader conditions (Yohe and Tol, 2002). Adaptive capacity is context-specific and varies from country to country, from community to community, among social groups and individuals, and over time (Smit Barry and JohannaWandel., 2006).

The IPCC definition suggests that the most vulnerable individuals, groups, classes, and regions or places are those that (1) experience the most exposure to perturbations or stresses, (2) are the most sensitive to perturbations or stresses (i.e., most likely to suffer from exposure), and (3) have the weakest capacity to respond and ability to recover (Schiller, *et al.*, 2001).

2.1.4 Urban Heat Vulnerability Concept

Urban is defined as an environment where the density of population and economic activities are more than in other places with higher rate of destruction of natural resources (Toy, *et al*., 2007). With higher rate of economic development, urbanization coupled with population growth continue in developing countries, anthropogenic heat increases as well (Ichinose, and Bai, 2000). As a result of the constraints by urbanization and global climate change Ndetto and Matzarakis, (2013) suggested that better understanding of urban microclimate and bioclimatic condition of any city requires urgent attention today.

Urban heat vulnerability arise through characteristics of cities that include replacement of vegetation with impervious, heat-absorbing surfaces such as concrete and bitumen, installation of tall buildings that reduce airflow and ventilation, and generation of heat and greenhouse gases through human activities (Cisneros *et al*., 2018). Similarly, Odindi *et al.*,(2015) stated that the conversion of urban greenery to impervious landscapes has been identified as a key factor influencing the distinctive urban heat and associated consequences. highest green area has great a role both ecologically and in urban cool island (Ilestari, *et al*., 2018). Furthermore, the characteristics of individuals and communities, access to safe drinking water impact the ability of human populations to respond to and cope with these exposures (Conlon *et al*., 2020).

Research on urban heat vulnerability as impact conceives vulnerability as an outcome determined by exposure to hazards such as temperature, sensitivity of urban populations and the resulting or potential impacts (Romero-lankao *et al*.,2012). Furthermore, Loughnan, *et al.,(*2013) was also interpreted extreme urban heat vulnerability as a function of both the sensitivity of a population to heat and the adaptive capacity decision for higher temperature change.

In response to urban heat vulnerability, researchers are tasked with developing preparedness, response, and mitigation plans and policies that protect those who are experiencing and who will experience most of the health burden related to extreme temperature (Conlon *et al*., 2020). Recent advances in geospatial research methods and analysis tools allow for spatially explicit characterization of extreme heat vulnerability in urban environments (Wilhelmi *et al., 2004)*. Although the selection of the specific indicators to be examined is subjective, they can be used to provide an estimate of a population's sensitivity and adaptive capacity to urban heat vulnerability (Luis *et al*., 2016).

2.1.5 Causes of Urban Heat Vulnerability

Understanding drivers of heat vulnerability are fundamentally very important for analyzing vulnerability level, in terms of environmental justice and ultimately the different societal impacts of extreme heat (Romero-lankao *et al.*, 2012). In large sprawling cities, with a highly variable socio-economic fabric, uneven infrastructure and uneven accessibility is continuing as a challenge because of urban growth (Luis *et al.*, 2016). As well as, urban environments are especially vulnerable to heat due to increase in land surface temperature (Rasul and Ibrahim, 2017). impervious surface like concrete and building materials that retain heat, population density levels and nonexistence of green areas have been identified as main drivers of urban heat vulnerability (Conlon *et al*., 2020).

Increased population in the city also promotes warming from anthropogenic heat release. Hence, those that live in inner city areas are subsequently exposed to the UHI effect and can be under increased heat risk (Lindley *et al.*, 2011). High population density has been shown to correlate with areas of higher temperatures, and is to be expected given that high population density is often within inner city areas that are also impacted by the UHI (Hajat and Kosatky, 2010).

Many studies on urban thermal environment indicate that settlement and impervious surfaces are highly expanded at the expense of green areas, and open spaces (Mutiibwa, *et al.,*2014). In the same way, Odindi *et al.,*(2015) indicated that the conversion of urban greenery to impervious landscapes has been identified as a key factor influencing the distinctive urban heat and associated consequences. Heat stress becomes aggravated due to reduced levels of evapotranspiration and occurs in high-density and industrial, thus affecting public health (Baklanov *et al.*, 2016).

In high-income and some middle-income nations, virtually all the urban population is served by drinking quality water piped to the home 24 hours a day (Satterthwaite, *et al*., 2014). However, as Medhin, *et al* (2017) most water supply services of cities in Ethiopia are unreliable, particularly in providing an adequate amount. And also stated, almost all cities in the country have frequently experienced service failures and a lack of an adequate amount of drinking water supply. Although, lack of basic sanitation, limited access to safe drinking water supply has impacts on personal hygiene practice and adequate hydration in the face of high ambient heat, leaving them vulnerable to illness (FDRE Ministry of Health, 2015)**.**

2.1.6 Impacts of Urban Heat Vulnerability

Scientists have reached a consensus that the global annual average temperature is likely to be 2 °C above pre-industrial levels by 2050 and a 2 °C warmer world will experience more intense rainfall that lead to frequent floods, more intense droughts, heat waves, and other extreme weather events (IPCC, 2014b; Abbasnia, *et al.,* 2016). Temporal variations in climate are harmful to the interaction between natural systems and health. Those variations lengthen the transmission season for vector-borne diseases in some areas and can be a significant threat to human health (Ludena, *et al*., 2015). For example, an increase in mean temperatures has been observed to increase the geographic distribution of mosquitoes and shorten the incubation period of the pathogen within the vector, which is likely to increase the risk of vector-borne diseases such as malaria and Dengue fever (Füssel and Klein, 2006; Strand *et al.*, 2010). Recent evidence reveals re-emergence of Dengue fever in eastern parts of Ethiopia; Dengue fever is among climate sensitive diseases that are believed to intensify with the rise of temperature(FDRE Ministry of Health, 2015).

Climate change is an emerging threat to global public health. Studies of the relationship between heat and health have noted that the measure of daily mean temperature is a better predictor of health impact than maximum temperature alone (Hajat and Kosatky, 2010). Given concerns over increasing temperatures and the serious health effects that have already been demonstrated in recent heatwaves, several jurisdictions have started to develop spatial vulnerability assessments for heat (Rinner *et al*., 2010).

The population’s heat health threat has been investigated in several cities. The studies showed that the high rate of heat vulnerability has effect on the health of people thereby leading to heat related diseases such as fatigue, sunstroke, muscle cramps, heat stroke and heat exhaustion (Alaigba, *et al.*, 2017). In addition a combination of factors diminishes the older person’s ability to maintain a normal body temperature and adequate hydration in the face of high ambient heat, leaving them vulnerable to illness and death (Hajat and Kosatky, 2010). The extent of the impact depends on the magnitude of climatic changes affecting a particular system (exposure), the characteristics of the system (sensitivity) and the ability of people and ecosystems to deal with the resulting effects adaptive capacities of the system (IPCC, 2014b).

2.1.7 UHV Mitigation through Increased Urban Vegetation and Water Supply Coverage

Climate change is predicted to increase the intensity and negative impacts of urban heat events, warning the need to develop preparedness and adaptation strategies that reduce societal vulnerability to extreme heat (Wilhelmi and Hayden, 2010). Climate change effect is considered together with other environmental and social stresses, and adaptations are mostly integrated or mainstreamed for practical implementation of adaptations at the community scale (Smit and Johanna, 2006). Siti Zakiah, (2004) anticipated to deliver a basis for understanding and create awareness on the importance of comfortable outdoor living environment for comfortable human life and living with serious attention on issues of urban heat and the effective use of natural elements such as plants and water as heat ameliorator for Kuala Lumpur City.

A number of studies on vulnerability to climate change have recognized the necessity of local scale exploration of vulnerability to identify adaptation measures (Ludena, *et al*., 2015). The literature on benefits of green space for mitigation of urban heat vulnerability is extensive. Such as, in the Netherlands literature started to increase after the release of the '*Vitamin G'* study in 2006, but there was still little focus on the profitable motivation of green and blue infrastructure (Maas, 2008). Urban vegetation can reduce temperatures in urban areas by providing shade, evaporative cooling through evapotranspiration, and reduced heat storage capacity compared to bricks and other building material (Rasul and Ibrahim, 2017). Reports indicate that, increased area of urban green spaces in Shanghai was deemed to be an important factor in reducing the health impact of heat waves from 1998 to 2003 (Tan *et al*., 2007).

Ethiopian Demography Health Survey (2014), define improved drinking water sources as water from a source that is more likely to provide "safe" water (i.e., these are household connection (piped into a dwelling, compound, outside compound or bottled water) and as overall, there is a growing trend of access to improved drinking water supply coverage; For instance, Harari, Dire Dawa and Addis Ababa had significantly higher improved water supply coverage compared to the national average. Existing water supply system of the Dire Dawa City comes from ground water sources (Abate, 2010). According to integrated development plan (IDP, 2006), study urban water supply coverage in 2006 was estimated to be about 72 percent. However, in 2020 the percentage of access to water becomes 76%. Yet, a percentage of access to safe water per kebele is also being like chalk and cheese.

2.1.8 Indicator Selection Process and Selection Criteria

Indicator selection needs to consider the heterogeneity of the region, the objectivity and the availability of data, and the actual situations in deferent countries (Guo et al., 2019). Therefore, the selection of indicators has not yet formed a unified standard, but there is a great similarity in the selection of indicators. Most social vulnerability indices adopt one of three commonly used structural designs: (a) deductive; (b) hierarchical; or (c) inductive (Tate, 2012). None of these architectures is inherently better or worse than another, but they may vary in robustness and performance depending on the index configuration(Tate, 2012).

The deductive approach is theory-driven and typically synthesizes a relatively small set of indicators (Vincent, 2007; Hinkel, 2011). Hierarchical designs commonly synthesize roughly 10 to 20 indicators arranged into sub-indices representing major themes or core domains, enabling meaningful positioning of each indicator to represent distinct components of the system of analysis (Maggino and Zumbo, 2012; Tate, 2012). The inductive approach to composite index development is primarily data-driven and tends to begin with a large set of candidate indicators (more than 20 variables), which is reduced to a smaller set prior to aggregation (Vincent, 2007; Tate, 2012).

Many studies are based on local situations and the availability of data using local characteristics, such as tribes and caste conditions (Azhar, 2017). Therefore, this study adopted deductive approach. A review of Sabelli, (2011) on vulnerability case studies carried out across the globe at different scales using the indictors-based approach demonstrated that this kind of evaluation is useful in countries with significantly lack of data, technical and financial resources to undertake more complex modeling simulations mainly at small scales, showing the practical application of this approach.

2.1.9 Urban Heat Vulnerability Mapping

Mapping and visualizing intra-urban heat vulnerability offers opportunities for presenting information to support decision-making; for example the visualization of the spatial variation of heat vulnerability has the potential to enable local governments towards identify hot spots of heat vulnerable location to allocate resources and increase assistance to people in areas of greatest need (Wolf *et al.,* 2015). From the research scale, foreign studies often use census tract or block group (Reid, *et al.,* 2009) and neighborhood (Jenerette, 2016) as the basic research units, and domestic studies are usually based on sub cities (Feyissa, 2019).

Analyzing urban heat vulnerability for communities offers opportunities for presenting information to support decision-making (Sun, *et al.*, 2018). Spatial analysis is common in vulnerability research, often result in vulnerability index maps, where indices are constructed as cumulative composites of multiple factors (Luis *et al*., 2016). Several studies have used different methods to quantify and map the urban heat vulnerability, which inevitably varies from location to location. However, the choice of method was depend on objectives, data availability, funding, and the time frame for the assessment (Sherbinin, 2014). The additive approach is favorable when it is assumed that each vulnerability factor adds a different element of vulnerability to the overall composite index (Abson, *et al.*, 2012). Historically, a common approach has been used to aggregate the individual indicators into an overall score, referred to as an index, For example, the Human Development Index (HDI) is a composite of indicators, transformed into standard scores and differentially weighted (UNDP, 1999). Alternative strategies include expert judgment(Brooks *et al.*, 2005; Ozceylan and Coskun, 2012) or multivariate statistical techniques such as principal component and factor or cluster analysis (Cutter *et al.*, 2003).

2.2. Empirical Review

Remote sensing applications play a key role in visualization, summarizing and obtaining the information on intra-urban heat vulnerability. Mainly the satellite application of thermal remote sensing is always important to monitor the land surface temperature (Feyissa, 2019). Satellite remote sensing has provided major advances in understanding the climate system and its changes, by quantifying processes and spatio-temporal states of the atmosphere and land (Yang, *et al.*, 2013). With the development of remote sensing technology, satellite imagery based estimation of land surface temperature that derived from thermal infrared imagery becomes more effective in interpreting UHI effect because, it provides a relatively rapid and low-cost data information on landscape scale (Juntao Tan and Hung, 2018). In the absence of a dense network of land-based meteorological stations, the spatiotemporal distribution of land surface temperature from thermal remote sensing imagery can be used as information to support UHI management and potentially countermeasures (Feizizadeh, et al., 2013).

Increasing urban temperature due to urbanization has been studied in Cities around the world such as Atlanta (Weng, 2017), Dhaka (Ahmed, 2015) and Ho Chi Minh City (Doan and Kusaka, 2016). To comprehend the influence of LULC change on the thermal environment of the urban areas, Ding and Shi, (2013) utilized the Landsat images of Beijing and related LULC with LST. Kuang, *et al.*, (2015) utilized in situ observations and concluded that LST differences were found for different LULC classes. They also pointed out that impervious surfaces are warmer than green areas.

According to (Tong and XuCheng , 2018), UHIs may adversely affect physical and mental health, as well as promote cardiovascular disease and chronic kidney disease. Research shows that homeless populations are vulnerable during extreme heat events. In the 2006 Phoenix, Arizona heat wave, there were 13 heat stroke deaths, 11 of which were homeless people (Kovats and Osborn, 2016). A study in Maricopa County, Arizona found that 66% of heat-related mortality occurred in outdoor workers. The majority of these outdoor deaths were in people younger than 65 years (Yip *et al.*, 2008). Presently, most cities in the world are greening their cities. For example, the city of Rotterdam in the Netherlands implements the greening concept in city planning and development (Bolund, 2015).

2.3. Conceptual Framework

The theoretical framework presented the review of literature on different theories related to spatial quantification and mapping of heat vulnerability hotspots and integration of these all together for enhanced resilience planning. Especially the role of identifying urban heat vulnerability hotspots zones are used to mitigate urban heat vulnerability effects. Also different methods of measuring vulnerability, classifying heat vulnerability to identify urban heat vulnerability hotspot zones by using geospatial technologies tools can highlight contributory features that can assist the government and its agencies to implement corrective measures at such spots and reduce the effect of urban heat vulnerability on the environments. To quantify urban heat vulnerability levels as “high” vulnerable zones, the original heat vulnerability indicator were normalized and aggregated to HVI then after, categorized by five levels from “very low” to “very high” with geometrical interval classification scheme (ESRI, 2016 ; Tomlinson et al., 2011b ; Guo et al., 2019). Summary of the studies about heat vulnerability are presented in table 2.1 below.

Table: 2. 1 Summary of the previous studies about heat vulnerability assessments

	Author (Time, Location)	**Variables (Numbers)**	**Methods**
1	Tomlinson et al. (2011, Birmingham)	land surface temperature, elderly, ill, density of households, flat (5)	normalization, equal weight
2	Chow, *et al.* (2012, Phoenix)	mean summer maximum/minimum temperature, mean normalized difference vegetation index, elderly, income, foreign-born noncitizens, immigrants (7)	normalization, equal weight
3	Aubrecht, *et al.* (2013, U.S. National Capital Region)	heat wave day count, elderly, living alone, poverty, poor English skills, education, vegetation (7)	normalization, equal weight
4	Wolf and Mcgregor, (2013, London)	land surface temperature, households in rented tenure, flat, population density, households without central heating, elderly, self-report bad health status, receiving social benefit, single pensioner households, ethnicity (10)	Principal component analysis, spatial clustering analysis
5	Dong, *et al.* (2014, Beijing)	heat wave days, extremely high temperature days, population density, elderly ratio, income level, land use/cover (6)	normalization, equal weight
6	Vescovi, *et al.* (2005, Southern Quebec)	hot days, consecutive hot days with Tmax > 30°C and Tmin > 22°C, elderly, poverty, isolation, education (6)	normalization, equal weight
7	Harlan, *et al.*, (2013, Maricopa county)	ethnicity, immigrant, poverty, education, central AC, elderly, elderly and living alone, living alone, vegetated area (mean), unvegetated area (SD), surface temperature (11)	Principal component analysis, local indicators of spatial association (HVI/aggregated)

CHAPTER III: MATERIALS AND METHODS

3.1. Description of the Study Area

Dire Dawa Administration, in eastern Ethiopia, was established in 1902 as a relatively lowland with elevation of 1200m above sea level and Dire Dawa Administration is a chartered as Administration that consists of 9 urban and 38 rural kebeles (IDP, 2006). Dire Dawa City is located between latitude and longitude of 9°35'00"N to 9°40'00"N and 41°44'00"E to 41°53'30"E respectively. Dire Dawa City, administration share boundaries with East Hararge Administrative zone of Oromia Regional State borders it in the south and southeast and Shinele zone of Somalia Regional State in the north, east and west (UN-Habitat, 2015). The map that describes the location of the study area is shown in figure 3.1 as follows.

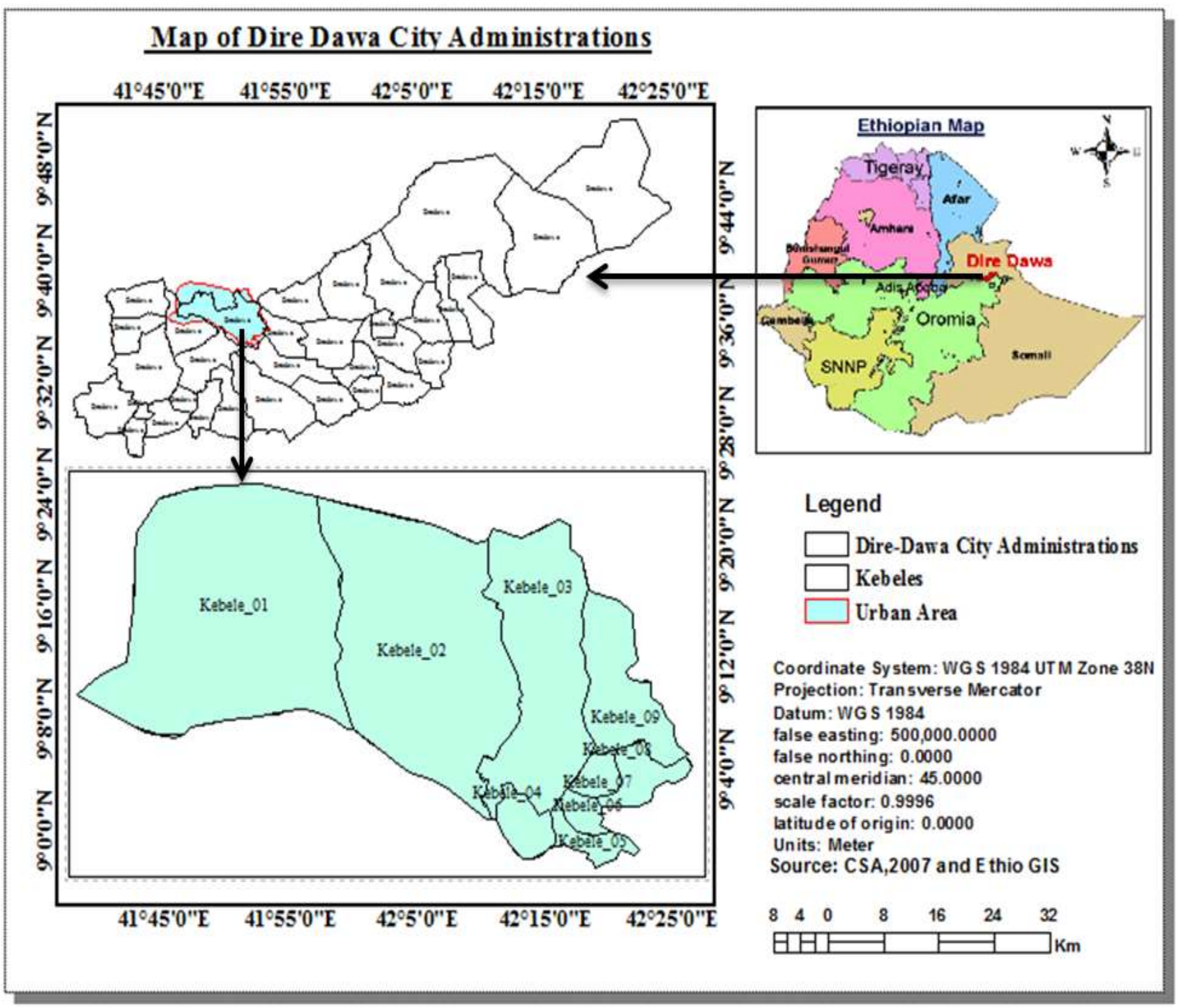

Figure: 3. 1 Location of the study area

Dire Dawa city is accessible by airplane, train and cars, and is about 515 km road distance to the east of Addis Ababa and 311km to the west of Djibouti port. In the south Dire Dawa city is connected to Addis Ababa and Harar, in the east to Djibouti and west to Hurso by a paved road. This makes the city close proximity to the middle east of the import and export destination. In all, the Administration has a total land size of 1,300 square kilometer or 130,000 hectares, of which 94.65% accounts for the size of the rural area, while the remaining 5.34% covers the land size of the urban areas found in the Administration (D.D.E.P.A, 2019).

Although Dire Dawa city is primarily known by its trading centers, it also has its own numerous and precious cultures and heritages of glorious attractions. Out of this, Lagaoda Ancient Cave, Africans Graveyard built after the Second World War, in memory of members of British Air Force and African soldiers who sacrificed their lives for the freedom of Ethiopia against the Italian invasion during World War II, Ancient Railway Station (Kezira) and (Qafira) open market are among the enormous potentials that the City Administration has as real glories or tourism attractions and related activities.

Demographic Characteristics: According to Central statistical Agency, 1994 Census report for the year 1995 the population number was about 177,251. In the next Census of 2007, the population of the city was increased to 233,224. In addition, According to Dire Dawa Administration statistical Bureau (D.D.A.S.B) (2013), Report on the population projections for the years between 2007 and 2037, the population of the Dire Dawa City is expected to be about more than 323 thousands in 2020.

Climate: Dire Dawa City has a hot semi-arid climate (koppen climate classification Bsh). The mean annual temperature of the provisional administration is about 26.61°C with average maximum temperature of 32.78°C, while its average minimum temperature is about 19.12°C. For the last two decades, the average annual temperature of the City was increasing by 0.6°C per decade, especially in the cool months(D.D.E.P.A, 2020). Monthly average temperature of the city is shown in Appendix 1.

Dire Dawa City has two rain seasons; that is, a small rain season from March to April, and a big rain season that extends from August to September. The administration has a warm and dry climate with a low level of precipitation. The administration has an average annual rainfall of 604 millimeters (D.D.E.P.A, 2019).

3.2. Data Sources

Primary and ancillary data used in this study were collected from different sources. The primary data source involves a direct collection of information on the field using handheld GPS and observations. The secondary data source involves sourcing information from existing records i.e., from three meteorological stations within and nearby the study area, Central statically agency (Dire Dawa City branch) and an aerial photo of the study area from the land administration of the City.

3.2.1. Remote Sensing Data Acquisition

Due to historical archival availability, Landsat images of 1995 and 2020 were downloaded from the website of earth explorer; usgs.gov, United States Geological survey (USGS). Both Landsat 5 TM (1995) and Landsat 8 OLI/TIRS (2020) cloud free image of the study area with the path of 166 and row 053 images with similar seasonal properties have been chosen. In addition, within this season, the study area has clear sky with no cloud. The Acquired Landsat images were used to extract LST, NDVI and LULC. The January 16th and February 6th image was also selected for the reason that it falls within the early part of the warm season when green vegetation is likely to be in abundance. The presence of green vegetation is paramount to a study concerned with the association between LST and NDVI; since NDVI is an indicator of green vegetation and is therefore impacted by seasonal changes (Yuan and Bauer., 2007). Thus, a study which attempts to establish an understanding of how natural solutions might help alleviate UHV through the analysis of intra-urban relationships between land surface temperature and vegetation density. Specification of Landsat images used in the study was shown in the following table 3.1.

Table: 3.1 Specification of Landsat Images used in the study

Date of Acquisition	Sensor	Path	Row	Multispectral Band	Thermal Band
16/01/1995	TM	166	53	1 to 5 and 7	6
06/02/2020	OLI/TIRS	166	53	1 to 7 and 9	10 and 11

[Source: Landsat-5 and Landsat-8 Meta data, obtained from USGS, 2020]

Primary and ancillary data used in the study were collected from different sources as shown below in table 3.2.

Table: 3.2 List of data, materials, software packages and equipment used for the study

A.	Used Data	Purpose	Sources
1	Landsat 5, and 8 image (1995 and 2020)	For extractions of LU/LC, LST and NDVI.	http://earthexplorer.usgs.gov
2	Aerial photo and Google Earth	To get updated information this may not exist on map.	Land administration of the City and Earth explorer
3	Geographic coordinates of land use locations	For accuracy assessment	Field Survey
4	Meteorological data 1995 to 2020 (monthly)	For land surface temperature validation	Meteorological stations.
5	Demographic data	To construct heat vulnerability index	Central Statically Agency (Dire Dawa City Branch)
6	Accessibility of clean water	To construct heat vulnerability index	Dire Dawa City water supply and sewerage authority.

B. Software Used			
No.	**Name**	**Version**	**Purpose**
1	ArcGIS	10.8	For extractions of LU/LC, LST and NDVI. For integration and management of spatial information and statistical analyses.
2	ERDAS IMAGINE	2014	To process Landsat imagery including, preprocessing and for LU/LC classification.
3	Microsoft word and Microsoft excel	2020	For the thesis report documentation and To analyze data's in spreadsheets (e.g. bar graph)
4	Mendeley Desktop	1.14	To insert citation and references used for the study.
C. Equipment Used			
1	Hand held GPS	Garmin64	For classification accuracy assessment

3.3. Methods of Data Analysis

In this study, the method used to achieve the objectives of the research was begun with the acquisition of Landsat imagery for the years 1995 and 2020 from the website of earth explorer (USGS). Then after, by using Geographic Information System (GIS) and ERDAS Imagine 2014 software both Landsat5 TM and Landsat8 OLI /TIRS were preprocessed to drive LULC, LST, and NDVI. LULC patterns were mapped by using supervised classification technique with a maximum likelihood algorithm. Subsequently, LST was derived from thermal bands of Landsat5 TM using band 6 and Landsat8 OLI /TIRS using band 10 and band 11. The image was processed in Arc Map using raster calculator. As well as, vegetation density was derived by using the normalized difference vegetation index algorithm. Moreover, zonal statistics as table and regression analysis tools were used to examine the correlation between vegetation density (NDVI) and LST based on LULC. Methodological frame work that adopted for the study is shown in figure 3.2 as follows.

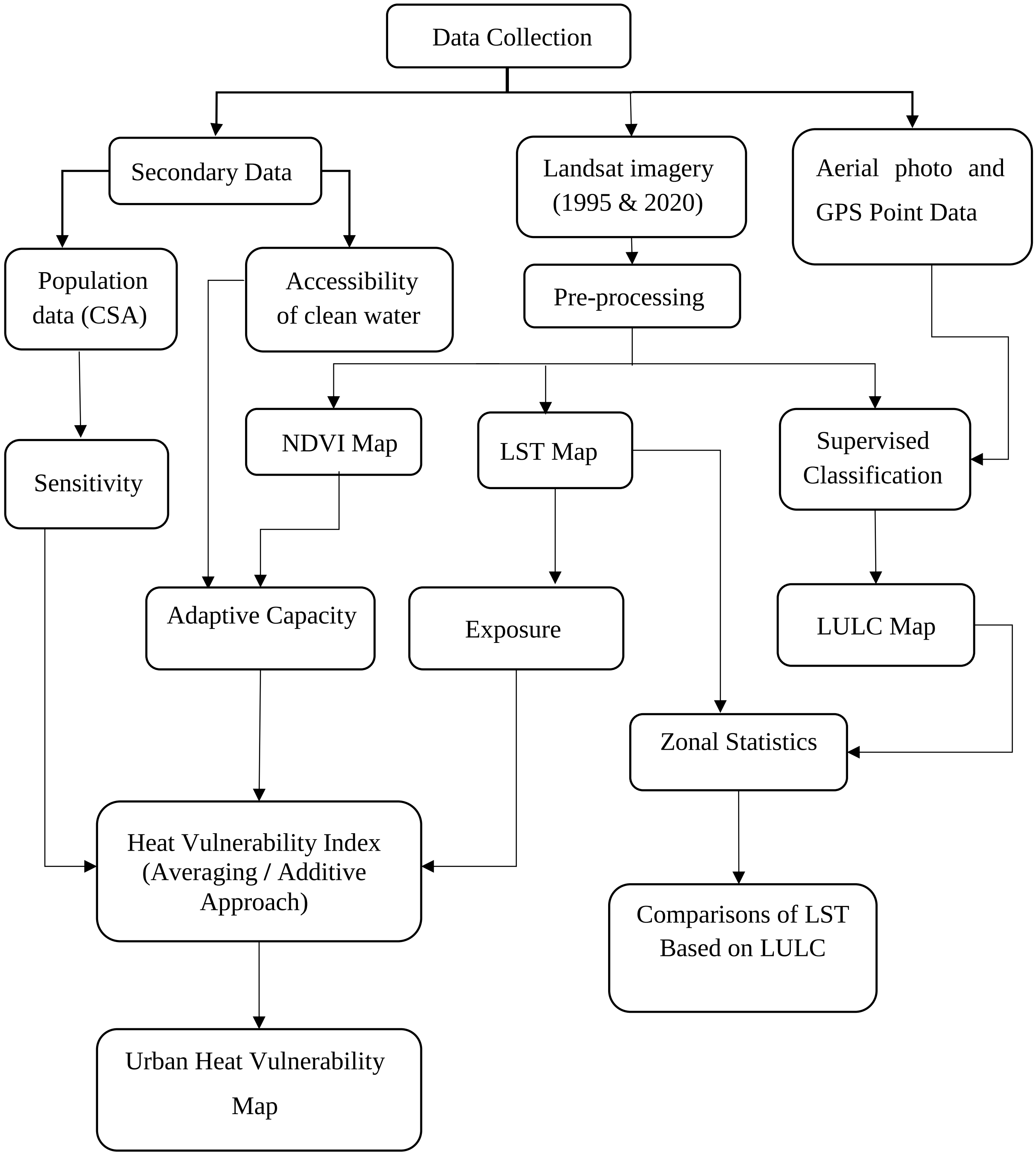

Figure: 3.2 Flowchart of methodology adopted for the study

3.3.1 Digital Image Preprocessing

Before processing the data, image pre-processing activities were done. Preprocessing includes importing, layer stacking, and sub setting of the image based on the boundary of Dire Dawa City Administration, geometric correction, radiometric correction and other image enhancement techniques. Radiometric correction is a removal of atmospheric noise to make more representatives of the ground truth conditions based on the sensors and the main purpose of image enhancement is to advance the interpretability of information in images for viewers, or to provide better input for other automated digital image processing techniques. These all previously mentioned activities were done to improve visual interpretability of an image by increasing apparent distinction between the features in the scene. In addition, the image was also geo-referenced using boundary of the Dire Dawa City Administration. During geo-referencing and re-projecting process WGS(1984) datum and UTM Zone 38N coordinate system was followed for raster and vector data in the study to maintain uniformity.

3.3.2 Image Classification (LU/LC Extraction)

In remote sensing, Image classification is the task of extracting information classes from a multiband raster image or extracting information based on the reflectance of the object and it serves specific aims; which is converting image data into thematic data. Image classification uses the reflectance statistics for individual pixels; Digital image classification techniques assemble pixels to represent LU/LC classes (Tafesse, 2017). In this research land-use/ land-cover pattern was mapped by using supervised classification with the maximum likelihood classification algorithm in ERDAS Imagine 2014 software.

Maximum likelihood classification algorithm is one of the most known methods of classification in remote sensing, in which a pixel with the maximum likelihood classification is classified into the matching classes (Asubonteng, 2007; Pansi and Yang, 2015). It is a statistical decision measure to assist in the classification of overlapping signatures; pixels are assigned to the class of the highest probability and considered as more accurate than parallelepiped classification (Coppin *and Bauer*., 1996). The supervised classification image of each year involves pixel categorizations activity was done by taking training site, areas as sample training area for class of LU/LC classification. After the training area assigned for each classes, the classification activity was performed (Mohan, M. and Pathan, 2011).

After all classification activity has been completed, the accuracy of the classification was checked. The classification accuracy requires the collection of some original data or a prior knowledge about some parts of the landscape, which can then be compared with classified map (Tafesse, 2017). The field survey data's were used for evaluation of the LU/LC classification accuracy. The Accuracy was analyzed by using a contingency matrix which is a square matrix that comprises the number of pixel classification (error matrix or confusion matrix). The mathematical formula that used to calculate overall accuracy is shown below:

Overall accuracy = (Total diagonal / Total column)*100………………………… Eq. (3.1)

Post classification is among the most widely used approach for change detection purpose (Chen, 2000 ; Bekele, 2019). The first task was to develop a table indicating the area coverage in square kilometers and the percentage change for each year 1995 and 2020 measured against each LU/LC classes. Therefore, to calculate LU/LC in percentage equation (eq 3. 2) were used (Lambin, *et al.*,2001).

$$\text{Percentage Change} = \frac{\text{Observed Change}}{\text{Sum of Area}} * 100 \qquad \text{Eq. (3.2)}$$

According to Dire Dawa Administrative Agricultural Development Office (2018), the land use/land cover types have been grouped into four major classes. In line with the major class identified by the office, these studies adopt four major classes; table: 3.3. Shows description land use/land-cover classes of the study area.

Table: 3.3 Description of Land-use/land-cover classes for the study area.

No	Type of LULC	Description
1	Built up Area	classified into different categories like residential, recreational, industrial transport, communication, utilities etc.
2	Shrub land	Area which is covered with dense shrub, open shrub land (*Prosopis Juliflora* plantation) and Eucalyptus plantation
3	Sparse vegetation	Lands with a mosaic of forests, woody plants, trees, natural vegetation, gardens, parks and vegetated lands, agricultural lands, and crop fields
4	Barren land	Open spaces, bare lands and soils, sands, dunes and excavation sites

(**Source**: Dire Dawa Administrative Agricultural Development Office.)

Steps or processes that followed to classify land-use/land-cover from a Landsat image are presented below in figure 3.3.

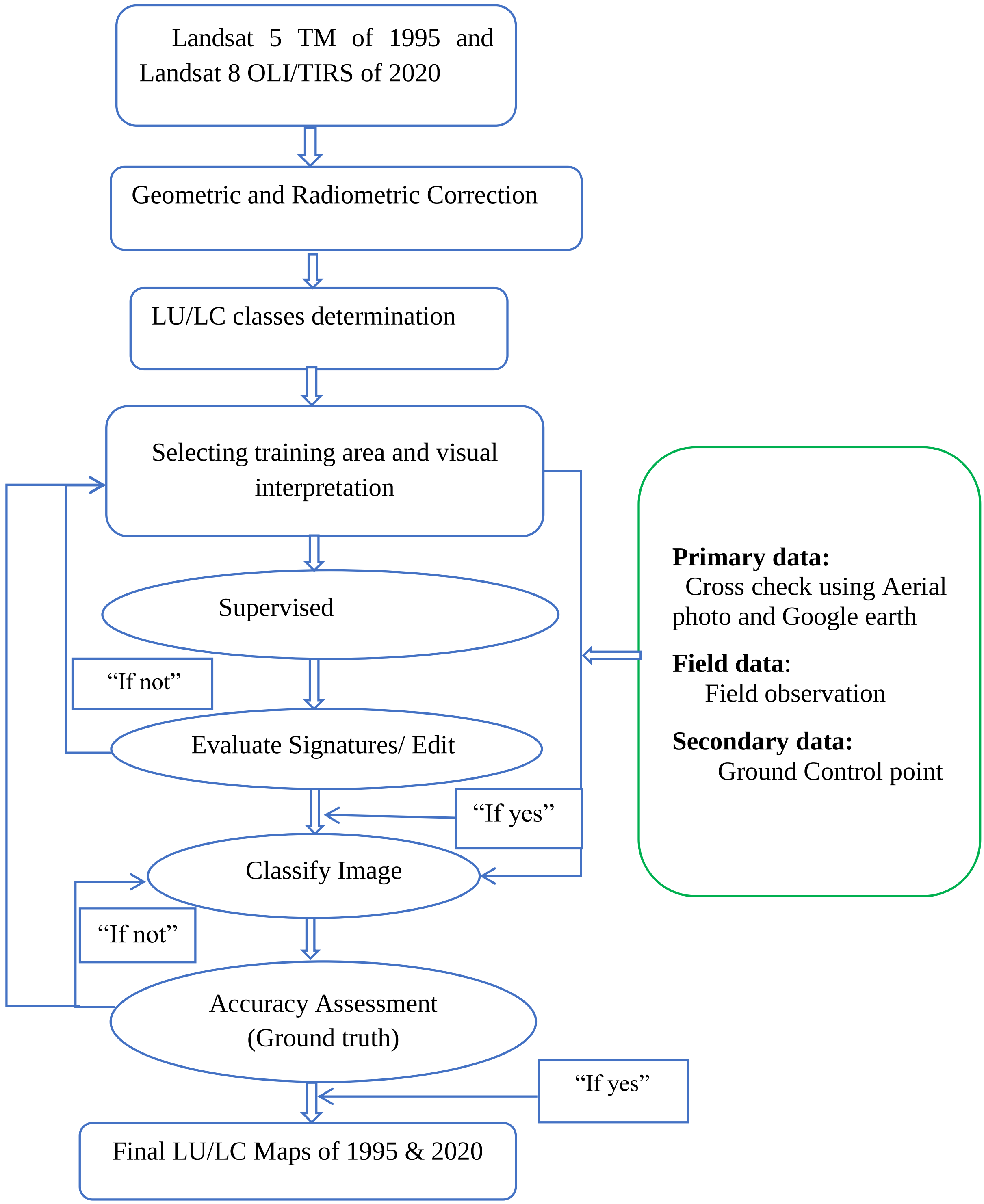

Figure: 3.3 Steps followed to classify land-use/land-cover from a Landsat image.

3.3.3 Normalized Difference Vegetation Index (NDVI) Extraction

The Normalized Difference Vegetation Index (NDVI) is a standard algorithm designed to estimate the amount of the above-ground green vegetation cover from measurements of red and near-infrared reflectance, which help in delineating vegetation and non-vegetation areas (Panahi, 2013). The value of NDVI is between -1 and 1(Cisneros *et al.,* 2018). Landsat5 TM sensor reflects both near IR in band 4 and visible red (R) in band 3, But in case of Landsat 8 NIR is band 5 and the red band is a band 4 (Weng, 2017). Equation 3.3 was used to calculate NDVI from Landsat 5 TM sensor of 1995 and Landsat 8 OLI/TIRS of 2020.

$$\mathrm{NDVI} = \frac{\mathrm{NIR} - \mathrm{R}}{\mathrm{NIR} + \mathrm{R}} \quad \text{Eq. (3.3)}$$

Where, NDVI: Normalized Difference Vegetation Index, NIR: is the near infrared band, R: is the red band.

3.3.4 Derivation of Land Surface Temperature

The land surface temperature data can be derived from the TIR band of the Landsat images. It should be mentioned that in addition to the method developed by (Artis and Carnahan, 1982), a few other methods have been developed for deriving LST from Landsat imagery. These include the mono-window algorithm (Qin *et al.*, 2001) and the Radiative Transfer Equation (Sobrino *et al.*,2004). However, these other methods require additional input parameters (such as atmospheric water vapor content and near-surface air temperature) from ground-based observations captured simultaneously with the satellite passes, which are usually unavailable (Ma *et al.*, 2010). For this reason, the method developed by (Artis and Carnahan, 1982), which necessitates no additional input parameters, was chosen for this research.

Radiometric Correction: Radiometric correction needs converting a remote sensing digital number to spectral radiance values. Image processing procedures that are used to correct errors, converting digital number (DN) values to radiance and then reflectance was categorized as a radiometric correction (Prata, 1999; Farina, 2012). To perform the conversion of digital number to spectral radiance equation (3.4) was used.

$$L\lambda = Lmin + (Lmax - Lmin) * DN/255 \quad \text{Eq. (3.4)}$$

Where,

$L\lambda$=spectral radiance,

Lmin=spectral radiance of DN value 1,

Lmax=spectral radiance of DN value of 255,

DN=Digital Number

Conversion at Sensor Spectral Radiance: In radiometric calibration, pixel values which were represented by Q in remote sensing raw data and unprocessed image data, were transformed into absolute radiance values (Tafesse, 2017). Equation (3.5) was used to perform the conversion at sensor spectral radiance or satellite data scaled into 8 bits.

$$\mathbf{L\lambda} = (Lmax\lambda - Lmin\lambda) / (Qcalmax - Qcalmin) * (Qcal - Qcalmin) + Lmin\lambda \text{............. Eq. (3.5)}$$

Where;

$L\lambda$: Spectral radiance at sensors aperture or the calculated radiance associated to the ground area enclosed in the pixel and referred to the λ wavelength range of specific band.

Lmaxλ=spectral at Sensor Radiance that is scaled to Qcalmax

Lminλ=Spectral at Sensor Radiance that is scaled to Qcalmin

Qcalmax=Maximum Quantized Calibrated Pixel values corresponding to Lmaxλ

Qcalmin=Minimum Quantized Calibrated Pixel values corresponding to Lminλ

Qcal=Quantized Calibration Pixel value (DN).

Conversion of Radiance into Brightness Temperature: Thermal infrared data can be converted from atmosphere reflectance ($L\lambda$) to effective sensor Brightness Temperature (BT) using thermal constants provided in the Meta data file (Zhao *et al.,* 2014). Remote sensing data (Landsat imagery) thermal band that is band 6 on thematic mapper and band10 and band11of OLI/TIRS were used from a sensor spectral radiance to effective at sensor brightness temperature. Brightness temperature is the radiance travelling upward from the top of earth atmosphere. To covert $L\lambda$ (spectral radiance) to BT (brightness temperature) equation 3.6 was used (Landsat Project Science Office, 2001).

$$BT = \frac{K2}{\ln(\frac{K1}{L\lambda + 1})} - 273.15 \text{...Eq. (3.6)}$$

Where;

TB= effective at satellite brightness temperature (unit in Kelvin)

K2= calibration constant,

Ln= natural logarithm

K1= calibration constant,

$L\lambda$: spectral radiance at sensors aperture.

Generally, to calculate LST for the sensor subtracting 273.15 from the existed result that is performed from effective at satellite temperature formula in Kelvin. Table 3.4 and table 3.5 shows the calibration constant used during performing the formula for brightness temperature.

Table: 3. 4 Thermal Band Calibration Constant of Landsat 5 TM for 1995

Satellite	Sensors	Categories	Band 6
		K1	607.76
		K2	1260.56
		Radiance_maximum_band	15.303
		Radiance_minimum_band	1.238
		Quantize_cal_max	255
		Quantize_cal_min	1
		Map_projection	"UTM"
		Ellipsoid	"WGS84"
		Utm_zone	38
		Grid_cell_size_reflective	30

[Source: Landsat-5 Metadata, Obtained from USGS, 1995]

Table: 3. 5 Thermal Band Calibration Constant of Landsat 8 OLI/TIRS for 2020

Satellite	Sensors	Categories	Band 10	Band 11
		K1	774.8853	480.8883
		K2	1321.0789	1201.1442
		Radiance_maximum	22.0018	22.0018
		Radiance_minimum	0.10033	0.10033
		Quantize_cal_max	65535	65535
		Quantize_cal_min	1	1
		Resolution	100 * (30)	100 * (30)

[Source: Landsat-8 Metadata, Obtained from USGS, 2020]

Land Surface Emissivity (LSE): Emissivity is a ratio which compares the spectral radiant remittance of a surface to that of a blackbody at the same temperature (Artis and Carnahan, 1982). Calculation of land surface emissivity (LSE) is required to estimate land surface temperature (Jeevalakshmi, 2017) since, LSE is a proportionality factor that scales the black body radiance (Plank's law) to measure emitted radiance and it is the ability of transmitting thermal energy across the surface into the atmosphere (Jovanovska and Ugur avdan , 2016). Based on the previous result obtained from NDVI values; the proportions of vegetation was determined by using the following equation 3.7.

$$PV = \left(\frac{\text{NDVI}-\text{NDVImin}}{\text{NDVImax}+\text{NDVI min}}\right)^2 \text{...Eq. (3.7)}$$

Where, PV is proportion of vegetation, NDVI min and NDVI max: normalized difference vegetation index minimum and maximum value respectively.

Land surface emissivity is determined by several factors including the chemical composition, roughness and moisture content of a surface; the emissivity of a surface can have values between 0 and 1; however, for most objects spectral emissivity is very close to 1 (Jeevalakshmi, 2017). Equation 3.8 below was used to determine land surface emissivity.

LSE = 0.004Pv + 0.986................………. …………………...……........................... Eq. (3.8)

Where, LSE is land surface emissivity and PV is the vegetation proportion.

Land Surface Temperature (LST): The spatial distribution of LST of the study area was extracted and quantified using Landsat5 TM of 1995 and Landsat8 OLI/TIRS thermal bands of 2020. LST was derived from Landsat TM band 6 and OLI/TIRS using band 10 based on the following equation (Artis and Carnahan, 1982).

$$\mathbf{LST} = \frac{\text{TB}}{1 + \left(\lambda * \frac{\text{TB}}{\rho}\right) Ln\, \varepsilon} \text{.. Eq. (3.9)}$$

Where; TB is brightness temperature, λ is wavelength of emitted radiance, ρ is h×c/σ (1.438×10^{-2} m K), σ is Boltzmann constant (1.38×10^{-23} J/K), h is Planck's constant (6.626×10^{-34}Js), c is velocity of light (2.998×10^{8} m / sec), ε is the surface emissivity.

The activity of extracting land surface temperature (LST) data from Landsat image is summarized as follows in figure 3.4 below.

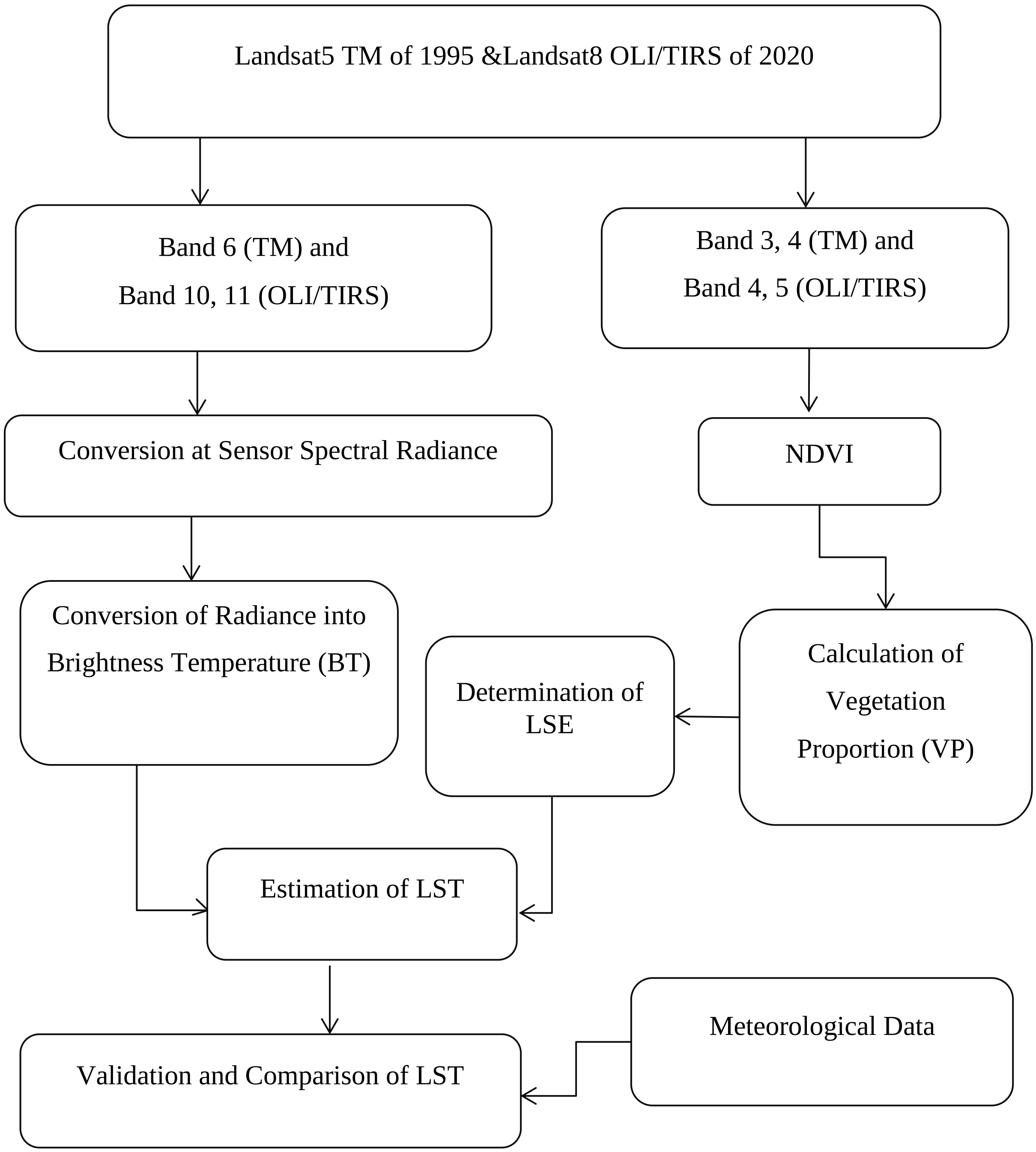

Figure: 3.4 Steps followed to extract LST from Landsat data.

3.3.5 Zonal Statistics

The application of GIS to analyze climate change vulnerability has grown highly in the last decade (Woodruff et al., 2017). The zonal statistics tool of ArcGIS was widely used in this study due to zonal statistics function summarizes the value of a raster within the zones of another dataset (either raster or vector) and reports the results as a table and figure. Zonal statistics tool is used in classifying and relating land surface in land use change in various studies (Younes zadeh, *et al.*, 2015; Rahmana, 2016). Maps of LU/LC, NDVI and LST were prepared for the year 1995 and 2020. To examine the spatial difference of LST according to varies land use land cover classes; the result was summarized using the zonal statistics tool of the Arc GIS10.8. Subsequently, summarized LU/LC, NDVI and LST data were analyzed using excel. Zonal statistics as table and figure is one of important methods that used to examine the correlation between Land use land cover, normalized difference vegetation index and land surface temperatures.

3.3.6 Spatial Interpolation

Spatial interpolation is the procedure of using points with known values to evaluate values at other unknown points. Interpolation predicts values for cells in raster from a limited number of sample data points. The available interpolation methods are Inverse Distance Weighted, Spline and kriging. No matter which interpolator is selected, however, the more input points and the greater their distribution, the more reliable the results (ESRI, 2016). In present study, meteorological data was used to interpolate and see the result and compare with the LST values that were done from Landsat thermal infrared bands. To interpolate temperature data Inverse Distance Weighted (IDW) interpolation method was used. Inverse Distance Weighted is the simplest interpolation method and deterministic models. Deterministic models include IDW, rectangular, natural neighbors and spine. Interpolation uses vector points with known values to estimate unknown locations to create raster surface covering an entire area (Legates and Willmott, 1990).

The reason why IDW interpolation method was used is that, in IDW interpolations different distances are integrated in the estimation; the distance weighting is able to precisely regulate the impact of the distances and it allows very fast and simple calculation (ESRI, 2016). Therefore, in the present study temperature data was interpolated using sample points in ArcGIS 10.8 environment and finally the interpolated maps were used for land surface temperatures validation.

3.3.7 Normalization of the Indexes

Normalization of the indicators were undertake to ensure the comparability of the indicators. This was carried out using the methodology developed for the calculation of the Human Development Index (UNDP, 2006) using equation (3.10). Then all the indicators assigned with values range from 0 to 1.

$$xij = \frac{X\,ij - \mathrm{Min}\,(Xij)}{\mathrm{Max}\,(Xij) \;- \mathrm{Min}(Xij)} \quad \ldots\ldots\ldots\ldots\ldots\ldots\ldots\ldots\ldots\ldots\ldots\ldots \quad (3.10)$$

Where X_{ij} is the separated value in the distribution, Min (X_{ij}) minimum value in the distribution and Max (X_{ij}) is the maximum value in the distribution, i is the kebele and j is number of indicators. The value of the normalized equation falls between 0 and 1. Where, 1 being the highest value and 0 with being the least vulnerable area for the indicators with positive relationship with vulnerability(Feyissa, 2019). Unless, if the indicators are assumed to be negative relationship with vulnerability, the above formula will be changed to the following as described in equation 3.11.

$$xij = \frac{\mathrm{Max}\,(Xij) - \;Xij}{\mathrm{Max}\,(Xij) \;- \mathrm{Min}(Xij)} \ldots\ldots\ldots\ldots\ldots\ldots\ldots\ldots\ldots\ldots\ldots\ldots\ldots\ldots \quad (3.11)$$

These study were used both positive and negative normalization technique to normalize urban heat vulnerability indicator values to 0 and 1. With negative normalization technique the highest normalized values 1 represented the least adapted (most vulnerable) sub-city, while the lowest normalized values 0, represented the most adapted (least vulnerable) sub-city (Feyissa, 2019). Normalization for individual variables were used in these study with the reference of other studies (Menezes *et al.,* 2018; Aubrecht and Ozceylan, 2013; Chow *et al.,* 2012; Dong, *et al.,* 2014; Tomlinson *et al.,* 2011; Vescovi, *et al.,* 2005). All normalized indicators were aggregated to heat vulnerability index (HVI) with a range between 0 and 1. Again, with 1 representing the highest level of heat vulnerability.

$$\mathrm{HVI} = \frac{\mathrm{EI+SI+AC}}{\mathrm{K}} \ldots\ldots\ldots\ldots\ldots\ldots\ldots\ldots\ldots\ldots\ldots \quad (3.12)$$

Where HVI is heat vulnerability index at kebele scale, EI represent the Exposure Index, SI represents the Sensitivity Index, AC represents the Adaptive Capacity Index and K is the total number of indicators. The value of (i) is kebele and j (indicators) is replaced with normalized HVI results in this study.

3.3.8 Heat Vulnerability Index

There are four approaches to aggregating or summarizing the information contained in the indicators in an overall index (the averaging/additive approach, principal components analysis, cluster analysis, and "geons"). Averaging/additive approach is the most frequently used approach in the IPCC definition of vulnerability framework. One advantage of the averaging/additive approach is that separate maps for each vulnerability component (e.g., into exposure, sensitivity and adaptive capacity) can help decision-makers to analyze adaptation options (Sherbinin, 2014).

The second approach to aggregation is Principal component analysis and one advantage of the principal component analysis is that it can help to illuminate the statistical relationships among the indicators used for a spatial vulnerability analysis. While, it may be challenging to attribute an intuitive meaning to a specific principal component analysis (Fekete, 2012). Sherbinin (2014) developed vulnerability maps for Mali using a number of data layers and aggregated them using both an averaging approach and PCA. For the averaging approach, each indicator was normalized to a 0–100 score, and then the components were averaged to produce an overall vulnerability index. The overall vulnerability maps are quite similar, but the individual IPCC component and PC maps reveal different patterns. Thus, a PCA approach can be complementary to the additive/averaging approach, providing additional information to policy makers; that said, there can be challenges in explaining the concept of principal components to stakeholders without much background in statistics (Sherbinin, 2014).

The third approach to aggregation is cluster analysis. In cluster analysis, the number of desired clusters is identified *a priori* and units are assigned to clusters on the basis of their profiles across all indicators (cluster might show the inverse); the resulting map will show patches of pixels with similar statistical profiles across the entire suite of indicators (Sherbinin, 2014). As with principal component analysis, some degree of interpretation is required to label the clusters (e.g., Kok *et al.*, 2010).

The fourth new approach to aggregation and regionalization is based on what are called "geons" (Lang, *et al.,* 2008; Hagenlocher *et al.,* 2013). Geon's are also independent of any given set of defined boundaries, as for example administrative boundaries, which are commonly used as reference units in the construction of composite indicators. While this approach has many strengths, it has yet to be widely adopted, perhaps because of the requirements for special software (e.g., eCognition) in data processing and analysis skills (Kienberger *et al.*, 2013 ; Sherbinin, 2014).

Four subcomponents of vulnerability indicators were used to identify vulnerable areas to heat by aggregating vulnerability component (exposure, sensitivity, and adaptive capacity) to Heat Vulnerability Index. Table: 3.6 shows the list of identified indicators for calculating the heat vulnerability index and their relationship with study by vulnerability components.

Table: 3. 6 Lists of Selected Indicators of Exposure, Sensitivity and Adaptive Capacity

Components	Indicators	Relation-ship	Layers in Sullivan Definition	Data Source
Exposure Layers	Mean LST Change	posative(+)	Geospatial	Extracted from Landsat
Sensitivity Layers	Population density	posative(+)	Environment	CSA (Dire Dawa city)
Adaptive Capacity Layers	Vegetation cover	Negetive (-)	Environment	Extracted from Landsat
	Access to tap water (%)	Negetive (-)	Access	Dire Dawa city water supply and sewerage authority.

[Adopted from, Feyissa, (2019)]

For these study the chosen method is to aggregate many heat vulnerability indicators into a single score that known as Heat Vulnerability Index (HVI) to represent the place with high heat risks. Heat vulnerability index through aggregation (additive approach) are a widely used methods in composite spatial indices of vulnerability (Harlan, *et al.*, 2006; Aubrecht, and Ozceylan, 2013; Zhu *et al.*, 2014; Janicke, *et al.*,2018). Finally, by using the geometrical interval classification scheme creates class breaks based on class intervals that have a geometrical series. The algorithm creates geometric intervals by minimizing the sum of squares of the number of elements in each class; This ensures that each class range has approximately the same number of values with each class and that the change between intervals is fairly consistent (ESRI, 2016). This algorithm was specifically designed to accommodate continuous data and it is a compromise method between equal interval, natural breaks (Jenks), and quantile (ESRI, 2016 ; Tomlinson *et al.*, 2011b; Guo *et al.*, 2019). It creates a balance between highlighting changes in the middle values and the extreme values, thereby producing a result that is visually appealing and cartographically comprehensive (ESRI, 2016). The results were mapped using ArcGIS 10.8 package.

CHAPTER IV: RESULTS AND DISCUSSIONS

This chapter presents the results of the analysis conducted to identify the co-location of hot spots kebele across the urban environment of Dire Dawa City. The chapter begins with an analysis of the land use land cover changes, changes on vegetation abundance, land surface temperature changes and percentage of access to safe water (improved drinking water supply coverage). All of the above important and valuable indicators are included in this study to estimate the degree of urban heat vulnerability in Dire Dawa City.

4.1. Characteristics of Land-Use/Land-Cover change

According to Dire Dawa Administrative Council Office and Dire Dawa Administrative Agricultural Development Office, the land use/land cover types have been grouped into four major classes. They are designated as urban built up, physiognomic (shrub) vegetation types, cultivated land (sparse vegetation), and bare land (D.D.A.I.D.P, 2012). In line with the major class identified by the office, the study adopts four major classes; the classification was intended to explore the influence of urban land use land cover change on land surface temperature. Land use land cover map of Dire Dawa City with four major categories namely, bare land, built-up area, sparse vegetation and shrub lands were generated for the year of 1995 and 2020 is presented in below Figure 4.1 and 4.2.

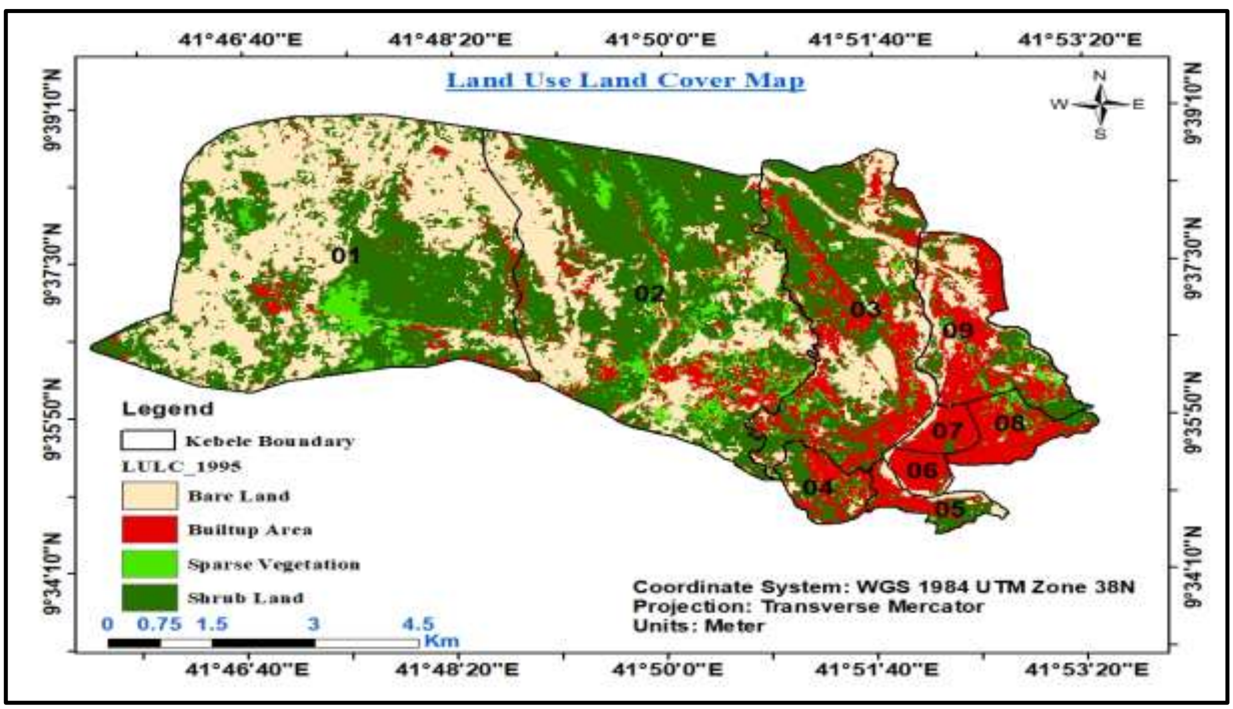

Figure: 4.1 Land Use Land Cover Maps of the Study Area for the year 1995.

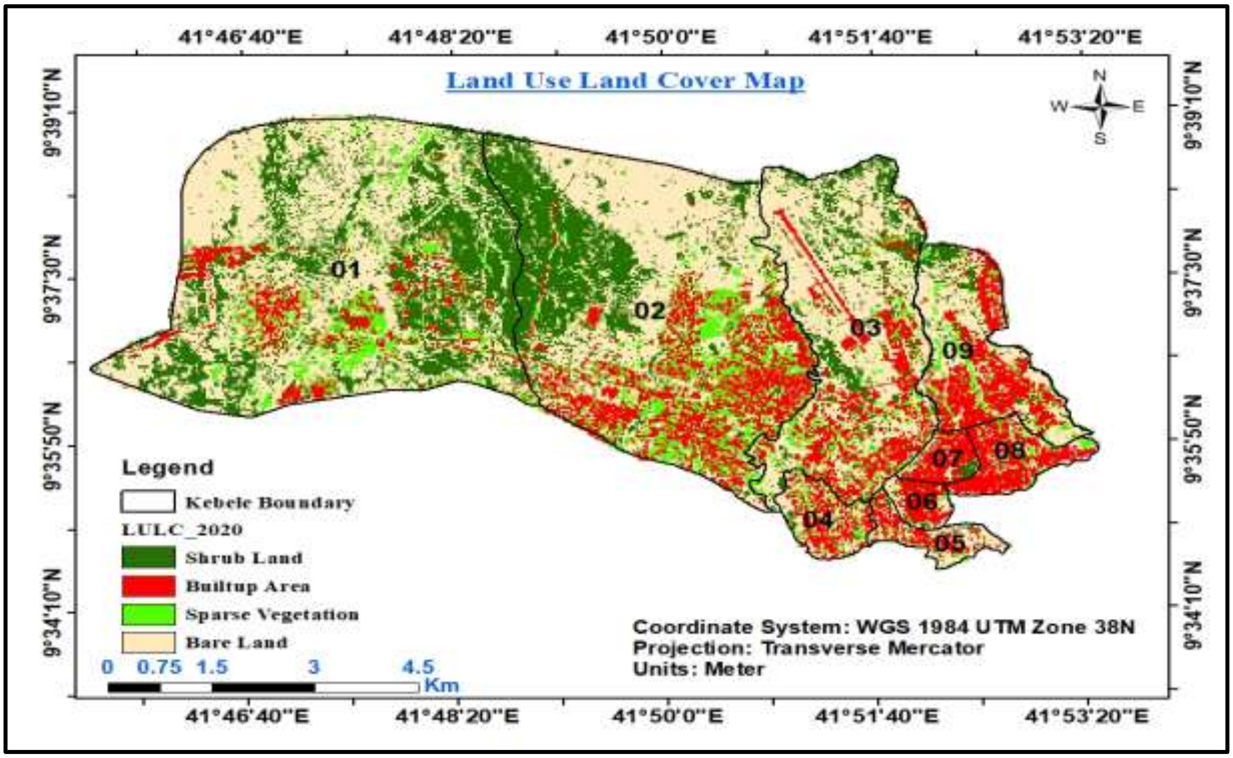

Figure: 4.2 Land Use Land Cover Maps of the Study Area for the year 2020.

Land-use/land-cover classes which comprise built up, barren land, sparse vegetation, and shrub land and area coverage of 1995 and 2020 is summarized in the Table 4.1.

Table: 4.1 Land-Use/Land-Cover classes and area coverage for 1995 and 2020.

		1995		**2020**		
No.	**Class Name**	**Area (km^2)**	**Percentage (%)**	**Area (km^2)**	**Percentage (%)**	**Net changing (1995-2020 in km^2)**
1	Bare Land	24.04	34.93	20.54	29.84	-3.50
2	Built-up Area	14.26	20.71	19.63	28.52	+5.38
3	Sparse Vegetation	13.79	20.03	11.72	17.02	-2.07
4	Shrub Land	16.75	24.33	16.95	24.62	+0.20
Total		**68.84**	**100.00**	**68.84**	**100.00**	

As shown in (Table 4.1), In 1995, LU/LC of bare land ($24.04km^2$) and shrub land ($16.75km^2$) takes the largest share followed by built-up area ($14.26km^2$) and sparse vegetation ($13.79\ km^2$). After 25 years in 2020, the total area of bare land is greater ($20.54km^2$) and followed by Built-up Area ($19.63km^2$). Shrub land area had also a total area of ($16.95km^2$) and followed by sparse vegetation ($11.72km^2$). Therefore, As shown previously in (Figure.4.1 and 4.2), in both study years the most dominant class of Land-use/land-cover was bare land and also the least dominant type of LU/LC was sparse vegetation.

As shown in (Table 4.1), the extent of built-up area in 2020 increased by $5.38km^2$ from 1995 than shrub land which is increased by $0.2km^2$. However, in comparative to Built-up area and shrub land, bare land has shown a considerable decrease in areal extent from $24.04km^2$ (34.93%) in 1995 to $20.54km^2$ (29.84%) in 2020; Thus, a total area of $3.50km^2$ has been converted in to other LU/LC classes. In addition, sparse vegetation has been gradually decline from $13.79\ km^2$ (20.03%) in 1995 to $11.72km^2$ (17.02%) in 2020 which is about $2.07km^2$; Subsequently, $2.07km^2$ of sparse vegetated areas were converted in to other land use land cover classes (built-up area and shrub lands). Land-use/land-cover classes and area coverage of 1995 and 2020 is presented Figure 4.3 below.

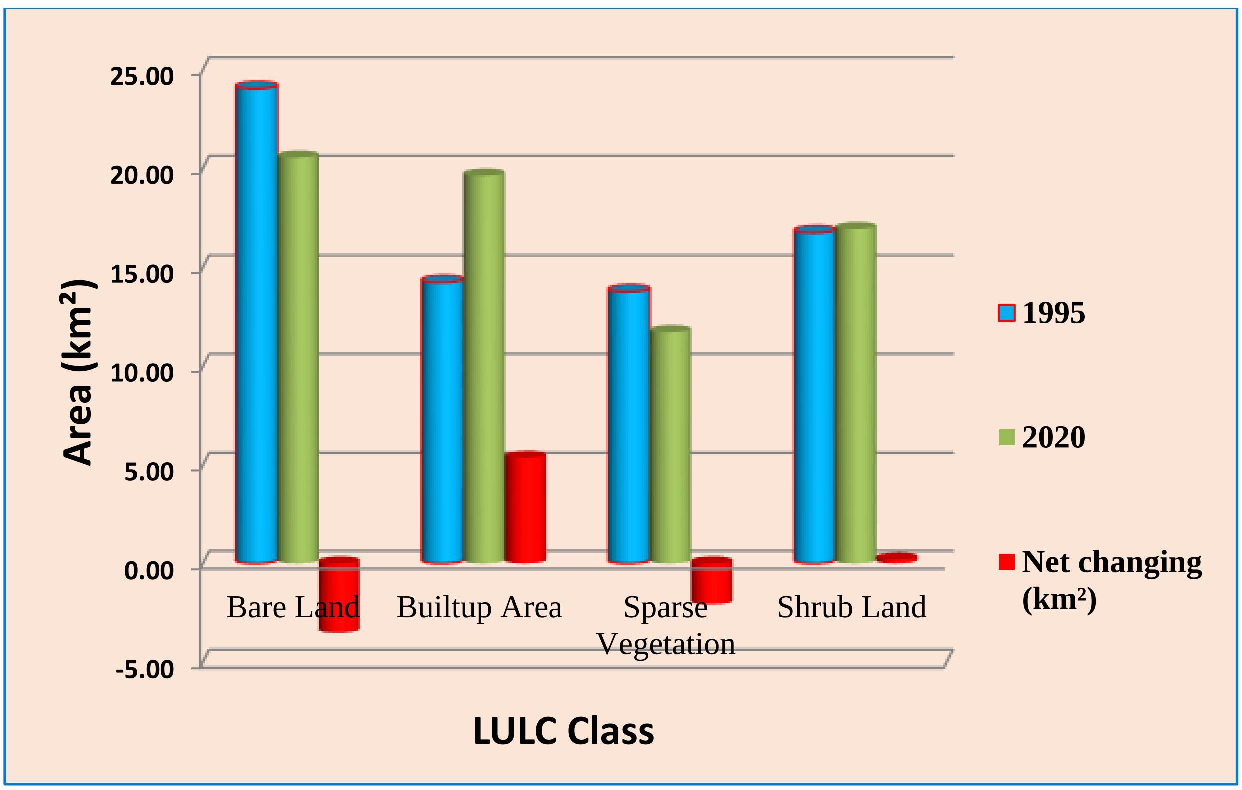

Figure: 4.3 Land-Use/Land-Cover change and area coverage for 1995 and 2020.

Accuracy assessment

Accuracy assessment determines the quality of the map created from remotely sensed data. The users and producer's accuracy assessment also calculated for each land classes and indicated acceptable agreement. Moreover, the overall accuracy was calculated by summing the number of pixels classified correctly and dividing by the total number of pixels sample. The accuracy assessment of LU/LC classification for the years 1995 and 2020 recorded the overall classification accuracy of 0.875 (87.50%) and 0.9125 (91.25%) respectively. Additionally the overall kappa statistics for the year 1995 and 2020 values are 0.8637 and 0.8937 respectively. The detailed information of producers and users accuracy is indicated in (Appendix 4 and 5) and table 4.2 below.

Table: 4.2 Statistical information of accuracy assessment for the year 1995 and 2020.

Class Name	1995		2020	
	Producers Accuracy (%)	**Users Accuracy (%)**	**Producers Accuracy (%)**	**Users Accuracy (%)**
Bare Land	83.33%	83.33%	85.71%	92.31%
Built-up Area	90.91%	90.91%	95.45%	91.30%
Sparse Vegetation	92.91%	88.89%	85.00%	89.47%
Shrub Land	80.00%	84.21%	95.83%	92.00%
Over all Classification Accuracy	87.50%		91.25%	
Overall Kappa Statistics	86.37%		89.37%	

Kappa coefficient was computed to measure the actual agreement and a chance agreement between the reference data and the classified data; this would be expressed in terms of the percentage of strong, moderate and poor agreement i.e. a value >0.80 (80%) strong agreement; a value b/n 0.40 and 0.80 (40 to 80%) represents moderate agreement; and a value < 0.40 (40%) represents poor agreement (Bekele, 2019). Therefore, the computed kappa hat value of 0.8637(86.37%) and 0.8937 (89.37%) for the year 1995 and 2020 indicates a better accuracy in the classification that was resulted from random sample classes classification. Since the kappa hat value fell above 80%, it represents strong agreement.

An important aspect of change detection is to determine what is actually changed to the other land use class. Land-use/land-cover changes between (2020 and 1995) years were calculated using change detection matrix to point out the rate of change and conversion. Clearly, as table 4.1 and figure 4.1 shows, for the last 25 years there has been a radical increase in areal extent and coverage of built-up area from 14.26km² (20.71%) to 19.63km² (28.52%) which is about 5.38km² area and followed by shrub land area 16.75km² (24.33%) to 16.95km² (24.62%) which is about 0.2km². Built-up area shows rapid expansion than other land use land cover classes. The land use land cover change map during the study period is shown in figure 4.4 below.

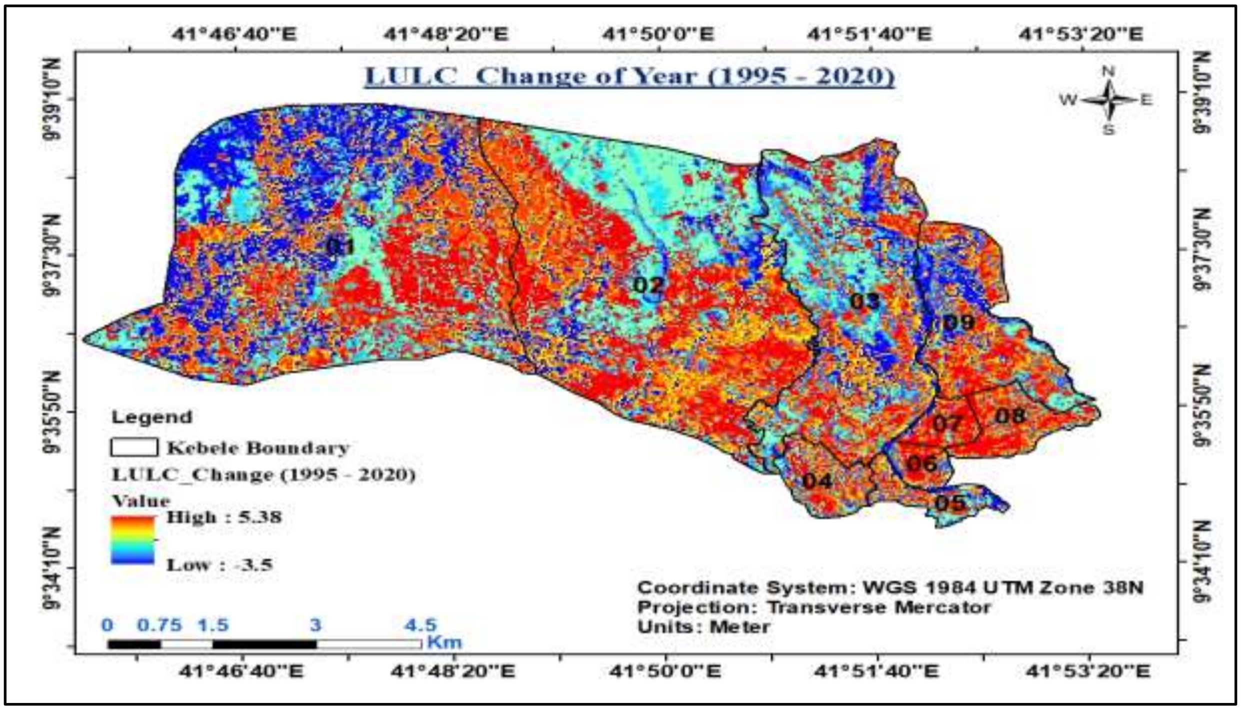

Figure: 4.4 Land Use Land Cover change Maps for the year between 1995 and 2020.

In developing countries, urbanization is rapid for three reasons: population growth caused by natural increase, migration toward urban areas and the reclassification of rural areas as urban centers (Maktav and Erbek, 2005; Wilhelmi and Hayden, 2010). Similarly, the number of population in the City was increased due to most of the country's industrial and commercial activities are concentrated there. Consequently, as the population increases, more specifically, the urban built-up area will be constantly expanding and it causes dynamic changes in LU/LC. The hospitality and sociability of the city's population at large is also worth mentioning in attracting development and investment activities in the near future. As a result, land-use/land-cover change could not be stopped easily.

4.2. Normalized Difference Vegetation Index (NDVI)

The general quantification of vegetation cover was done by using normalized difference vegetation index values, which allow making comparisons between different dates of imaging; the results of NDVI for two different years (1995 and 2020) were used to detect changes in vegetation cover and the overall NDVI values shows that vegetation density was in extensive reduction. NDVI maps of the study area for the year of 1995 and 2020 is presented in below Figure 4.5 and Figure 4.6.

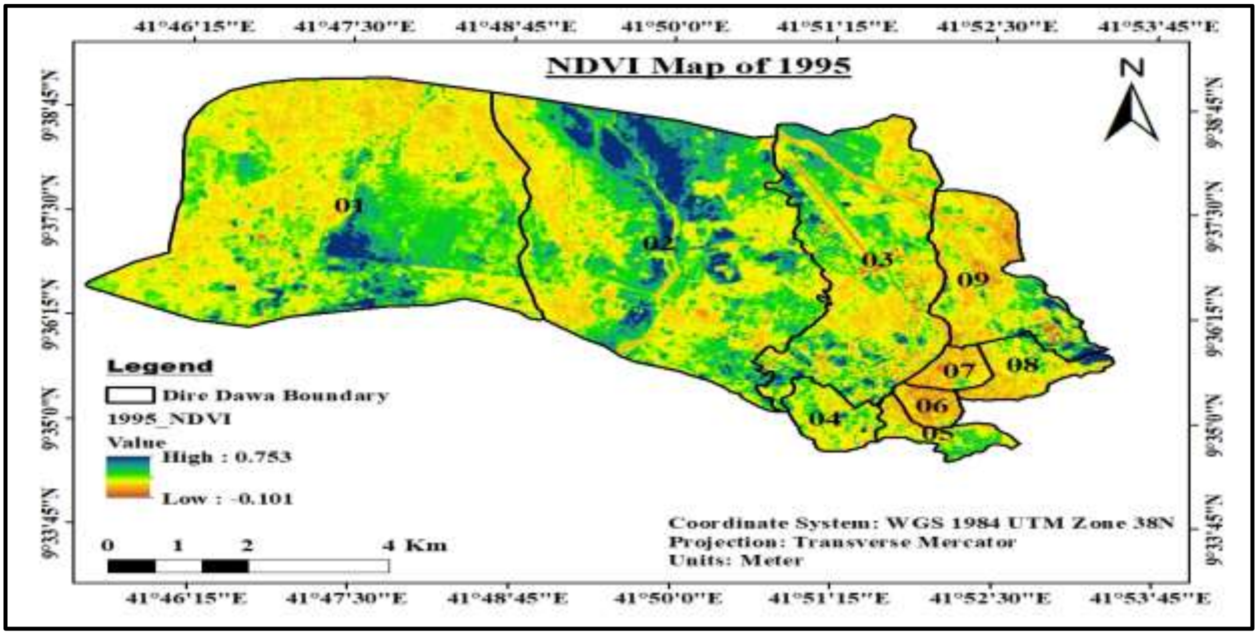

Figure: 4.5 Normalized Difference Vegetation Index Maps of the Study Area in 1995.

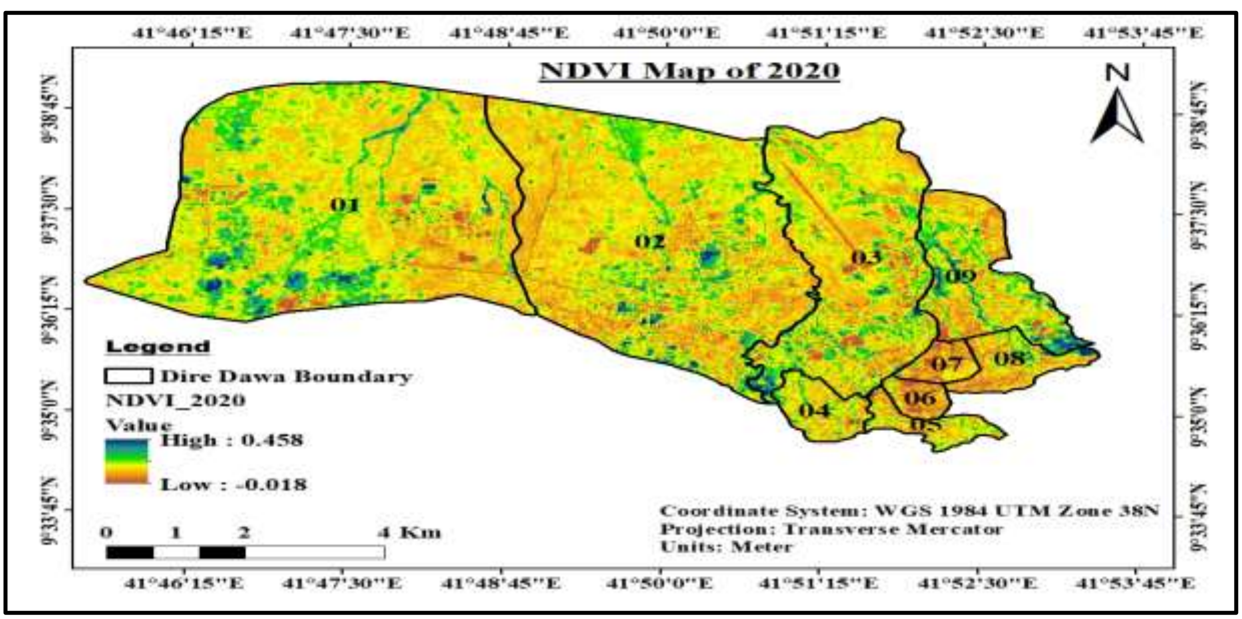

Figure: 4.6 Normalized Difference Vegetation Index Maps of the Study Area in 2020.

The Normalized Difference Vegetation Index (NDVI) is a vegetative index used in remote sensing analysis to assess whether or not a target contains live green vegetation. NDVI values were typically range between -1 and 1; 1 where the higher the value, the healthier and denser the vegetation. Moreover, values greater than 0.2 usually indicate vegetation, whereas values below 0.2 generally indicate soil, rock, or man-made materials. Water bodies typically give negative NDVI values (Liao *et al.,* 2005; Tam *et al.,* 2010). By using zonal statistics tool the maximum, minimum and mean value of NDVI were extracted and tabulated as shown in below table 4.3.

Table: 4.3 Statistical information of NDVI value per kebele.

No.	Kebele Name	NDVI 1995			NDVI 2020			Mean NDVI Change (1995-2020)
		Max	Min	Mean	Max	Min	Mean	
1	kebele 01	0.754	-0.031	0.151	0.403	-0.015	0.160	0.010
2	kebele 02	0.610	-0.034	0.199	0.459	-0.011	0.150	-0.049
3	kebele 03	0.598	-0.101	0.147	0.417	-0.007	0.155	0.007
4	kebele 04	0.574	0.019	0.142	0.403	-0.011	0.153	0.012
5	kebele 05	0.318	-0.013	0.129	0.304	0.013	0.145	0.016
6	kebele 06	0.253	-0.021	0.057	0.242	0.002	0.110	0.053
7	kebele 07	0.298	-0.048	0.071	0.284	-0.018	0.113	0.042
8	kebele 08	0.606	-0.037	0.125	0.373	0.039	0.144	0.019
9	kebele 09	0.551	-0.069	0.119	0.429	0.003	0.161	0.041

According to Table 4.3 the mean range of NDVI value per kebele level was 0.057 to 0.199 in 1995 and 0.110 to 0.160 in 2020. In 1995 the highest NDVI mean value of 0.199 was obtained in kebele 02 and the lowest NDVI mean value 0.057 was found in kebele 06. While, in 2020 the highest density of vegetation with mean value of 0.161 was obtained in kebele 09 and the lowest density of vegetation with mean value 0.110 was also in kebele 06. In 1995, kebele 02 (Sabian) had highest mean value of NDVI 0.199 followed by kebele 01 (Melka jebdu), kebele 03 (Kazira) and kebele 04 (Ganda Kore) by having mean value of 0.151, 0.147 and 0.142 respectively. In addition, kebele 05 (Addis Katama) and kebele 08 (Lege Hare) also had moderate mean value of NDVI 0.129, 0.125 respectively. Moreover, the lowest mean value of NDVI result that ranges below 0.125 was found in kebele 09, kebele 07 and kebele 06. Based on mean value of NDVI the abundance of vegetation in the Afata Issah and Dachatu kebele was relatively very low.

In 2020, the highest mean value of NDVI 0.161 was obtained in kebele 09 (Ganda Gerada). Followed by kebele 01(Malka jebdu) and kebele 03 (Kazira) by having mean value of 0.160 and 0.155 respectively. As well, modest mean value of NDVI was found in Kebele 04 (Ganda Kore), kebele 02(Sabian) and kebele 05 (Addis Katama) with mean value of NDVI 0.153, 0.150 and 0.145 respectively. Furthermore, the lowest mean value of NDVI was found in kebele 07 (Afata Issah) and kebele 06 (Dachau) by having mean value of NDVI 0.113 and 0.110 respectively. Generally, the result showed that the maximum density of vegetation (NDVI) value was drastically decreased from 0.753 in 1995 to 0.454 in 2020. Particularly, the highest negative change in abundance of vegetation is found in Kebele 02 (Sabian). Despite this, with the increasing depletion of grass, local communities tend to slice the leaves and branches of trees to feed their animals.

4.2.1 Relationship between LU/LC and NDVI

Normalized difference vegetation index maps that extracted from near infrared and red-bands of the study periods indicated that different land use land cover classes has reflect different NDVI values. So as to comprehend the NDVI value via LU/LC, the green space signature of each land use land cover classes was extracted by using zonal statistics tool. Table: 4.4 shows Statistical information of NDVI values by LU/LC classes.

Table: 4.4 Statistical information of NDVI values by LULC type for (1995 and 2020)

		1995 NDVI			**2020 NDVI**		
No.	**Class Name**	**Max**	**Min**	**Mean**	**Max**	**Min**	**Mean**
1	Bare Land	0.337	-0.145	0.096	0.227	0.027	0.127
2	Built up	0.467	-0.013	0.227	0.354	0.012	0.183
3	sparse vegetation	0.745	0.165	0.455	0.453	0.234	0.343
4	shrub land	0.556	0.097	0.326	0.428	0.169	0.298

In contrast to each LU/LC class, barren land has shown lowest mean value of NDVI 0.096 followed by built up area with moderate mean value of 0.227 in 1995. During the same study year, sparse vegetation recorded highest NDVI mean value of 0.455 followed by shrub land 0.326. Yet, in 2020 the mean NDVI value of sparse vegetation and shrub land was high 0.343 and 0.298 respectively. The least NDVI mean value was recorded for barren land 0.127 and built up 0.183.

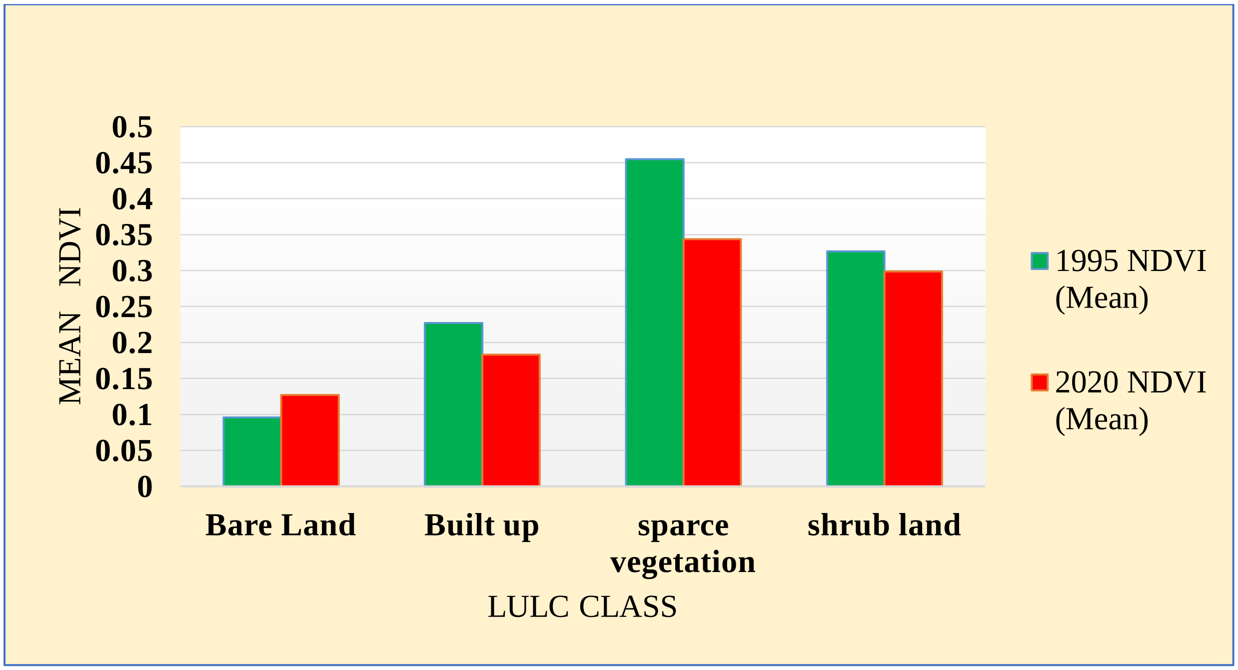

Figure: 4.7 Zonal statistical description of NDVI by LU/LC classes.

As NDVI is related with the vegetation condition, the value varies from area to area based on vegetation intensity of the sites. Similarly, the above Table: 4.4 and Figure 4.7 shows that the LU/LC type of sparced vegetation exhibited the highest mean NDVI value due to the predominance of vegetated land cover type. This was closely followed by the LU/LC types of shrub land which also showed high mean NDVI values. While, the LU/LC types of Built up area including (residential, industrial, commercial, public, public units and associated land) and bare land also showed low mean NDVI values.

4.3. Land Surface Temperature (LST)

The spatial distribution of land surface temperature of the study area was extracted and quantified by using Landsat 5 TM of 1995 and Landsat 8 of 2020 TIRS thermal bands. The results of land surface temperature over Dire Dawa City in year 1995 was ranged from 12.21°C to 31.96°C with mean land surface temperature value of 26.75 °C and in 2020 extended from 24.20°C to 36.70°C with mean land surface temperature value of 32.82°C. The mean land surface temperature change between 1995 and 2020 over the cities were 6.07°C. Table 4.5 presents the minimum, maximum and mean land surface temperature of Dire Dawa City in per kebele which was generated by zonal statistics tool. Land surface temperature (LST) maps of the study area in 1995 and 2020 is also presented in below Figure 4.8 and Figure 4.9.

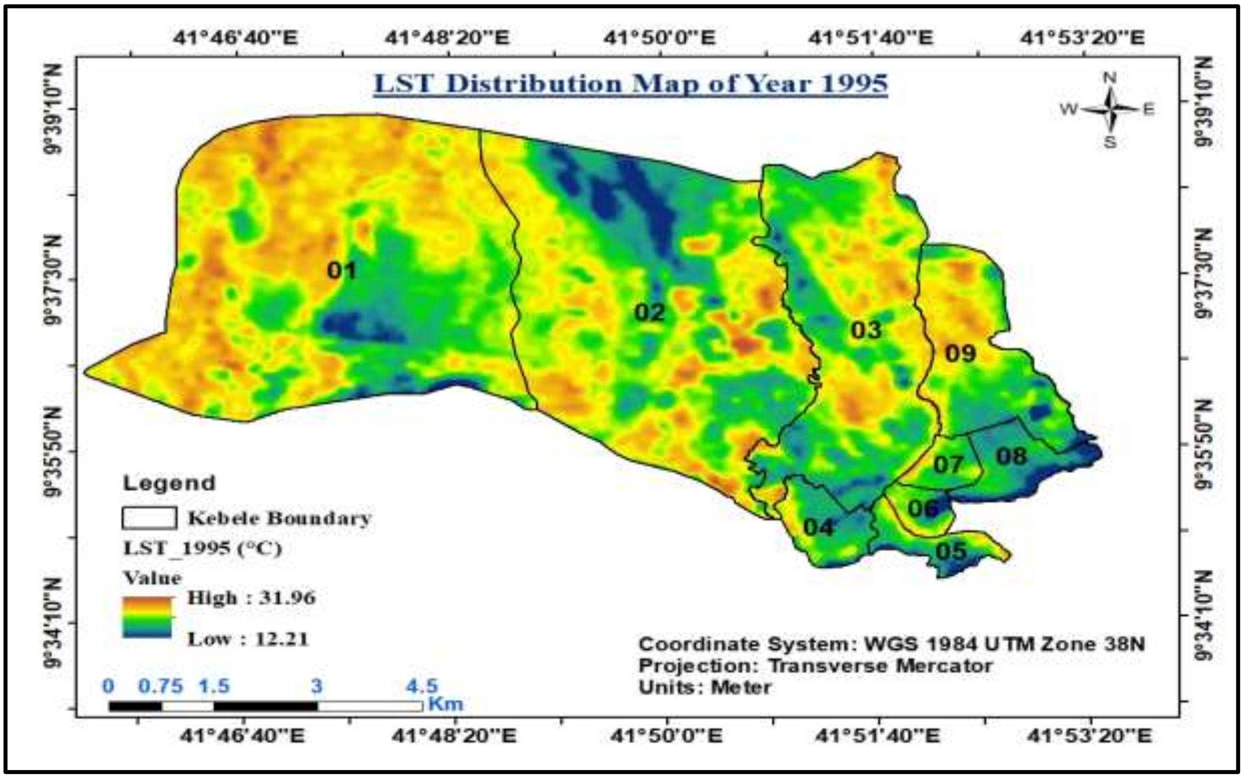

Figure: 4.8 Land Surface Temperature Maps of 1995.

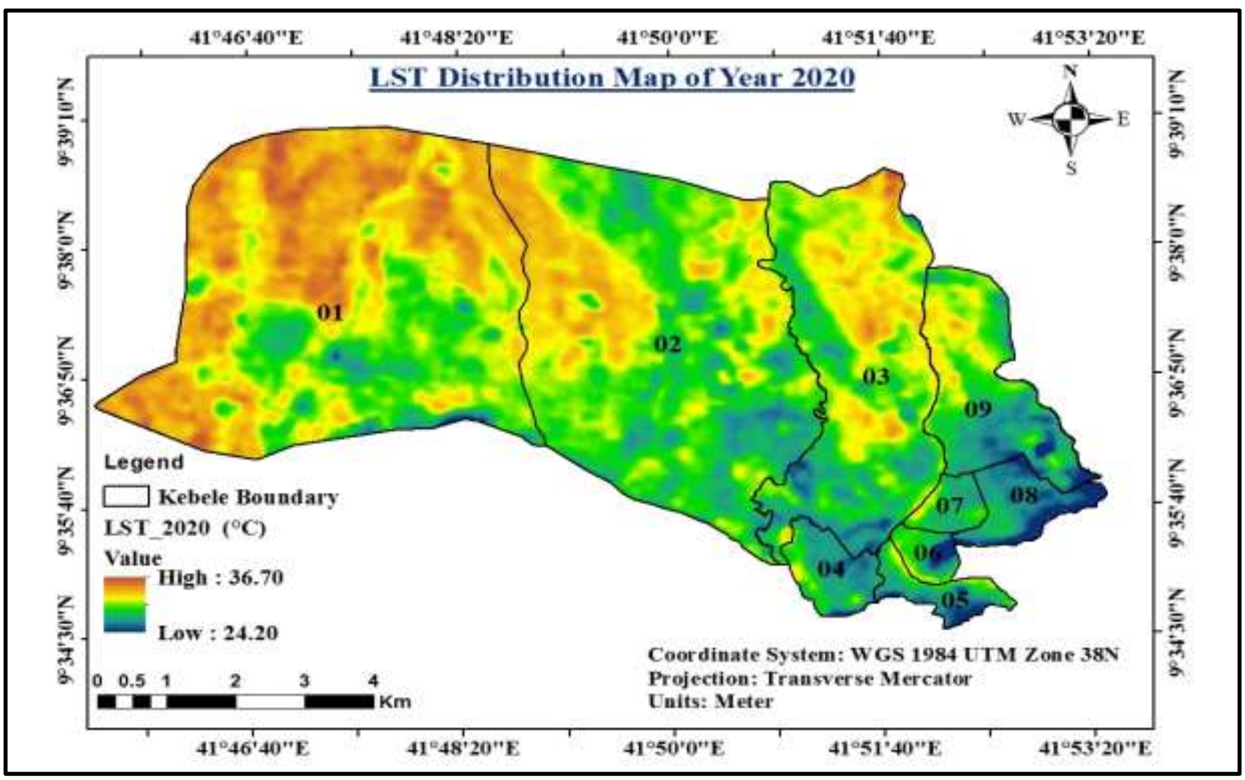

Figure: 4.9 Land Surface Temperature Maps of 2020.

Table: 4.5 Trends in minimum, maximum and mean LST distribution in 1995 and 2020.

No.	Kebele Name	1995 LST			2020 LST			Mean LST Change (°C)
		Min	Max	Mean	Min	Max	Mean	
1	kebele 01	20.32	31.56	27.62	28.24	36.70	33.84	6.21
2	kebele 02	20.32	31.96	26.74	29.60	36.53	33.61	6.87
3	kebele 03	22.47	30.76	26.86	28.82	36.68	32.58	5.72
4	kebele 04	21.18	29.55	25.54	28.43	33.88	30.90	5.36
5	kebele 05	19.44	30.36	25.57	26.91	33.76	30.88	5.31
6	kebele 06	19.88	29.15	25.84	26.99	33.56	31.14	5.30
7	kebele 07	24.17	29.55	26.43	30.18	34.03	32.49	6.06
8	kebele 08	17.68	27.51	24.01	25.61	32.11	29.77	5.76
9	kebele 09	12.21	30.76	26.87	24.21	36.17	32.73	5.86

Where, Min = Minimum, Max = Maximum, STD = Standard deviation.

In 1995 the highest mean land surface temperature distribution was found in kebele 01(Melka jebdu), Kebele 09(Ganda Gerada) and kebele 03(Kazira) by having mean LST value of 27.62°C 26.87°C and 26.86 °C respectively. Followed by kebele 02(Sabian) and kebele 07 (Afata Issah) with mean land surface temperature of 26.74°C and 26.43°C individually. On the other hand, relatively the moderate mean land surface temperature was obtained in kebele 06 (Dechatu) and kebele 05 (Addis Katama) by having mean land surface temperature value of 25.84°C and 25.57 °C separately. However, as shown in the above table 4.5 in 1995 the lowest mean land surface temperature of 24.01°C and 25.54°C was in kebele 08 (Lege hare) and kebele 04 (Ganda kore).

The distribution of mean land surface temperature over the city in 2020 shows that the highest mean LST value 33.84°C is found in kebele 01(Melka jebdu). It is followed by kebele 02(Sabian) with mean LST Value 33.61°C. The third highest mean LST value of 32.73°C and 32.58°C was located in Kebele 09(Ganda Gerada) and kebele 03 (Kazira) each individually. It is followed by Kebele 07 (Afata Issah) with 32.49°C. On the other hand, kebele 06 (Dechatu), kebele 04 (Ganda kore) and kebele 05 (Addis Katama) have almost equivalent mean LST value of 31.14°C, 30.90°C and 30.88°C each separately. Comparatively, the lowest mean land surface temperature of 29.77°C was in kebele 08 (Lege hare).

Generally, as the above table 4.5 shows, the highest mean land surface temperature change between (1995- 2020) is found in Kebele 02 (Sabian) and Kebele 01 (Melka jebdu), Kebele 07 (Afata Issah). Whereas, relatively the lowest mean land surface temperature change was occur in kebele 06 (Dechatu), kebele 05 (Addis Katama) and kebele 04 (Ganda Kore); As a result, the land surface temperature in the southeast of the City was lower than the surrounding temperature. Furthermore as the figure 4.8 and 4.9 shows, in 1995 the highest land surface temperature distributions were located along the northeast and northwest direction; as well as, in 2020 the highest land surface temperature distribution was oriented in to northwest directions.

4.3.1 Relationship between LULC and LST

To recognize the effects of the Land-use/land-cover dynamics on land surface temperature, the land surface temperature values on each Land-use/land-cover type were acquired by overlaying land surface temperature image with a Land-use/land-cover map of the same date. The mean values of land surface temperature for the different Land-use/land-cover types are extracted by using zonal statistics tool and summarized as shown in below Table 4.6.

Table: 4.6 Statistical information of LST over different LU/LC classes.

LULC Class	**1995 Mean LST(ºC)**	**2020 Mean LST(ºC)**	**Mean LST Change in ºC (1995 – 2020)**
Shrubs Land	24.79	28.12	3.33
Sparse Vegetation	21.41	26.44	5.03
Built-up Area	26.17	31.29	5.12
Bare Land	28.36	32.76	4.40

As observed in the above table 4.6, Land-use/land-cover categories that received minimum temperature were sparse vegetation and shrub land respectively. Comparatively, the highest land surface temperature value was recorded in bare land and built-up area. Scholars have also witnessed that the highest values of land surface temperature are in the urban or built-up areas and other impervious surfaces, while the lower land surface temperature values were found around highly vegetated areas like urban green space (Honjo and Takakura, 1990).

In contrast towards each LU/LC class in 1995, the highest mean LST value of 28.36ºC was recorded on barren land. Followed by built up area with mean LST value of 26.17ºC. During the same study year, sparse vegetation recorded lowest mean LST value of 21.41ºC and followed by shrub land 24.79ºC. On the other hand, in 2020 the lowest mean LST value of 26.44 ºC was spotted in sparse vegetation land cover but, mean LST was increased by 5.03 ºC. And the mean LST of shrub land is 28.12 ºC; it was also greater than before by 3.33 ºC. Whereas, the highest mean LST of 32.76 ºC was recorded in barren land, Yet again the mean LST was raised up by 4.40 ºC. Moreover the mean LST of built up area was raised up by 5.12 ºC (from 26.17 ºC to 31.29 ºC). The comparisons of mean land surface temperature in different land-use/land-cover classes during the study period (1995 – 2020) year is shown in Figure 4.10 below:

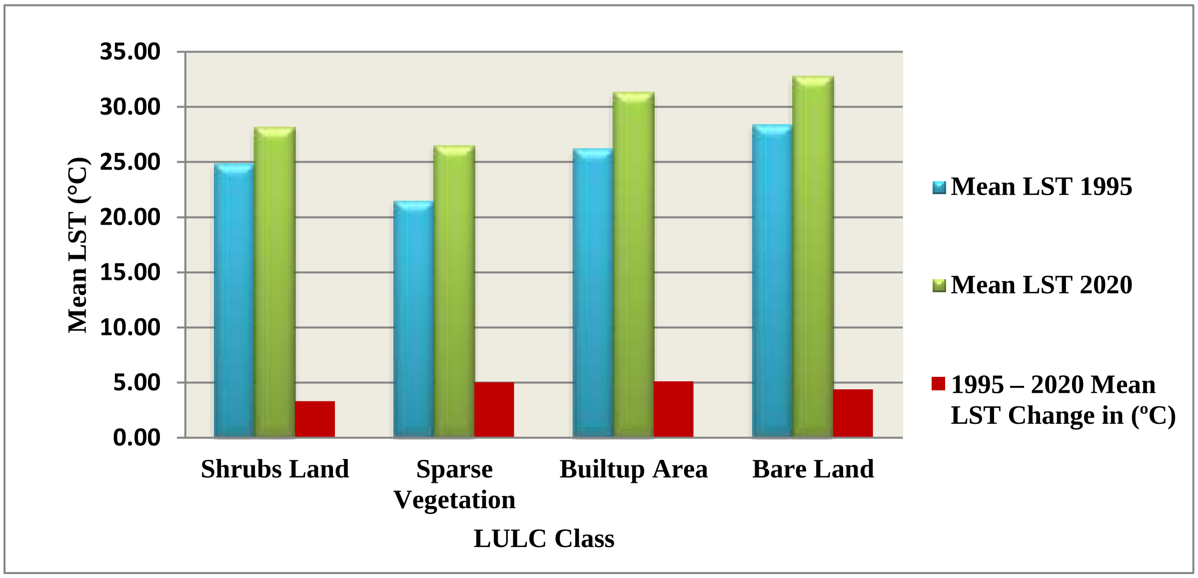

Figure: 4.10 Comparisons of mean LST in different LU/LC classes.

As observed in the above (Table 4.6 and Figure: 4.10), Results from land use land cover dynamics in relation to land surface temperature changes between 1995 and 2020 revealed that, a noticeable increase in built-up area by 5.38 km² exhibited a high change of surface temperature 5.12ºC. While, sparse vegetation has been gradually decline by 2.07 km² exposed the values of surface temperature to increase by 5.03ºC. From perspective of the impact of land use land cover change on land surface temperature, the finding of this study is consistent with previous studies that show an increase in built-up area, while decreases in other land cover types, primarily sparced vegetation areas, lead to an adverse effect of urban heat island at different times (Haylemariyam, 2018 ; Jifar, 2020).

4.3.2 Relationship between NDVI and LST

Normalized Difference Vegetation Index (NDVI) is typically used as the indicator of vegetation abundance and it's widely used in various study to estimate the LST - Vegetation relationship. According to Mihai, (2012) and Weng, *et al.*, (2004), Normalized Difference Vegetation Index is found as an acceptable indicator of land surface temperatures and dryness. A regression analysis between LST and NDVI for both study years was conducted. The regression between NDVI and LST is obtained as 0.9556 (95.56%) and 0.9713 (97.13%) in the 1995and 2020 respectively. These results show that, in 1995, about 95.56% value of LST variability was due to the difference in NDVI value, the coefficient variation values are also familiar for 2020. Land surface temperature and normalized difference vegetation index correlation for the years 1995 and 2020 are also shown in figure 4.11 and 4.12.

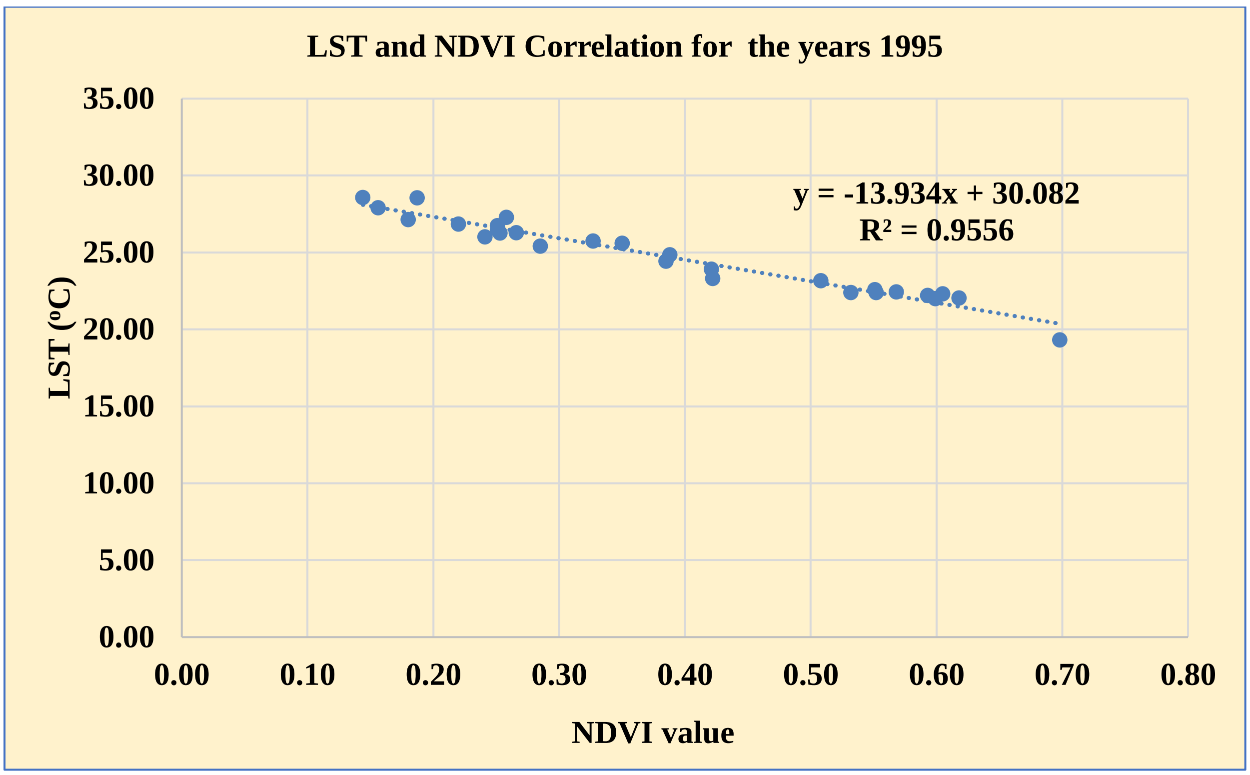

Figure: 4.11 linear regression scatter plot of LST and NDVI for 1995.

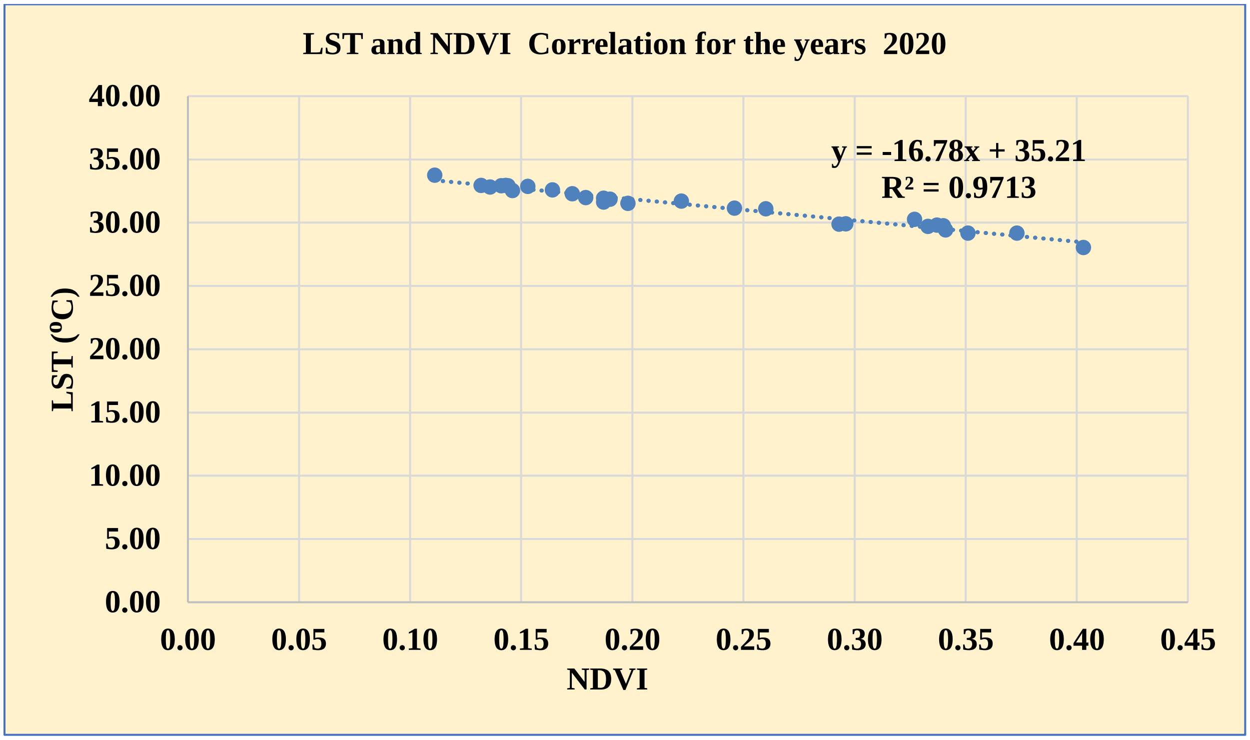

Figure: 4.12 linear regression scatter plot of LST and NDVI for 2020.

As shown previously in (Figure.4.5 and 4.6), the mean value of NDVI from 1995 to 2020 exhibits a significant decrease, while the mean value of LST from 1995 to 2020 indicates a significant increment (Figure.4.8 and 4.9). From the analyzed Landsat images of the years 1995 and 2020, it is evident that the LST is strongly and negatively correlated with NDVI. It means that where NDVI is lower, there is a higher land surface temperature and where NDVI is higher, there is a lower land surface temperature. Hence, areas with the least vegetation are experiencing higher land surface temperatures. This shows vegetated area played crucial role in minimizing the land surface temperatures.

Different researchers used Landsat imagery to study normalized difference vegetation index and land surface temperatures relationship. for instance, Gebrekidan Werku (2016) used Landsat imagery to study LST situation of Addis Ababa City and founds negative linkage in NDVI and LST values. The finding of this study is coincides with those of studies that found a strong association between the land surface temperature distribution and vegetation density. Therefore, this indicates that increasing the amount of vegetation with the goal of decreasing heat intensity, is more effective.

4.3.3 Validation of Land-Surface Temperature

In this study, Interpolation of temperature were done based on the meteorological data collected from three stations within and nearby the study area. These stations were; Dire Dawa, Kersa and Dengego. Land surface temperature was verified by using average monthly meteorological data. There is a strong relationship between the land surface temperature extracted from Landsat thermal band of the study area and atmospheric temperature, which was interpolated from those three stations nearby the study area. Interpolated map of atmospheric temperature are presented in Figure 4.13 bellow.

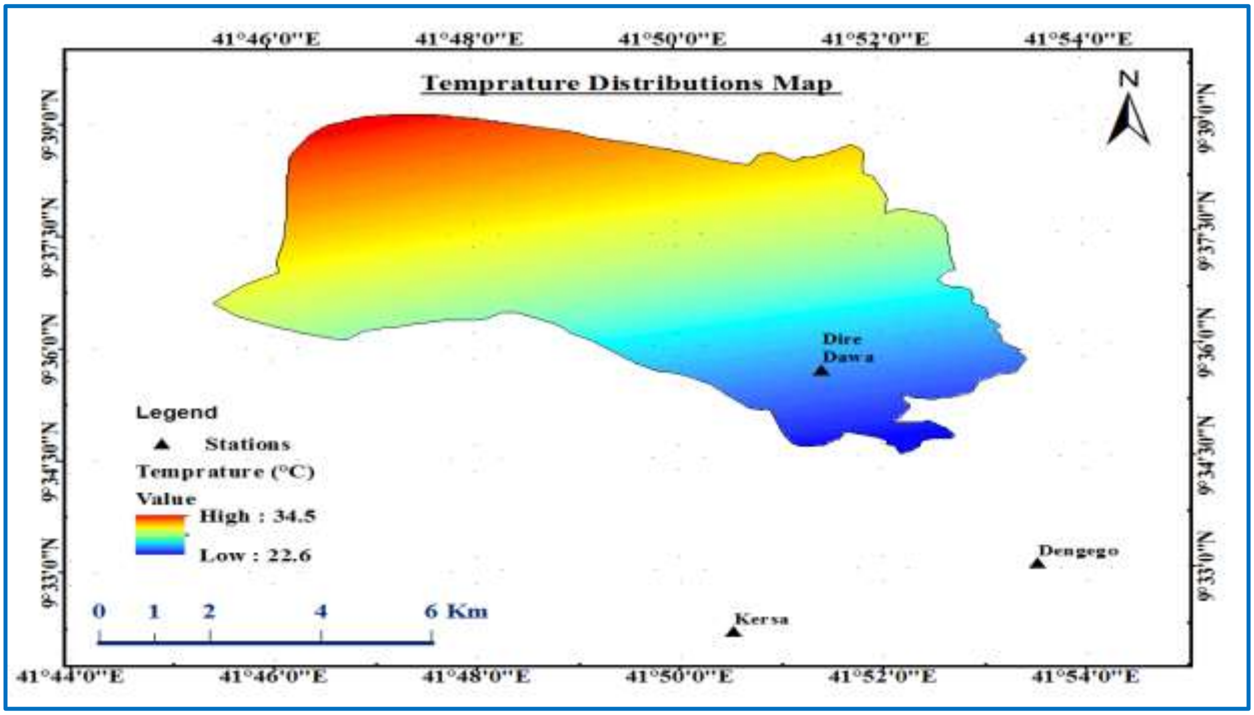

Figure: 4.13 Interpolated map of Temperature.

The land surface temperature, which was extracted from thermal bands of the study period (2020), was ranged from 24.20ºC to 36.70ºC. While, the interpolated atmospheric temperature map result ranged from 22.6ºC to 34.5ºC. Consequently, both land surface temperature map extracted from Landsat thermal bands and interpolated map shows the same result around the central part of the study area; which shows comparatively medium temperature. The result of land surface temperature extracted from Landsat thermal bands, also revealed that the north, central and some north eastern parts of the study area exhibited relatively high temperature value in each of the study periods, whereas the southeastern parts have lower temperature value than northwestern parts.

4.4. Urban Heat Vulnerability Quantification and Mapping

Urban heat vulnerability quantification and mapping was conducted based on indicators that reflect exposure, sensitivity of the population's and local adaptive capacity to mitigate urban heat vulnerability for the people who inhabited in the Dire Dawa City.

4.4.1. Exposure Component

Following the vulnerability concept, this study uses the mean land surface temperature change as an exposure to put a figure on the mean land surface temperature change in function of the geographic location. These indicator are extensively used in urban heat vulnerability analyses. The assumption was that the places with the highest land surface temperature change are more exposed to heat vulnerability. Land surface temperature is derived from consecutive Landsat satellite images, then after the mean land surface temperature were extracted by using zonal statistics as table tool. The quantified mean land surface temperature change presented in table 4.7 were normalized to evaluate highly exposed kebeles to heat vulnerability.

Table: 4.7 Exposure Indicator

No.	Kebele Name	1995 Mean LST (°C)	2020 Mean LST (°C)	Mean LST Difference (°C)	Normalized
1	kebele 01	27.62	33.84	6.21	0.58
2	kebele 02	26.74	33.61	6.87	1.00
3	kebele 03	26.86	32.58	5.72	0.26
4	kebele 04	25.54	30.90	5.36	0.03
5	kebele 05	25.57	30.88	5.31	0.01
6	kebele 06	25.84	31.14	5.30	0.00
7	kebele 07	26.43	32.49	6.06	0.48
8	kebele 08	24.01	29.77	5.76	0.29
9	kebele 09	26.87	32.73	5.86	0.35

(Source: Based on data from Landsat images, and extracted by author)

Based on results the change in spatial distribution of mean land surface temperature per kebele shows that highest change was found on kebele 02 (sabian) with 6.87 ^{0}C and kebele 01 (Melka jebdu) by 6.21 ^{0}C. On the other hand, the modest mean land surface temperature change was take place at kebele 07 (Afata issah) via 6.06 ^{0}C and kebele 09 (Ganda Gerada) by 5.86 ^{0}C. Whereas, the lowest mean land surface temperature change was take place at kebele 06 (Dechatu) by 5.30 ^{0}C, kebele 05 (Addis Katama) via 5.31 ^{0}C, kebele 04 (Ganda Kore) by 5.36 ^{0}C, kebele 03 (Kazira) in 5.72 ^{0}C and kebele 08 (Lege Hare) through 5.76 ^{0}C.

As shown previously in (table 4.7), the average value of exposure was found to be 0.333 (moderate). According to, the normalized scores of mean land surface temperature change per kebele shows, the highest scores of exposure was 1 which is found in kebele 02 (sabian) and followed by kebele 01 (Melka jebdu) through 0.58. Then again, the moderate value of exposure was take place at kebele 09 (Ganda Gerada) by 0.35 and kebele 07 (Afata issah) via 0.48. Whereas, comparatively the lowest value of exposure was transpire at kebele 06 (Dechatu) by 0.0, kebele 05 (Addis Katama) via 0.01, kebele 04 (Ganda Kore) by 0.03, kebele 03 (Kazira) in 0.26 and kebele 08 (Lege Hare) through 0.29. Normalized and reclassified map of exposure indicator is presented in below Figure 4.14 and in Appendix 7.

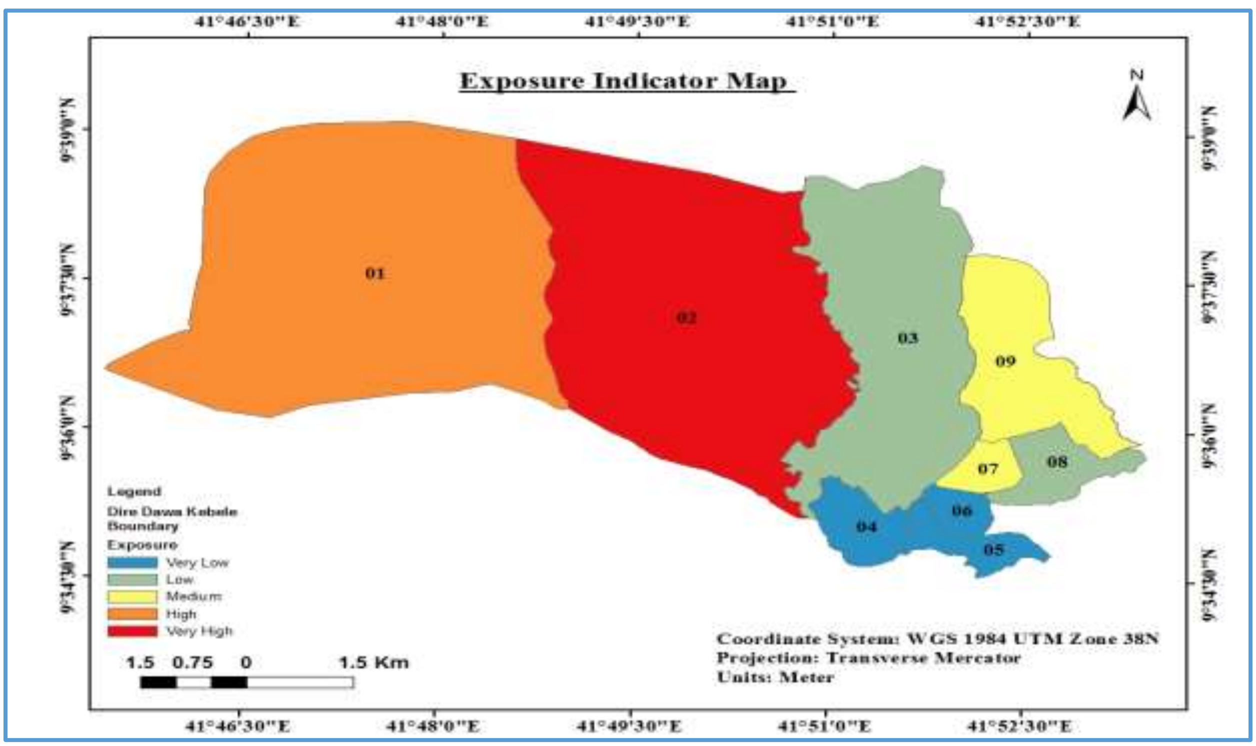

Figure: 4.14 Normalized and reclassified map of exposure indicator.

Figure 4.14 revealed that highly exposed kebeles to mean land surface temperature change were kebele 02 (Sabian) and kebele 01 (Melka Jebdu). On the other hand, the moderately exposed kebeles were kebele 07 (Afata issah) and kebele 09 (Ganda Gerada). Whereas, the lowest mean land surface temperature change was take place at kebele 06 (Dechatu), kebele 05 (Addis Katama), kebele 04(Ganda Kore), kebele 03 (Kazira) and kebele 08 (Lege Hare); for that reason, those kebeles were least exposed kebeles to heat. As result indicates the higher rate of mean land surface temperature change is found in western, northern, northwest directions and southeastern parts of the city. These results are agrees with previous study done over the study area at different time (Haylemariyam, 2018; Jifar, 2020)

4.4.2. Sensitivity Component

For the Sensitivity component the selected indicator was spatial distribution of population per kebeles. Sun, etal., (2019) used population density (persons per square km) as a sensitivity indicator with high number corresponding with a high sensitivity score, as denser populations are more sensitive to heat related health complications. The distribution of population over the City is shown in table 4.8 below and in Appendix 2:

Table: 4.8 Sensitivity Indicator

No.	Kebele Name	Area in Km^2	2020 Population per kebele	Normalized
1	kebele 01	25.09	25156	0.06
2	kebele 02	21.17	61156	0.99
3	kebele 03	11.82	27440	0.11
4	kebele 04	1.48	29045	0.16
5	kebele 05	1.11	24754	0.05
6	kebele 06	0.69	23007	0.00
7	kebele 07	0.8	31742	0.23
8	kebele 08	1.65	40901	0.46
9	kebele 09	4.87	61559	1.00

(Source: Based on data from, Dire Dawa City Central statistical Agency and constructed by author)

The distribution of population over the City in 2020 shows that the highest percentage, 18.96 % or 61559, of the city's population live in kebele 09, occupying an area of 4.87 km^2. It is followed by kebele 02 that accounts for 18.83 % or 61156 of the city's population and occupying an area of 21.17 km^2. The third largest is kebele 08 with 12.59 % or 40901 of the city's residents living in an area of 1.65 km^2. It is followed by kebele 07 and kebele 04 with 9.77% or 31742 and 8.94% or 29045 of the city's residents living in an area of 0.8 and 1.48 km^2 each respectively. Kebele 03 residents is 8.45% of the total population i.e. 27440 people is living with in the area of 11.82 km^2. On the other hand kebele 01 and kebele 05 residents is 25156 (7.75%) and 24754 (7.62%) is living with in the area of 25.09 and 1.11 km^2 each respectively. Moreover, the minimum population distribution in the city were located in kebele 06 with percentage of 7.08 % or 23007, occupying an area of 0.69 km^2. Distribution of population over the City for 2020 is shown in Appendix 6.

Based on the normalized and reclassified values of spatial distribution of population per kebele in 2020, the highest score for sensitivity was found in kebele 09 (Ganda Gerada) and kebele 02 (Sabian) via 1 and 0.99 respectively. While, the lowest score ranged from (0.0 to 0.16) was found in kebele 06 (Dechatu), kebele 05 (Addis ketema), kebele 01 (Melka Jebdu) and kebele 03 (Kazira). Normalized and reclassified sensitivity indicator map are presented in below Figure 4.15 and in Appendix 8.

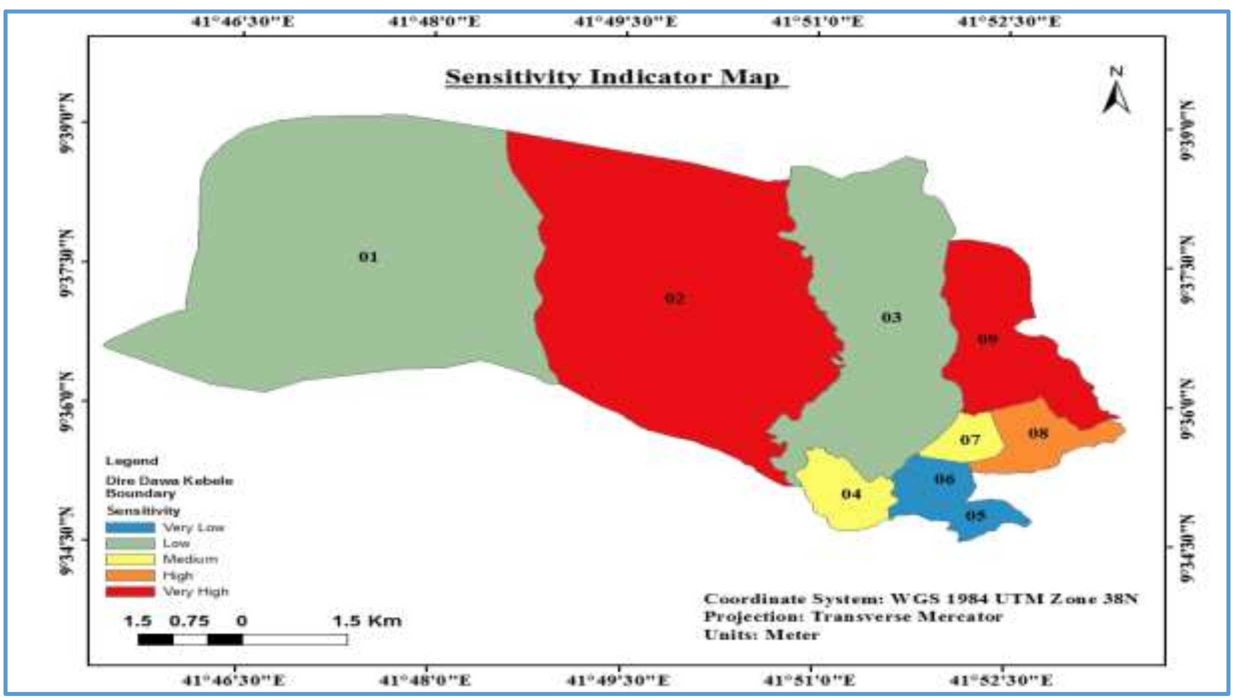

Figure: 4.15 Normalized and reclassified map of sensitivity indicator.

As shown in Figure 4.15, reclassified map for sensibility of population to heat indicates kebele 09 (Ganda Gerada), kebele 02 (Sabian) and kebele 08 (Lege Hare) were highest sensitive kebele. Which is found in the eastern, central and southeastern parts of Dire Dawa City. Whereas, based on the spatial distribution of population kebele 06 (Dechatu), kebele 05(Addis ketema), Kebele 01 (Melka Jebdu) and kebele 03 (Kazira) were comparatively low sensitive. On the other hand, in kebele 04 (Ganda kore) and kebele 07(Afata Issah) the density of population is described as moderate; as a result, sensitivity to heat is medium.

4.4.3. Adaptive Capacity Component

In these studies, two adaptive capacity indicator have been selected to reduce the adverse impacts of urban heat vulnerability. These are green infrastructure (vegetation abundance) and a percentage of access to water (only access to water provided by tap in their house or compound, whether it is shared or private). In vulnerability studies, exposure and sensitivity are considered to have the potential to increase the vulnerability of a system, while adaptive capacity has the potential to decrease it (Menezes *et al.*, 2018). This logic was adopted in present study. Therefore, the highest normalized values represented the least adapted kebeles, while the lowest normalized values represented the most adapted kebeles. The normalized scores were presented in below table 4.9.

Table: 4.9 Adaptive Capacity Indicator

No.	Kebele Name	2020 NDVI (Mean)	Norm	% of access to water	Norm	Average Adaptive Capacity
1	kebele 01	0.160	0.01	78	0.59	0.30
2	kebele 02	0.150	0.21	85	0.26	0.24
3	kebele 03	0.155	0.12	90	0.00	0.06
4	kebele 04	0.153	0.15	71	0.90	0.53
5	kebele 05	0.145	0.30	76	0.69	0.50
6	kebele 06	0.110	1.00	70	0.99	1.00
7	kebele 07	0.113	0.94	72	0.86	0.90
8	kebele 08	0.144	0.34	73	0.83	0.59
9	kebele 09	0.161	0.00	69	1.00	0.50

(Source: Based on data from Landsat imagery and Dire Dawa City water supply and sewerage authority, constructed by author).

As Table 4.9 shows, in 2020 the highest mean value of NDVI 0.161 was obtained in kebele 09. Followed by kebele 01 and kebele 03 by having mean value of 0.160 and 0.155 respectively. As well, modest mean value of NDVI was found in kebele 04, kebele 02 and kebele 05 with mean value of NDVI 0.153, 0.150 and 0.145 respectively. Furthermore, the lowest mean value of NDVI was found in kebele 07 (Afata Issah) and kebele 06 (Dachau) by having mean value of NDVI 0.113 and 0.110 respectively. Based on the normalized indicators value of mean NDVI, kebele 06 (Dechatu), kebele 07 (Afata Issah), kebele 08 (Lege Hare) and kebele 05 (Addis Katama) kebeles of the cities have lowest green infrastructure. While, kebele 03 (Kazira), kebele 04 (Ganda kore) and kebele 02 (Sabian) have relatively medium green infrastructure. Kebele 09 (Ganda Gerada) and kebele 01 (Melka jebdu) have comparatively highest green infrastructure.

Based on existing data's from Dire Dawa City Water Supply and Sewerage Authority, the percentage of access to safe water per kebele is widely divergent. For instance, the highest percentage of accessibility to safe water is found in kebele 03 (Kazira) and kebele 02 (Sabian) by having 90% and 85% water supply coverage. Followed by kebele 01 (Melka Jebdu) with 78% and kebele 05 (Addis Katama) with 76%. While, the lowest percentage of water supply coverage with values ranging from 69% to73%; which is found in Kebele 09 (Ganda Gerada) by having 69%, kebele 06 (Dechatu) via 70%, kebele 04 (Ganda Kore) 71%, kebele 07 (Afata Issah) 72%, kebele 08 (Lege Hare) 73%. Increased access to improved drinking water in areas with the least access to safe water can help to enhance urban heat vulnerability across a range of possible future climates.

Generally, as table 4.9 and figure 4.16 of normalized and reclassified average adaptive capacity (the mean vegetation abundance and the percentage for accessibility of safe water per kebele) indicates, the average value of adaptive capacity was 0.51. The kebeles with the highest average adaptive capacity were kebele 03 with (0.06) and kebele 02 by (0.24); both located in the central portion of the City and kebele 01 (0.30) located in western region. Whereas, kebele 04 (Ganda kore), kebele 08 (Lege Hare), kebele 07 (Afata Issah) and kebele 06 (Dechatu) have the lowest adaptive capacity with values ranging from 0.53 to 1.00. Normalized and reclassified average adaptive capacity indicator map are presented in below Figure 4.16 and in Appendix 9.

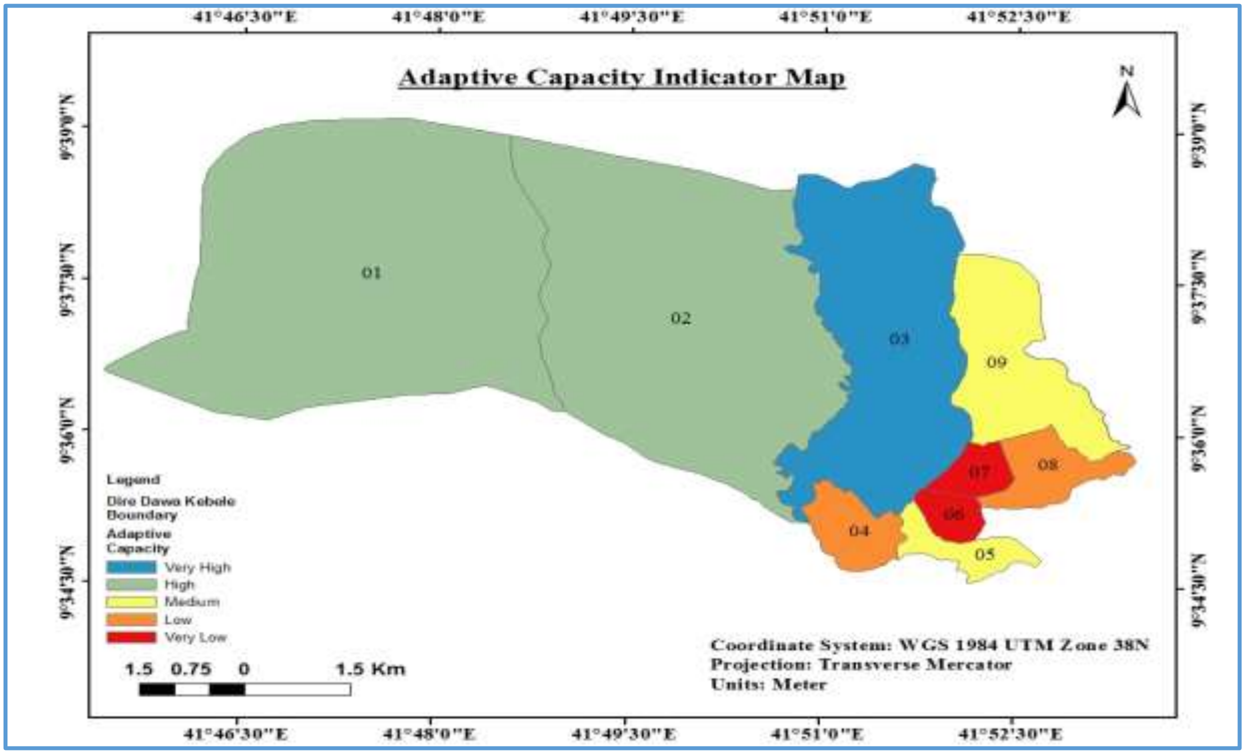

Figure: 4.16 Normalized and reclassified map of adaptive capacity indicator.

4.4.4. Urban Heat Vulnerability Map

The urban heat vulnerability maps that developed for Dire Dawa City are able to identify *not only* where are the hottest areas are located but also where the most vulnerable people of the city are located in the City. In addition, there are also able to visualize the current state of adaptive capacity to extreme heat based on the availability of greenery, water accessibility for public health etc. Therefore, government officials, environmental experts, and other interested parties in making decisions can pinpoint where to develop heat mitigation projects. By helping the City prioritize its actions, the map maximizes the efficiency of the City's efforts to become more resilient.

Urban heat vulnerability analysis is conducted to identify areas where high vulnerability to heat might be expected, i.e., focus on areas with higher urban heat vulnerability relative to baseline; in combination with selected heat vulnerability indicator attributes. Normalized score of exposure, sensitivity, adaptive capacity indices and heat vulnerability index for each kebele of the Dire Dawa City are summarized in below Table 4.10; the highest normalized score of heat vulnerability index presented in the below Tables 4.10 and Figure 4.17 represented the most vulnerable kebeles, while the lowest normalized score of heat vulnerability index symbolized the least vulnerable kebeles.

Table: 4.10 Normalized Exposure, Sensitivity and Adaptive Capacity layers

No.	Kebele Name	Exposure	Sensitivity	Adaptive Capacity		Heat Vulnerability index
		1	2	3	4	
1	kebele 01	0.58	0.06	0.01	0.59	0.31
2	kebele 02	1.00	0.99	0.21	0.26	0.61
3	kebele 03	0.26	0.11	0.12	0.00	0.12
4	kebele 04	0.03	0.16	0.15	0.90	0.31
5	kebele 05	0.01	0.05	0.30	0.69	0.26
6	kebele 06	0.00	0.00	1.00	0.99	0.50
7	kebele 07	0.48	0.23	0.94	0.86	0.63
8	kebele 08	0.29	0.46	0.34	0.83	0.48
9	kebele 09	0.35	1.00	0.00	1.00	0.59

Table Legend: mean land surface temperature change (1), the spatial distribution of population per kebele (2), vegetation abundance (3), Percentage of access to water (4).

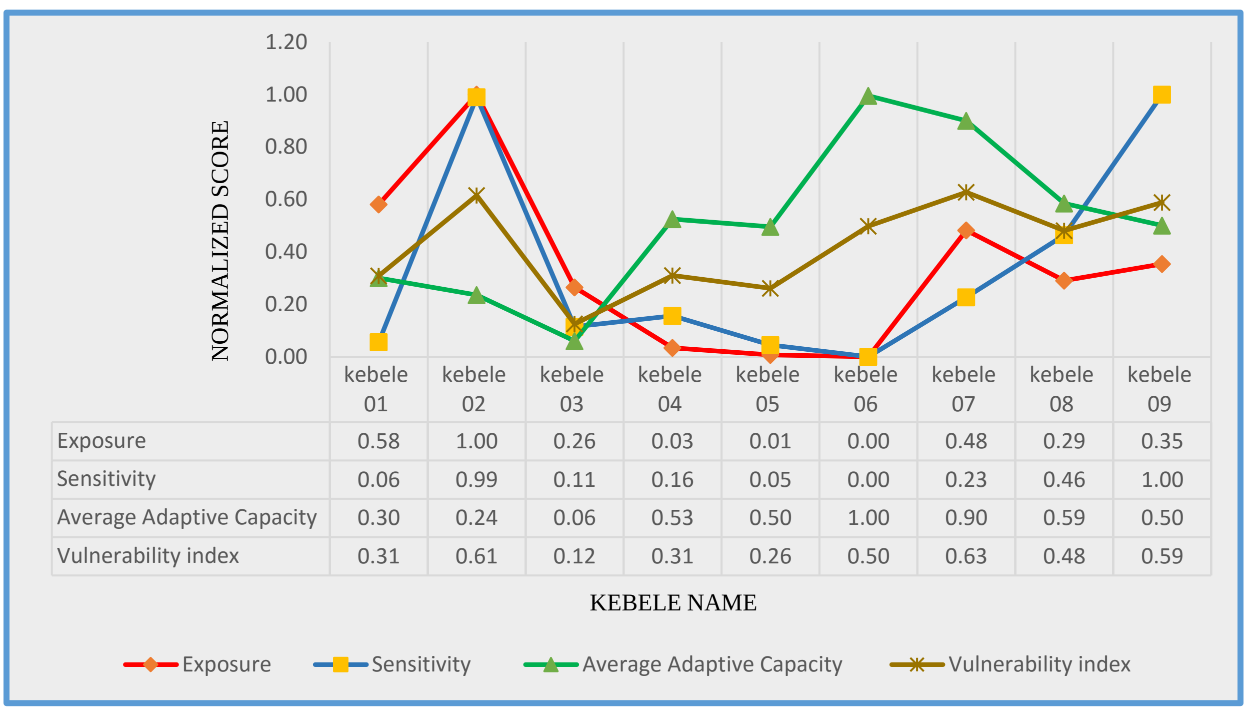

Figure: 4.17 Heat Vulnerability Index

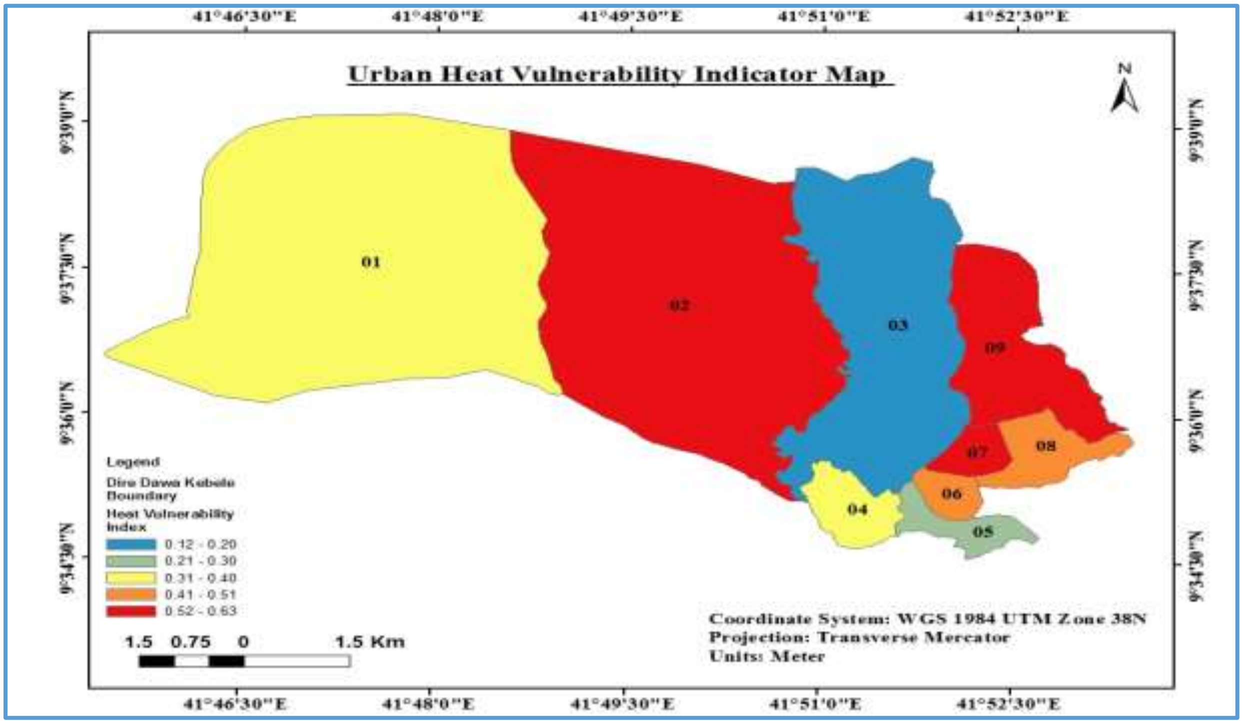

Figure: 4.18 Normalized and reclassified map of urban heat vulnerability indicator.

Relative heat vulnerability index, scores range from a lowest heat vulnerability score of 0.12 in kebele 03 (Kazira), goes to the highest heat vulnerability score of 0.63 found in kebele 07 (Afata Issah); the highest-scoring kebele are located towards the southeastern of the City. As the aggregated heat vulnerability index, shows the highest scores of heat vulnerability index is found in kebele 07 (Afata Issah) with 0.63 and followed by kebele 02 (Sabian) and kebele 09 (Ganda Gerada) with 0.61 and 0.59 respectively. Kebele 06 (Dechatu) and kebele 08 (Lege Hare) also have high values of HVI with 0.50 and 0.48. Then again, the medium heat vulnerability index scores were found in kebele 01 (Melka Jebdu) and kebele 04 (Ganda Kore) by having the same values 0.31. While, lower HVI scores were found in kebele 03(Kazira) and kebele 05 (Addis Katama) with values ranging from 0.12 to 0.26.

Generally, the highest urban heat vulnerability clusters are the result of higher exposure, higher sensitivity of the population to heat and lower adaptive capacity. By superimposing the heat vulnerability index, Kebele 07 (Afata Issah), kebele 02 (Sabian), kebele 09 (Ganda Gerada), Kebele 06 (Dechatu) and kebele 08 (Lege Hare) kebeles were identified as highly vulnerable to heat incidence. Urban heat vulnerability indicator maps are presented in below Figure 4.19.

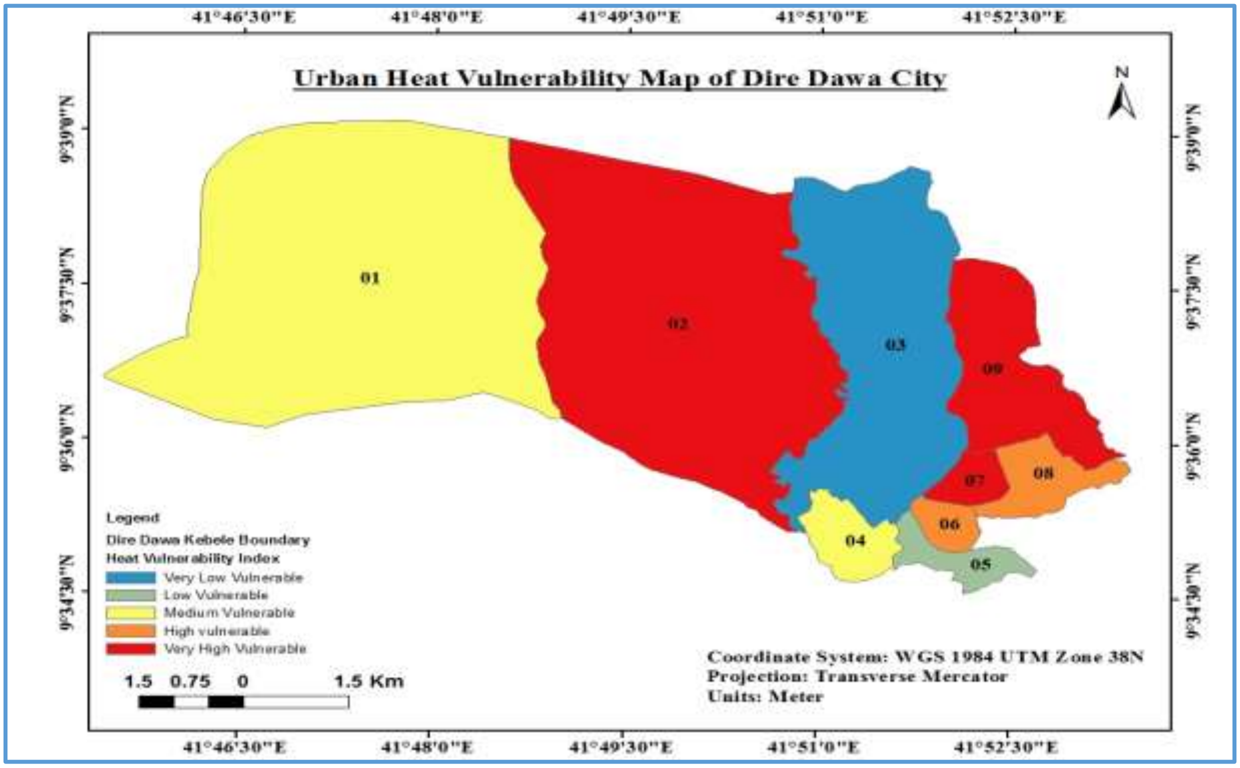

Figure: 4.19 Urban Heat Vulnerability Map of Dire Dawa City.

Urban heat vulnerability large concentration areas appeared in central portion of the city (e.g. kebele 02 (Sabian)) and also in eastern and southeastern part of the city; such as, kebele 07 (Afata Issah), kebele 09 (Ganda Gerada), kebele 06 (Dechatu) and kebele 08 (Lege Hare) have higher heat vulnerability. Eventually, the central and eastern parts of the City derive their high vulnerability from factors associated with high mean land surface temperature change and population density. Many studies have correlated urban areas with high temperatures, where dense populations (Reid et al., 2009); in another studies also, high population density has been shown to correlate with areas of higher temperatures (Coutts, *et al*., 2007). While, lower heat vulnerability were found in kebele 03 (Kazira) and kebele 05 (Addis Katama) located in the inner of the city and in southern areas of the city. Specially, in kebele 03 (Kazira) which is located in the inner region of the city more natural environment was well-preserved. This confirms those large green areas definitely have positive effect on reducing the temperature of surrounding areas.

CHAPTER V: CONCLUSIONS AND RECOMMENDATIONS

5.1. Conclusions

Landsat imageries are useful source of data to examine the spatio-temporal variation of land surface temperature with in relation to the land-use/land-cover change dynamics. The present study has used Landsat 5 TM, 1995 and Landsat 8 OLI/TIRS, 2020 images. The result shows that, for the last 25 years, the portion of land under built-up (settlement) area have shown significant expansion due to urban growth; a noticeable increase in built-up area exhibited a high change of surface temperature. On the other hand, bare land and sparse vegetation have shown decrease in territorial extent from 1995 to 2020. The shrinking of dense vegetation cover continuously worsens the thermal condition of the City, which contributes its part in increasing land surface temperature and air temperature.

Urban heat vulnerability is measured by the exposure level, sensitivity's strength and adaptive capacity. The finding of this study reveals that, for the last 25 years, between 1995 and 2020 the changes of mean land surface temperature over the cities were 6.07°C; due to higher mean land surface temperature change; there is higher level exposure. For instance the western part of the City kebele 02 (Sabian) and kebele 01 (Melka jebdu) and also, some eastern part of the city such as kebele 07 (Afata Issah) and kebele 09 (Ganda Gerada) was highly exposed to land surface temperature changes, again spatial distribution of population was higher on central and some eastern part of the City. Furthermore, limited green area coverage's, and also poor accessibility water of safe water leads kebele 08 (Lege Hare), kebele 07 (Afata Issah) and kebele 06 (Dechatu) to least adopted area.

Vulnerability to heat in Dire Dawa City is characterized by its spatial variability, In broad-spectrum, out of the total 9 kebele of the study area about 5 kebeles were identified as vulnerable area; there is strong statistical evidence for the clustering of high vulnerability areas in the western and eastern parts of the City; highest heat vulnerability are derived from factors associated with the raised land surface temperature, high population density, limited green area coverage's and poor accessibility of water. These altogether makes kebele 07 (Afata Issah), kebele 02 (Sabian), kebele 09 (Ganda Gerada), kebele 06 (Dechatu) and kebele 08 (Lege Hare) vulnerable to heat. Therefore, with the intention of reducing urban heat vulnerability increasing the accessibility of safe water and green space could help to improve human health, social wellbeing, and environmental quality.

5.2. Recommendations

❖ The incorporation of urban heat vulnerability responsive design strategies can helps to achieve the city's vision to be sustainable, livable, attractive and thriving city. Regarding urban heat vulnerability the finding showed that, most of western and northeastern regions and the southeastern portion of the city were more vulnerable to heat. This shows that these areas are indeed worthy of more attention from policymakers, who could formulate strategies that consider the actual situation of the Dire Dawa City to improve the well-being of residents.

❖ The high activity in urbanization which mainly focuses on house construction with little attention to urban green space development makes the land surface temperature changes higher overtime. If the condition continues without any intervention mechanism, the urban thermal comfort condition of the Dire Dawa City is under high influence. As a result, this study suggests, plans for reducing heat vulnerability could consider urban reforestation as a key role. Since, urban reforestation is the most powerful heat abatement strategy available to cities today. These studies also recommends that, paying attention to improve the accessibility of water on locations of having lowest accessibility of safe water, could be underlined to mitigate the adverse effects of urban heat vulnerability.

❖ Vulnerability mapping helps to target vulnerable hotspots and recommend appropriate interventions. The results of kebele scale vulnerability analysis are believed to be important for decision makers and a good starting point for different urban heat vulnerability study. However, it is recommended that detailed assessment of heat vulnerability at the smallest geographical unit (e.g. census tracts level) and then at national level can be done using more diverse indicators for further refinement of the result of this study.

REFERENCES

Abate, E. (2010). Anthropogenic impacts on groundwater resources in the urban environment of Dire Dawa, Ethiopia. In DUO – Digitale Utgivelser ved uio.

Abbasnia, M., and Toros, H. (2016). Future changes in maximum temperature using the statistical downscaling model (SDSM) at selected stations of Iran. model. earth syst. environ, 2, 1–7. https://doi.org/https://doi.org/10.1007

Abson, and Dougill, (2012). Using principal component analysis for information-rich socio-ecological vulnerability mapping in Southern Africa. appl geogr, 35, 515–524. https://doi.org/10.1016/j.apgeog.2012.08.004

Adger and Kelly,. (1999). Social vulnerability to climate change and the architecture of entitlements. mitigation and adaptation strategies for global change 4,. 253–266.

Adger, W. (2006). Vulnerability. glob environ chang., 16(3):, 268–281.

Ahmed.M (2015). Climate risks in megacities of the global south: focus on Dhaka, Bangladesh. in the “state of drr at the local level” a report on the patterns of disaster risk reduction at local level. Geneva, Switzerland, pp, (43),121–234.

Alaigba, Fabiyi, and Akinnawo, (2017). GIS in the assessment of the impact of microclimatic variables on. 7(1), 64–74.

Alexander, Eric and Michael, J. (2010). Climate change and urban water utilities: challenges & opportunist. water p-notes, world bank report. no. 50; 55828(1), 1-4.

Artis, and Carnahan. (1982). Survey of emissivity variability in thermography of urban areas. remote sensing of environment, 313–329.

Asubonteng. (2007). Identification of land use/cover transfer hotspots in the Ejisu-Juabeng.

Aubrecht and Ozceylan, D. (2013). Identification of heat risk patterns in the U.S. National Capital region by integrating heat stress and related vulnerability. environ. int., 56, 65–77.

Azhar, G. (2017). Heat wave vulnerability mapping for India. environ. res. public health, 14, 10.

Baklanov, Molina, and Gauss. (2016). Megacities, air quality and climate. atmospheric environment, 235–49.

Bao, Li and Yu. (2015). The construction and validation of the heat vulnerability index , a review. 7220–7234. https://doi.org/10.3390/ijerph120707220

Bauer and Coppin (1996). Digital change detection in forest ecosystems with remote sensing imagery. remote sensing reviews, 13(3-4), 207–234.

Bekele, T. (2019). Groundwater potential zone delineation using gis and remote sensing techniques in Sululta and surrounding watershed , Ethiopia.

Beyene, A. (2016). Precipitation and temperature trend analysis in Mekelle city, Northern Ethiopia, the case of Illala meteorological station. earth sci clim change, 7:1. http://dx.doi.org/ 10.4172/2157-7617.1000324

Bolund.(2015). Rotterdam programme on sustainability and climate change 2015-2018; City of Rotterdam: Netherlands, 2015, 1-12.

Brooks, Adger and Kelly,. (2005). The determinants of vulnerability and adaptive capacity at the national level and the implications for adaptation. glob. environ. chang. 15, 151–163.

Brooks, N. (2003). Vulnerability, risk and adaptation: a conceptual framework. tyndall centre for climate change research, (working paper 38,).

Buytaert and Bievre. (2012). Water for Cities: the impact of climate change and demographic growth in the tropical. water resources research, 48(8). http://doi.org/10.1029/2011wr011755.

Chang and Akpina, (2014) Effects of urban parks on the local urban thermal environment. urban for. urban green. urban for. urban green13, 672–681, 1-19.

Chemonics International. (2015). Climate variability and change in Ethiopia summary of findings. prepared for United States Agency for International Development Climate Change Adaptation Thought Leadership and Assessments (ATLAS).

Chen, X. (2000). Using RS and GIS to analyze land-cover change and its impacts on the regional sustainable development. international journal remote sensing. (23), 107–113.

Chow, Chuang and Gober, P. (2012). Vulnerability to extreme heat in metropolitan Phoenix: spatial, temporal, and demographic dimensions. prof. geogr., 64, 286–302.

Cisneros, Andrea, Laura, and Cintia, (2018). Spatial and temporal analysis of the LST-NDVI relationship for the study of land cover changes and their contribution to urban planning in Monte. 64, 25–47.

Conlon, Mallen, Gronlund, Berrocal, Larsen, and Neill, M. (2020). Mapping human vulnerability to extreme heat : a critical assessment of heat vulnerability indices created using principal components analysis. 128(september).

Conway and Schipper, (2011). Adaptation to climate change in Ethiopia: 21(1) (opportunities identified from Ethiopia, global environmental change), 227–237. https://doi.org/10.1016/

Coppin, B. (1996). Digital change detection in forest ecosystems with remote sensing imagery. remote sensing reviews, 13(3-4), 207–234.

Cutter, Carolina, Boruff, Carolina, Shirley, and Carolina, S. (2003). Social vulnerability to environmental hazards n. 84(2).

D.D.A.I.D.P. (2012). Dire Dawa Administrative Council Integrated Resource Development Master Plan Study Project.

D.D.A.S.B. (2013). Dire Dawa Adminstration Statistical Bureau,Dire Dawa Adminstration Statistical Abstract(2007-2037).

DDAADO. (2018). Dire Dawa Administrative Agricultural Development Office.

DDEPA. (2019). Dire Dawa Environmental Protection Authority. In international journal.

Ding, and Shi, W. (2013). Land-use/land-cover change and its influence on surface temperature: A case study in Beijing City. int. j. remote sens. 34, 5503–5517.

Doan and Kusaka. (2016). Numerical study on regional climate change due to the rapid urbanization of greater Ho Chi Minh City's. .int. j. climatol, 36, 3633–3650.

Doll, P. (2009). Vulnerability to the impact of climate change on renewable groundwater resources:environmentalresource.lett.4(1).,aglobal-scaleassessment. https://doi.org/ 10.1088/ 1748-9326/4/3/035006

Dong, Liu, Zhang, Tang, Liao, and Li,. (2014). Assessing heat health risk for sustainability in Beijing's urban heat island. sustainability, 6, 7334–7357.

EDHS. (2014). Ethiopia Demography Health Survey.

ESRI.(2016). Environmental Systems Research Institute; arcgis desktop help 10.4. Redlands, CA.

Farina, A. (2012). Exploring the relationship between land surface temperature and vegetation abundance for urban heat island mitigation in Seville , Spain. 15.

FDRE Ministry of Health. (2015). Federal Democratic Republic of Ethiopia Ministry of Health vulnerability and adaptation assessment of health to climate change in ethiopia final report. september.

Feizizadeh, Blaschke, Nazmfar, Akbari, and Kohbanani, H. (2013). Monitoring land surface temperature relationship to land use/ land cover from satellite imagery in Maraqeh County, Iran. journal of environmental planning management.

Fekete, (2012). Spatial disaster vulnerability and risk assessments: challenges in their quality and acceptance. natural hazards, 61(3), 1161-1178. retrieved from 10.1007s11069-011-9973-7.

Feyissa, N. (2019). Climate change trends , projections and vulnerability integration to enhance urban resilience planning : the case of Addis Ababa City.

Fussel and Klien. (2006). Climate change vulnerability assessments: an evolution of conceptual thinking,", 75(3):(climatic change), 301–329.

Gebrekidan, W. (2016). Modeling land surface temperature from satellite data, the case of Addis Ababa. ESRI, Eastern Africa education GIS conference. held at Africa hall, United Nations conference center from23-24 sept. 2016, Addis Ababa.

Gizachew and Shimelis, (2014). Analysis and mapping of climate change risk and vulnerability in central rift valley of ethiopia. African crop science, 22(vi), 807–818.

Guo, Huang, and Jia,. (2019). Estimating fine-scale heat vulnerability in Beijing through two approaches : spatial patterns , similarities , and divergence.

Hagenlocher, Lang, Holbling, Tiede and Kienberger, (2013). Modeling hotspots of climate change in the Sahel using object-based regionalization of multidimensional gridded datasets. ieee journal of selected topics in applied earth observations and remote sensing.

Hajat and Kosatky. (2010). Heat-related mortality: a review and exploration of heterogeneity. epidemiol commun, 753–760.

Hanak and Lund, (2011). Adapting California’s water management to climate change. climatic change, 28. http://doi.org 10.1007/s10584-011-0241-3.

Harlan, Declet-Barreto, Stefanov and Petitti, (2013). Neighborhood effects on heat deaths: social and environmental predictors of vulnerability in Maricopa County, Arizona. environ., 121,(health perspect.), 197–204.

Harlan, Brazel, Prashad and Stefanov (2006). Neighborhood microclimates and vulnerability to heat stress. soc sci med, 63:, 2847-2863.

Haylemariyam, M. (2018). Detection of land surface temperature in relation to land use land. journal of remote sensing & gis, 7(3). https://doi.org/10.4172/2469-4134.1000245

Hinkel, J. (2011). Indicators of vulnerability and adaptive capacity: towards a clarification of the science– policy interface. global environmental change, 21(1), 198-208.

Honjo and Takakura, (1990). Simulation of thermal effects of urban reen areas on their surrounding areas. energy build, 16, 443–446. https://doi.org/doi:10.1016/1212-f,

Huang, Zhou and Cadenasso, (2011). Is everyone hot in the City? spatial pattern of land surface temperatures, land cover and neighborhood socioeconomic characteristics in Baltimore. environmental manag, 92, 1753–1759.

Hunt, A., and Watkiss, P. (2010). Climate change impacts and adaptation in cities: a review of the literature. climatic change, 104(1), 13–49. https://doi.org/10.1007/s10584-010-9975-6.

Ilestari, Dewi, Pratama, Bramono, Nurvaridzi, and Widyatmanti, (2018). Utilization of remote sensing and GIS to identify radius of urban cool island for planning open green area in urban area (case study of Yogyakarta). iop publishing, 169(iop conference series :earth and environmental science). https://doi.org/doi :10.1088/1755-1315/169/1/012005

Ichinose, T. and Bai, Y. (2000). Anthropogenic heat emission in Shanghai City. 28(proceedings of annual meeting of environmental systems research), 329 –337.

IDP. (2006). Integrated Development Program. International Journal.

Inostroza, Palme, and Barrera, (2016). A heat vulnerability index : spatial patterns of exposure , sensitivity and adaptive capacity for Santiago de Chile. 1–26. https://doi.org/10.1371/journal.pone.0162464

IPCC. (2014a). Climate change. impacts, adaptation, and vulnerability WGII. AR5 summary for policymakers. 2014.

IPCC. (2014b). Contribution of working group II to the fifth assessment report of the intergovernmental panel on climate change.

Janicke, Holtmann, Kim, Kang, and Fehrenbach, (2018). "Quantification and evaluation of intra-urban heat-stress variability in Seoul, Korea,." int journal of biometeorology, 63, n, 1–12,.

Jeevalakshmi, D. (2017). Land surface temperature retrieval from landsat data using emissivity estimation. 12(20), 9679–9687.

Jenerette, (2016). Micro-scale urban surface temperatures are related to land-cover features and residential heat related health impacts in Phoenix, AZ USA. landsc. ecol, 31, 745–760.

Jifar, A.(2020). Analyzing the effect of optimizing the spatial locations of green infrastructure on land surface temperature: the case of Dire Dawa City.

Jovanovska and Ugur Avdan (2016). "Automated mapping of land surface temperature using landsat 8 satellite data",. journal of sensors,.

Juntao Tan and Hung. (2018). Assessment with satellite data of the urban heat island effects in Asian mega Cities. int. j. appl. earth obs. geoinf. 2006, 34–48.

Kelly, P Mick, and Neil Adger. (2000). Theory and practice in assessing vulnerability to climate change and facilitating adaptation. 4(climatic change), 325–352.

Kienberger, S., Hagenlocher, M., and Zeil, P. (2013). Mapping hotspots of vulnerability to vector-borne diseases in East Africa. paper presented at the presentation at the global geospatial conference, Addis Ababa, Ethiopia.

Klok, Zwart, Verhagen, and Mauri, E. 2012). The surface heat island of Rotterdam and its relationship with urban surface characteristics. resources, 64, 23–29.

Kok, Lüdeke, Sterzel, Lucas, Walter, Janssen, and de Soysa, I. (2010). Quantitative analysis of patterns of vulnerability to global environmental change: Netherlands environmental assessment agency.

Kovats and Osborn. (2016). UK climate change risk assessment evidence report; people and the built environment: report prepared for the adaptation sub-committee of the committee on climate change London.

Kuang, Dou, Zhang, Chi, Liu, Zhang and Liu, J. (2015). Quantifying the heat flux regulation of metropolitan land use/land cover components by coupling remote sensing modeling with in situ measurement. 120, 113–130. j. geophys. res. atmos.

Lambin, Turner, Geist, Agbola, Angelsen, Bruce and George,. (2001). The causes of land-use and land-cover change: moving beyond the myths. global environmental change, 11(4), 261–269.

Landsat Project Science Office. (2001). Landsat science data user's handbook (goddard space flight center). available online at: http://landsathandbook.gsfc.nasa.gov/handbook handbook_htmls chapter11/chapter11.html (accessed 21 april 2021).

Lang, Zeil, Kienberger and Tiede, D. (2008). Geons – policy-relevant geo-objects for monitoring high-level indicators. paper presented at the geospatial crossroads @ gi_forum. proceedings of the second geoinformatics forum, Salzburg, Germany.

Legates and Willmott, (1990). Mean seasonal and spatial variability in global surface air temperature. theoretical and applied climatology, 41(1), 11–21.

Lindley, O'Neill, Kandeh, Lawson, Christian, and O'Neill. (2011). Climate change, justice and vulnerability. in joseph rowntree foundation.

Loughnan, Tapper, Phan, Lynch, and Mcinnes,. (2013).Vulnerability analysis of urban populations during extreme heat events in Australian capital cities. in national climate change adaptation research facility, Gold Coast.

Ludena, Carlos Sánchez-aragón, and Leonardo Miller, (2015). Local vulnerability indicators and adaptation to climate change. https://doi.org/(idb-tn857)

Luis, Massimo, and Francisco. (2016). A Heat Vulnerability Index: spatial patterns of exposure, sensitivity and adaptive capacity for Santiago de Chile. 11(9). https://doi.org/10.1371/ journal.pone.0162464

Ma, Kuang, and Ningsheng, H. (2010). Coupling urbanization analysis for studying urban thermal environment and its interplay with biophysical parameters based on TM/ETM+ imagery. international journal of applied earth observation and geoinformation, 12, 110118.

Maas, R. (2008). Vitamine G, Green environments - Healthy environments. Phd thesis.

Maggino, and Zumbo, (2012). Measuring the quality of life and the construction of social indicators. michalos and sirgy (eds.), handbook of social indicators and quality of life research (pp. 201-238): springer netherlands. retrieved from http://dx.doi.org.

Maktav and Erbek (2005). Remote sensing of urban areas. international journal of remote sensing, 26:, 655-659.

Mccarty J, Leary O, Dokken N, (2001). Climate change 2001: impacts, adaptation, and vulnerability. contribution of working group II to the third assessment report of the intergovernmental panel on climate change.

Mcsweeney, New and Lizcano, G. (2010). General climate. Ethiopia, UNDP climate change country profiles ethiopia, 1–27. http://country-profiles.geog.ox.ac.uk

Medhin Shimelis, (2017). Gis based systematized water distribution network asset management system: case Of Harar Town, Ethiopia.

Menezes, Confalonieri, Madureira and De, I. (2018). Mapping human vulnerability to climate change in the Brazilian Amazon : the construction of a municipal vulnerability index. 1–30.

Mihai, V. (2012). Using satellite images landsat TM for calculating Normalized Difference Indexes for the landscape of Parang mountains.Lect.Ph.D.Eng.Banat University of agricultural sciences and veterinary medicine, Romania.

Mohan, M. and Pathan, S. (2011). Dynamics of urbanization and its impact on LULC: a casestudy of megacity Delhi. journal of environmental protection 2: 1274-1283.

Mulugeta, M., Tolossaa, D., and Abebe, G. (2017). Description of long-term climate data in Eastern and Southeastern Ethiopia. 26-36. https://doi.org/https://doi.org/10.1016/

Mutiibwa, Kilic and Irmak, S. (2014). The effect of land cover/land use changes on the regional climate of the USA high plains. 2(climate), 153–167. https://doi.org/https://doi.org/10.3390/

National Meteorological Agency (2020) Applied meteorological services case team climate information for the health sector may _ 2020; Ethiopia.

Ndetto and Matzarakis. (2013). Basic analysis of climate and urban bioclimate of Dar es Salaam, Tanzania. theoretical and applied climatology, 114, 213-226.

NMA. (2007a). National Adaptation Programme of Action of Ethiopia (NAPA).final draft report. National Meteorological Agency, Addis Ababa.

NMA. (2007b). National Meteorological Agency;Ethiopia.

Norton, Coutts, Livesley, Harris, Hunter, and Williams, (2015). Planning for cooler Cities: urban plan, 134(a framework to prioritise green infrastructure to mitigate high temperatures in urban landscapes.), 127–138.

O’Brien, Leichenko, Kelkar, Venema, Aandahl, and Tompkins,.(2004). Mapping vulnerability to multiple stressors: climate change and globalization in India. glob environ chang., 14(4):, 303-13.

Odindi, Bangamwabo and Mutanga,. (2015). Assessing the value of urban green spaces in mitigating multi-seasonal urban heat using MODIS land surface temperature (LST) and Landsat 8 data. 9(1), 9–18.

Ozceylan, D and Coskun, E. (2012). The relationship between Turkey’s provinces’ development levels and social and economic vulnerability to disasters. j. homel. secur. emerg. 9, doi 10.1515/1547-7355.1981.

Panahi,(2013). The relationship between NDVI and LST in urban area of Mashhad,. international conference on civil engineering architecture & urban sustainable development, 7.

Pansi, and Yang, L. (2015). Monitoring land use and land-cover change in the Eastern Gulf Coastal plain using multi tempora landsat imagery. j geophys remote sens, 9-14.

Prata. (1999). Thermal remote sensing of land surface temperature fromsatellites: status and future prospects. remote sensing rev., 12, 175–223.

Qin, Karnieli, and Berliner,. (2001). A mono-window algorithm for retrieving land surface temperature from landsat data and its application to the Israel-Eqypt border region. international journal of remote sensing, 22, 3719-3746.

Rahmana, M. (2016). Land use and land cover changes and urban sprawl in Riyadh, Saudi Arabia: an analysis using multi-temporal landsat data and shannon’s entropy index. the international archives of the photogrammetry, remote sensing and spatial information sciences, xli-b8,.

Rasul and Ibrahim, F. (2017). Urban land use land cover changes and their effect on land surface temperature : case study using Dohuk City in the Kurdistan region of Iraq. https://doi.org/10.3390/cli5010013

Reid, O’Neill, Gronlund, Brines, Brown, Diez-Roux, and Schwartz. (2009). Mapping community determinants of heat vulnerability. environ, 117(health perspect), 1730–1736.

Rinner, Patychuk, Bassil, Nasr, S., and Gower, S. (2010). The role of maps in neighborhood-level heat vulnerability assessment for the city of Toronto. geogr. inf. sci., 37, 31–44.

Rizwan, Dennis, and Chunho. (2008). A review on the generation, determination and mitigation of urban heat island. journal of environmental sciences, 120–8.

Romero-lankao, Patricia, Qin, H., and Dickinson, K. (2012). Urban vulnerability to temperature-related hazards : a meta-analysis and meta-knowledge approach. global environmental change, 22(3), 670–683. https://doi.org/10.1016/j.gloenvcha.2012.04.002

Sabelli. (2011). Scale counts: a review of indicator-based climate change vulnerability assessments. cidade do Panamaâ.

Santamouris, C. (2017). The role of green spaces in energy and climate in the urban built environment. USA, 2001; northeast institute of geography and agroecology, Chinese academy of sciences, changchun 130102,mdpi, 1-19.

Satterthwaite, Aragón-Durand, Corfee-Morlot, Kiunsi, Pelling, Roberts, and Solecki (2014). climate change impacts, adaptation, and vulnerability in urban areas. Part A: global and sectoral aspects. contribution of working group II to the fifth assessment report of the intergovernmental panel on climate change. Cambridge University Press, Cambridge, United Kingdom and New York, NY, USA,.

Schiller, Andrew, de Sherbinin, Alex, Hsieh, W., and Pulsipher, A. (2001). The vulnerability of global cities to climate hazards open meeting of the human dimensions of global environmental change research community. Rio de Janeiro, Brazil.

Sherbinin. (2014). Spatial climate change vulnerability assessments : a review of data , methods , and issues african and latin american resilience to climate change (issue august).

Siti Zakiah, (2004). The influence of urban heat towards pedestrian comfort and the potential use of plants and water as heat ameliorator in Kuala Lumpur City centre area, MSc. Thesis, University Putra Malaysia, Selangor, Malaysia.

Smit Barry, and johanna wandel. (2006). Adaptation , adaptive capacity and vulnerability. 16, 282–292. https://doi.org/10.1016/j.gloenvcha.2006.03.008

Sobrino, Jimenez-Munoz, and Paolini,. (2004). Land surface temperature retrieval from Landsat TM 5. remote sensing of environment, 90, 434-440.

Spronken-Smith, Oke, and Lowry,. (2001). Advection and the surface energy balance across an irrigated urban park. inter. journal of climatology, 20(9), 1033–1047.

Stone. (2012). The City and the coming climate: climate change in the places we live. Cambridge university press. https://doi.org/10.1017/cbo9781139061353.

Strand, Tong, Aird and McRae (2010). "Vulnerability of eco-environmental health to climate change: BMC public health, the views of government stakeholders and other specialists in queensland, 441-450.

Sun, Hurley, Amati, Arundel, Saunders, and Boruff,. (2019). Urban vegetation, urban heat islands and heat vulnerability assessment in Melbourne, clean air and urban landscapes hub, Melbourne, Australia.

Tafesse, B. (2017). Impact of land-use / land-cover changes on land surface temperature in adama zuria woreda , ethiopia , using geospatial tools.

Tan J: (2008). Commentary: people's vulnerability to heat wave. int j epidemiol, 37:, 318-320.

Tan, Zheng, Song, Kalkstein, Kalkstein, and Tang,. (2007). Heat wave impacts on mortality in Shanghai, 1998 and 2003. international journal of biometeorology, 193–200.

Tapsell, Penning-Rowsell, Tunstall, and Wilson,. (2002). Vulnerability to flooding: philos. trans. r. soc., 360 (health and social dimensions.), 1511–1525.

Tate, E. (2012). Social vulnerability indices: a comparative assessment using uncertainty and sensitivity analysis. natural hazards, 63, 325-347. retrieved from http://dx.doi.org/10.1007 s11069-0120152-2.

Tomlinson, Chapman, Thornes, and Baker,. (2011). Including the urban heat island in spatial heat health risk assessment strategies : a case study for Birmingham, UK. int. j. health geogr., 1–14. https://doi.org/doi:10.1186/1476-072x-10-42.

Tong and XuCheng. (2018). Heat wave and health events: a systematic evaluation of different temperature indicators, heatwave intensities. sci. total environ. 630,679–689.

Toy and Yilmaz,. (2007). Determination of bioclimatic comfort in three different land uses in the City of Erzurum, Turkey. 42(3)(building and environment), 1315–1318.

Turvey, R. (2007). Vulnerability assessment of developing countries: the case of small-island developing states. dev. policy rev., 25, 243–264.

Uejio, Wilhelmi, Golden, Mills, Gulino, and Samenow,. (2011). Health and place intra-urban societal vulnerability to extreme heat : the role of heat exposure and the built environment , socioeconomics, and neighborhood stability. 17, 498–507. https://doi.org/10.1016/j.

UNDP.(1999). United Nations Development Programme. New York: Human Development Index.

UNDP. (2006). United Nations Development Programme. human development report beyond scarcity: power, poverty and global water crisis. http://hdr.undp.org/sites/default/files/reports/267/hdr06-complete.pdf.

UNFCCC. (1992). United Nations Framework Convention on Climate Change.

Vescovi, Rebetez, and Rong, F. (2005). Assessing public health risk due to extremely high temperature events: clim. res., 30(climate and social parameters.), 71–78.

Vincent, K. (2007). Uncertainty in adaptive capacity and the importance of scale. global environmental change, 17(1), 12-24. http://dx.doi.org/10.1016/j.gloenvcha.2006.11.009.

Yue, Liu, and Zhou, (2019). Impacts of urban configuration on urban heat island. science of total environment, 671(an empirical study in China mega-cities), 1036–1046.

Weng, and Schubring, J. (2004). Estimation of land surface temperature–vegetation abundance relationship for urban heat island studies. remote sensing of environment, 89(4), 467– 483.

Weng. (2017). Responses of urban heat island in atlanta to different land-use scenarios. theor. appl. climatol., 1–13.

Wilhelmi, Purvis, and Harriss. (2004). Designing a geospatial information infrastructure for the mitigation of heat wave hazards in urban areas. natural hazards review, 147–58.

Wilhelmi, and Hayden (2010). Connecting people and place : a new framework for reducing urban vulnerability to extreme heat. 2010–2017. https://doi.org/10.1088/1748-9326/5/1/014021

WMO. (2020). World meteorological organization "what is the difference between climate variability and climate change." (accessed 20 th of october 2020). https://doi.org/ http://www.wmo.int/pages/prog/wcp/ccl/faqs.php

Wolf, mcgregor, and Analitis. (2014). Performance assessment of a heat wave vulnerability index for greater London,. United Kingdom weather climate society, 32–46.

Wolf, Chuang, and Mcgregor,. (2015). Do spatial heat vulnerability assessment studies influence policy ? 13321–13349. https://doi.org/10.3390/ ijerph 12101 33 21

Wolf, and Mcgregor,. (2013). The development of a heat wave vulnerability index for London , United Kingdom. weather and climate extremes, 1, 59–68. https://doi.org /10.1016/j.wace. 2013.07.004

Woodruff, Vitro, and bendor,. (2017). GIS and coastal vulnerability to climate change. university of North Carolina at Chapel Hill, Chapel Hill, NC, United States. 236-257. https://doi.org/ 10.1016 b978-0-12-409548-9.09655-x.

Yamin, (2005). "Vulnerability, adaptation and climate disasters: a conceptual overview." in ids bulletin 36, no. 4:1. (vol. 36).

Yang, Gong, Fu, Zhang, Chen, and Liang,. (2013). The role of satellite remote sensing in climate change studies. natural hazards review, 875–883. https://doi.org/10. 1038/nclimate1908

Yip, Flanders, Wolkin, Engelthaler, Humble, Neri, Lewis, Backer, and Rubin. (2008). The impact of excess heat events in Maricopa County, Arizona: 2000–2005. international journal of biometeorology, 52(8), 765–772.

Yohe, G., and Tol, R. (2002). Indicators for social and economic coping capacity—moving toward a working definition of adaptive capacity. global environmental change , 12, 25–40.

Younes zadeh, S., Amiri N, and Pilesjo, P. (2015). The effect of land use change on land surface temperature in the Netherlands. the international archives of the photogrammetry, remote sensing and spatial information sciences, xl-1/w5, 745-748.

Yuan and Bauer. (2007). Comparison of impervious surface area and NDVI as indicators of surface urban heat island effects. remote sensing of environment, 106, 375-386.

Zhang, and Murray, (2017). Optimizing green space locations to reduce daytime and nighttime urban heat island e ff ects in Phoenix , Arizona. landscape and urban planning, 165(april 2018), 162–171. https://doi.org/10.1016/j.landurbplan.2017.04.009

Zhao, H., Ren, Z., and Tan, J. (2014). The spatial patterns of land surface temperature and its impact factors : spatial non-stationarity and scale effects based on a geographically-weighted regression model. https://doi.org/10.3390/su10072242

Zhu, Liu, Lin, Xiao, Luo, Zeng, Zeng, Wei, Chu, and Baum. (2014). The spatial distribution of health vulnerability to heat waves in Guangdong Province, China. global health action. https://doi.org/10.3402

APPENDICES

1: Monthly, maximum, minimum and mean temperature of Dire Dawa City from 1995 and 2020

1995												
Month	Jan.	Feb.	Mar.	Apr.	May	Jun	Jul.	Aug.	Sep.	Oct.	Nov.	Dec.
Min	13.50	null	18.79	20.50	22.15	22.85	20.79	20.63	21.29	19.58	16.18	16.84
Max	28.67	null	30.18	31.41	35.09	36.06	33.50	33.00	33.98	33.17	31.16	29.63
Av.Temp.	21.09	Null	24.49	25.96	28.62	29.46	27.15	26.82	27.64	26.38	23.67	23.23
2020												
Month's	Jan.	Feb.	Mar	Apr.	May	Jun	Jul.	Aug.	Sep.	Oct.	Nov.	Dec.
Min.	15.5	17.5	19.9	21	22.2	23.2	20	20.9	20.2	18.9	15.7	14.4
Max	28.3	31	32.9	30.5	33.8	35.2	29.2	32.4	32.1	34.3	31.6	30.1
Av.Temp.	25.2	26.8	28.6	26.8	30.1	30.5	26	26.4	26	26.8	23.7	22.4

[**Source**: (Meteorological station, 2020)]

2: The distribution of population over the Dire Dawa City

No.	Kebele Name	Area in Km^2	Population distribution per Kebele		Population distribution change	Population density per Kebele		Population density change
			1995	**2020**	**(1995 - 2020)**	**1995**	**2020**	**(1995 - 2020)**
1	kebele 01	25.09	9033	25156	16123	360	1003	643
2	kebele 02	21.17	37565	61156	23591	1774	2889	1114
3	kebele 03	11.82	15112	27440	12328	1279	2321	1043
4	kebele 04	1.48	15996	29045	13049	10808	19625	8817
5	kebele 05	1.11	13633	24754	11121	12282	22301	10019
6	kebele 06	0.69	12670	23007	10337	18362	33343	14981
7	kebele 07	0.8	17482	31742	14260	21853	39678	17825
8	kebele 08	1.65	22525	40901	18376	13652	24788	11137
9	kebele 09	4.87	33235	61559	28324	6824	12640	5816

(Source: Based on data from, Dire Dawa City Central statistical Agency)

3: Coordinates of Sampled Locations within Dire Dawa City

LULC	Sample Location	EASTING_X	NORTHING_Y
Built Up Area	Oil libya Fuel Station	813715	1060947
	Niyala Hotels	814549	1061180
	meseret Pension	813859	1060600
	Dashen Banks	814509	1061208
	Jumma mosque	814782	1061177
	Tiawan indoor market	814743	1061809
	Dechatu bridge	814242	1061363
	Dire dawa palace	814037	1061330
	Mekonen bar and hotel	814019	1061628
	Besrate Gebriel	814439	1061901
	Post office	814060	1061645
	Dire Dawa Health bureau	813572	1061080
	Dire Dawa administration Council	814103	1062481
	Bilal Hospital	814498	1061305
	old resident Around Bilal Hospital	814483	1061335
	old resident Around Bilal Hospital 3	814595	1061270
	Education and civil service bureau (old building)	814153	1061721
	Garad commercial building	814487	1061143
	Cotton factory	816308	1062431
	Ethiopian Electric corporation	813598	1060418
	Ras-Hotel	813777	1061009
Bare Land	Prime minister Melezenawi Memorial park	813603	1063286
	New Referral Hospital	809097	1063723
	Ashewa market	814756	1062097
	Industrial zone	807885	1064530
	Defence Hospital	810042	1062950
	Christian cemetery	815053	1063404
	Christian cemetery	815070	1063778
	Dire Itl Air Port	813068	1064989
	Kefira open market	814503	1060587
	Around Dire Dawa university	812153	1064754
	franch Hospital	813415	1061197
Green Infrustructure	Tell communication (Kazira)	813891	1061406
	Cinima Empire (Tou info centr)	813654	1061300
	Goro green Area	812445	1061096
	Ethiopia Airline Ticket office(kazira)	814126	1061457
	Bus station trees	814089	1060790
	Dilchora Hospital	813848	1060949
	Prince Makonen palace	813677	1060998
	old cement factory	812450	1061529
	Pioneer Cement factory	805286	1062925
	Ture Cement factory	805886	1062956
	Balian Crematorium	816519	1061682
	Bangalo Recretional center	812813	1061901
	Millennium park	813933	1062772

4: Classification accuracy assessment report for the year 1995.

```
CLASSIFICATION ACCURACY ASSESSMENT REPORT LULC- 1995
                ----------------------------------------
Image File : c:/users/desktop/1995-image/1995-lulc-class.img
User Name  : User_Habtamu Lensha
Date       : Tue June 01 12:17:35 2021

ERROR MATRIX
-------------
ACCURACY TOTALS
----------------

         Class         Reference  Classified    Number    Producers     Users
          Name          Totals      Totals      Correct    Accuracy     Accuracy
    ----------     ----------  ----------   -------     ---------    --------
    Bare land           12          12         10        83.33        83.33
    Sparse Vegetation   26          27         24        92.31        88.89
    Built Up            22          22         20        90.91        90.91
    Shrub Land          20          19         16        80.00        84.21
        Totals          80          80         70

Overall Classification Accuracy = 87.50%
       ----- End of Accuracy Totals -----
KAPPA (K^) STATISTICS
---------------------
 Overall Kappa Statistics = 0.8637%
 Conditional Kappa for each Category.
  ------------------------------------
  Class Name          Kappa
   ----------         -----
 Unclassified         0.0000
 Bare land            0.8567
 Sparse Vegetation    0.8607
 Biult Up             0.8579
 Shrub Land           0.8516
      ----- End of Kappa Statistics -----
```

5: Classification accuracy assessment report for the year 2020.

CLASSIFICATION ACCURACY ASSESSMENT REPORT LULC- 2020

Image File : c:/users/desktop/2020-image/2020-lulc-class.img
User Name : User_Habtamu Lensha
Date : Sun June 18 16:35:55 2021

ERROR MATRIX

ACCURACY TOTALS

Class Name	Reference Totals	Classified Totals	Number Correct	Producers Accuracy	Users Accuracy
Bare land	14	13	12	85.71	92.31
Sparse Vegetation	20	19	17	85.00	89.47
Built Up	22	23	21	95.45	91.30
Shrub Land	24	25	23	95.83	92.00
Totals	80	80	73		

Overall Classification Accuracy = 91.25%

----- End of Accuracy Totals -----

KAPPA (K^) STATISTICS

Overall Kappa Statistics = 0.8937%

Conditional Kappa for each Category.

Class Name	Kappa
Unclassified	0.0000
Bare land	0.8768
Sparse Vegetation	0.8607
Biult Up	0.8879
Shrub Land	0.8569

----- End of Kappa Statistics -----

6: Spatial distribution of population maps in Dire Dawa City for the year 2020.

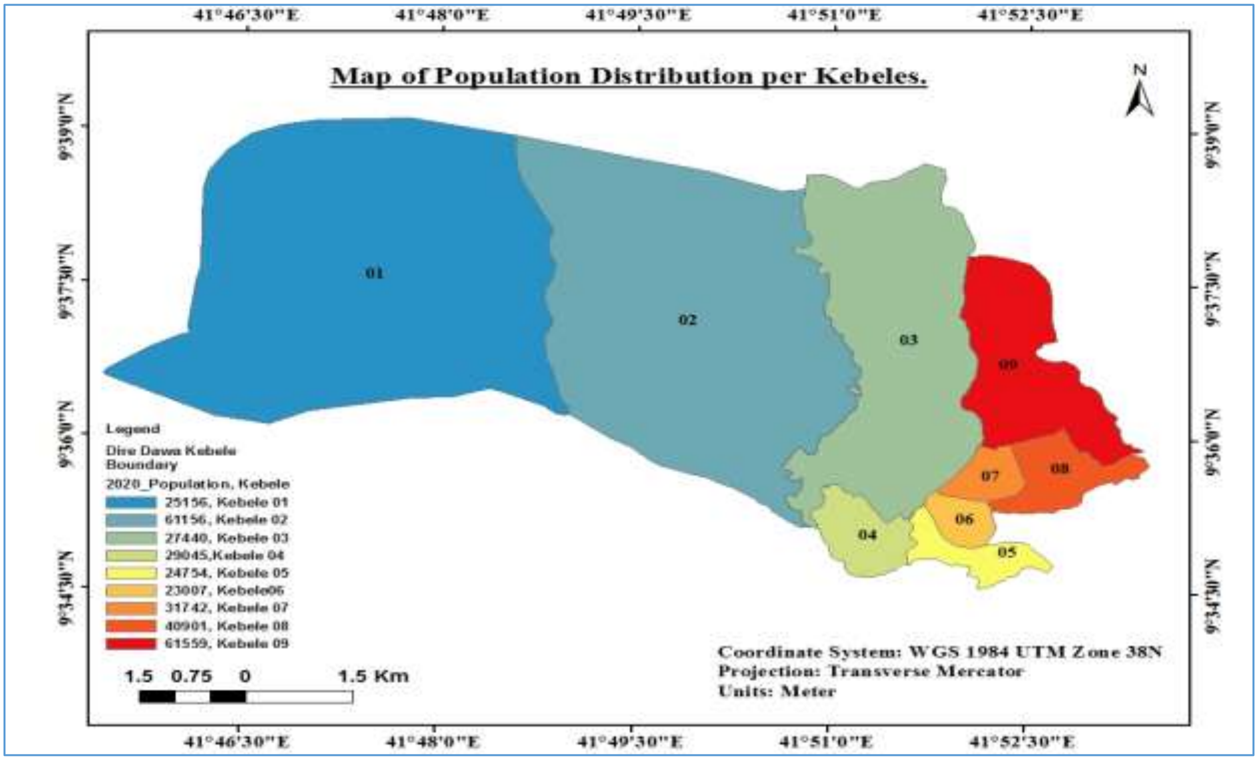

7: Normalized and reclassified exposure indicator map.

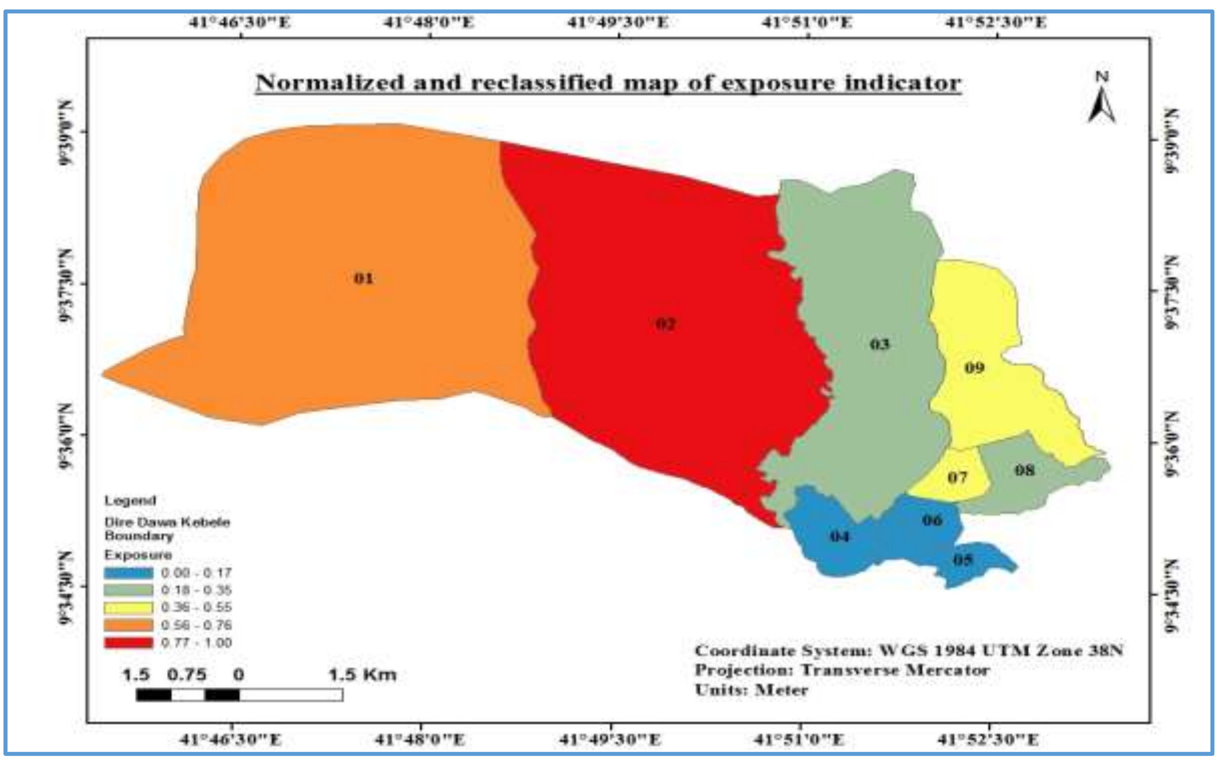

8: Normalized and reclassified sensitivity indicator map.

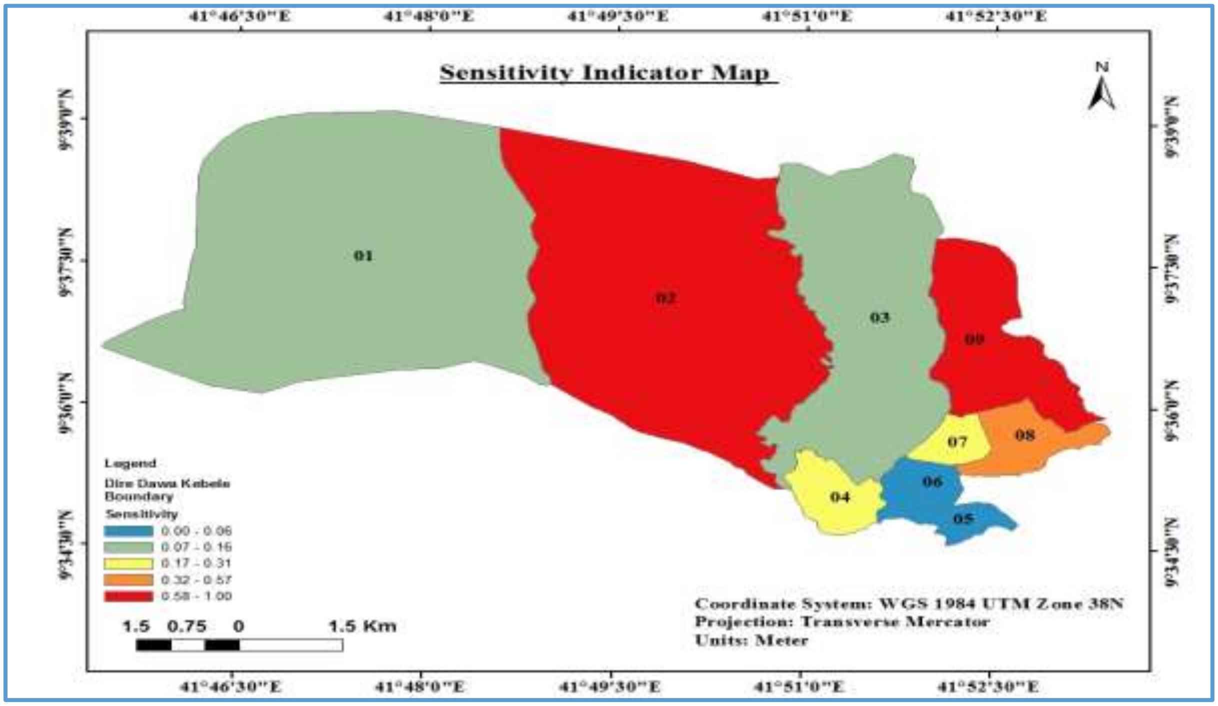

9: Normalized and reclassified average adaptive capacity layers map.